universität wien

MASTERARBEIT / MASTER'S THESIS

Titel der Masterarbeit / Title of the Master's Thesis

„Internalisation pathways of aichivirus A1 and productive infection of human cells and tissue"

verfasst von / submitted by

Konstantin Wiese BSc.

angestrebter akademischer Grad / in partial fulfilment of the requirements for the degree of

Master of Science (MSc)

Wien, 2022 / Vienna, 2022

Studienkennzahl lt. Studienblatt / degree programme code as it appears on the student record sheet:	UA 066 834
Studienrichtung lt. Studienblatt / degree programme as it appears on the student record sheet:	Master`s degree programme Molecular Biology
Betreut von / Supervisor:	Mag. Dr. Heinrich Kowalski

Acknowledgements

First of all, I would like to thank Mag. Dr. Heinrich Kowalski and Prof. Dieter Blaas for having me in their lab. It was a great experience working in such an innovative lab and with many exciting projects.

A huge thank you also contributes to Dr. Antonio Real-Hohn, who always had time for me and told and taught me so much about science and life. He was always positive and was incredibly good at thinking out of the box.

The same huge thank you goes to my other colleague Martin Groznica, who shared all the long hours in the lab with me and was there for any simple or absurd question I could have possibly asked.

You both helped me find solutions for everything and always brought the huge resort of positivity to move on, which is most important for science, in my opinion. Additionally, I never thought a coffee break with you two could be so efficient and inspiring.

I´m also thankful to Irene Gösler for helping me handle the cell culture and all the corresponding instruments.

The last thank you goes to my family, Sophia and Stefan. Thank you all for being there and always having my back!

Abstract

Kobuviruses comprise a large group of disease-causing agents, including human pathogens like aichivirus A1 (AiV-A1). This species has a high seroprevalence throughout all age groups and is detected in patients diagnosed with gastroenteritis. Even though this single-stranded positive-sense RNA virus, now assigned to the family of *Picornaviridae,* was first discovered in 1989, many features are still unknown: e.g. what kind of entry mechanism(s) are used. Preliminary data obtained with human lung cancer-derived A549 cells by others using an AiV-A1 strain isolated from a Taiwanese patient suggest that this virus may also infect the respiratory tract. The first part of this thesis, using RT-qPCR and immunofluorescence methods, therefore compares for the first time the infection of human lung 3D tissue models by the Taiwanese subtype. This demonstrates an enhanced susceptibility of the human airway epithelium for AiV-A1, strengthening the possibility of AiV-A1 being a human airway pathogen. The second part of this thesis characterizes the cell entry mechanism of AiV-A1 in the human lung cell line A549 cultivated under standard 2D conditions. By using different compounds known to interfer with cellular uptake and transport mechanisms it is shown here that AiV-A1 mainly uses clathrin-mediated endocytosis for entering A549 cells. Finally, we obtained strong evidence that AiV-A1 can disrupt the early endosome or the endocytic carrier vesicle membranes to either expose the RNA to the cytoplasm or the whole capsid.

Zusammenfassung

Kobuviren bilden eine große Gruppe von Krankheitserregern, darunter auch humanpathogene Erreger wie das Aichivirus A1 (AiV-A1). Diese Spezies hat eine hohe Seroprävalenz in allen Altersgruppen und wird bei Patienten mit diagnostizierter Gastroenteritis nachgewiesen. Obwohl dieses einzelsträngige (+)-RNA-Virus, das jetzt der Familie der Picornaviridae zugeordnet wird, erst 1989 entdeckt wurde, sind viele Merkmale noch immer unbekannt: zum Beispiel welche Art von Eintrittsmechanismen verwendet werden. Vorläufige Daten, die von anderen mit A549-Zellen aus menschlichem Lungenkrebs gewonnen wurden, wobei ein aus einem taiwanesischen Patienten isolierter AiV-A1-Stamm verwendet wurde, lassen vermuten, dass dieses Virus auch die unteren Atemwege infizieren kann. Im ersten Teil dieser Arbeit wird daher mit Hilfe von RT-qPCR- und Immunfluoreszenzmethoden zum ersten Mal die Infektion von menschlichen 3D Lungengewebemodellen durch den taiwanesischen Subtyp verglichen. Dies zeigt eine erhöhte Anfälligkeit des menschlichen Atemwegsepithels für AiV-A1, was die Möglichkeit wahrscheinlicher macht, dass AiV-A1 ein Pathogen der menschlichen Atemwege ist. Der zweite Teil dieser Arbeit charakterisiert den Zelleintrittsmechanismus von AiV-A1 in die menschliche Lungenzelllinie A549, die unter 2D-Standardbedingungen kultiviert wird. Durch den Einsatz verschiedener Substanzen, von denen bekannt ist, dass sie die zellulären Aufnahme- und Transportmechanismen stören, konnte gezeigt werden, dass AiV-A1 hauptsächlich die Clathrin-vermittelte Endozytose beim Eintritt in A549-Zellen nutzt. Schließlich haben wir deutliche Hinweise darauf erhalten, dass AiV-A1 die Membranen der frühen Endosomen oder der endozytischen Carrier-Vesikel zerstören kann, um entweder die RNA in das Zytoplasma freizugeben, oder das gesamte Kapsid freizusetzen.

Table of Contents

List of Figures

List of Tables

Abbreviations

(+)ssRNA	plus sense single-stranded RNA
°C	Degrees Celsius
µl	microliter
ACBD3	Acyl-coenzyme A binding domain containing 3
AiV-A1	Aichivirus A1 kvgh99012632/2010 Taiwan
bp	Basepairs
CAR	Coxsackie and adenovirus receptor
CCP	Clathrin coated pit
CCV	Clathrin coated vesicle
CLIC/GEEC	clathrin-independent carrier/glycosylphosphatidylinositol-anchored protein enriched early endocytic compartment
CME	Clathrin mediated endocytosis
CPZ	Chlorpromazine
CVB3	Coxsackievirus B3 strain Nancy
ECV	Endocytic carrier vesicle
EE	Early endosome
EpiAirway	EpiAirway AIR-100
ERC	Endocytic recycling compartment
FEME	fast endophilin-mediated endocytosis
GLS	Glycosphingolipids
HCEC	Human colon epithelial cells
HIV-1	Human immunodeficiency virus 1
ICAM-1	Intercellular adhesion molecule 1
IRES	Internal ribosomal binding site
LDL(R)	Low Density Lipoprotein (receptor)
M	Molar
mM	millimolar
MOI	Multiplicity of infection
MβCD	Methyl-β-cyclodextrin
ORF	Open reading frame
PAK	p21-activated kinases
PFU	Plaque-forming units
PI4KB	phosphatidylinositol-4 kinase B
PI4P	phosphatidylinositol-4-phosph
PKC	Protein kinase c
PLA2	phospholipase A_2-like

PLA2G16	phospholipase A_2 of group XVI
QC	Quinacrine
RE	Recycling endosome
RNA	Ribonucleic acid
rpm	Rotations per minute
RV-14	Rhinovirus B14
RV-A2	Rhinovirus A2
RV-A89	Rhinovirus A89
SARS-CoV-2	severe acute respiratory syndrome coronavirus type 2
$TCID_{50}$	Tisue culture infectious dose
UTR	Untranslated region
VP	Viral protein
x g	Times gravity

1. Introduction

1.1. Aichivirus A and its structure

The family *Picornaviridae* is presently divided into 63 genera. It comprises viruses with a plus sense single-stranded RNA ((+)ssRNA), including animal and human pathogens causing a broad diversity of diseases, such as the common cold, poliomyelitis, myocarditis and gastroenteritis. One of the viruses associated with gasterointestinal tract infections in people of all ages is the human aichivirus, now part of the genus *Kobuvirus*, classified in the picornavirus family and first identified in 1999. To the present day, there are three tentative and six officially recognized species assigned to the genus *Kobuvirus*. The three preliminary species are caprine kobuvirus, a viral genome collected from bat faeces through sequencing in the USA, and the Norway rat kobuvirus [1, 2]. The six confirmed *kobuviruses* include *aichivirus A-F*. Among these, only *aichivirus A1* (formerly called human aichivirus) comprises human pathogens. In contrast to other picornavirus strains, the A1 strains do not differ in antigenicity. Like the other members of the *Picornaviridae* family, AiV is non-enveloped and has an icosahedral morphology [3]. This thesis focused its work on the strain Aichivirus A1 kvgh99012632/2010 Taiwan (later referred to as AiV-A1, Accession number JX564249). This strain was first completely sequenced in 2013 by Chang *et al.* [4].

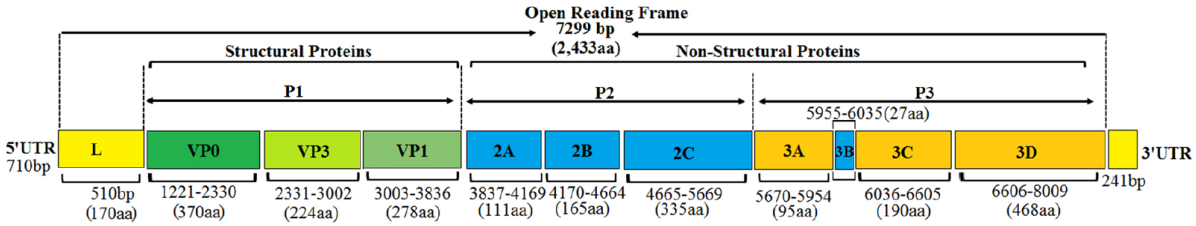

Figure 1 ***Genomic organisation of AiV-A1.*** *Beginning with the leader protein, the ORF comprises the structural proteins originally produced as a P1 precursor and non-structural proteins derived from P2 and P3 precursors. P1, P2, and P3 are in turn derived from proteolytic processing of a huge P1 polyprotein. Sadik et al. (2021)[5].*

The AiV genome codes for a large polyprotein, which is initially processed by virus-encoded proteases 3C, which liberates a leader protein L and the three precursor proteins P1, P2, and P3. Further cleavage of P1 by 3C and 3CD results in the three capsid proteins, VP0, VP3 and VP1, and proteolytic processing of P2 and P3 gives rise to non-structural proteins 2A, 2B, 2C, 3A, 3B, 3C, 3D and their immediate precursor such as 3CD and 3AB [6]. These are involved in replication of the viral RNA, defense against the antiviral immune response of the host and various other processes supporting virus growth and

survival. VP0 is unusually long with about 370 residues and is also not cleaved as in most other picornaviruses, where its is further split in VP2 and VP4 probably by an autocatalytic mechanism involving the encapsidated viral RNA [7]. Additionally, the genome shares only 15 to 34 % nucleotide identity with other picornaviruses. While featuring a typical myristoylation motif, it remains to be shown that the N-terminus of AiV VP0 is myristoylated as reported for several other picornaviruses [7]. The L protein was identified as a antagonist to the integrated stress response, to prevent a stress induced shutdown of translation. Rabouw *et al.*. showed in addition, that even at high levels of p-eIF2, the L protein of AiV-A1 rescued translation. P-eIF2 is a protein, that arrests translation [8]. The protein 2A instead is involved in the replication of the viral RNA, in both, the negative and the positive strand synthesis [9]. The open reading frame includes 7299 bp and is flanked by untranslated regions (UTRs), measuring 710 bp on the 5' and 241 bp on the 3' end. The 5'UTR also contains an internal ribosomal entry site responsible for recruiting ribosomal subunits, initiating translation, which works cap-independent [5, 10]. It also contains a packaging signal [11].

AiV-A1 presents a unique capsid, distinct from previously described structures of picornaviruses. It comprises plateaus surrounding the 3-fold axes, small protrusions around the icosahedral 5-fold axes and moderate depressions around the 2-fold axes.

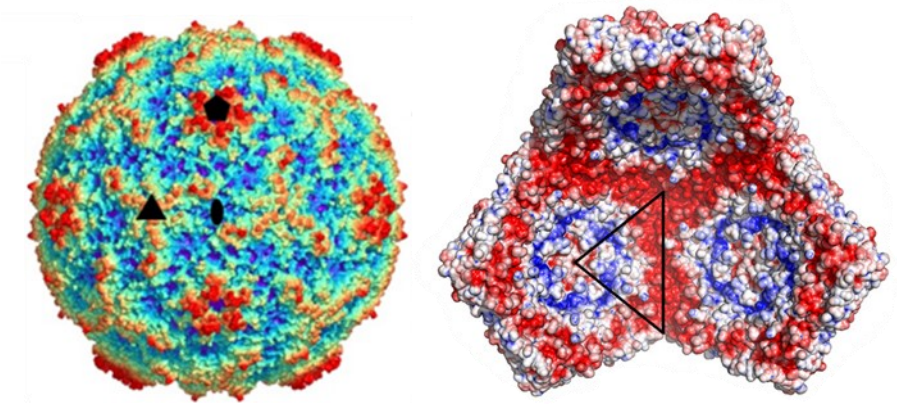

Figure 2 ***The capsid structure of AiV-A1.*** *Shown is the native virion of AiV-A1 and a close up of a trimer of pentamers. The location of the five-fold, three-fold and two-fold symmetry axis are indicated by black symbols. The black triangle shows one viral protomer and labels the sites where the later mentioned canyons are located on the outside of the capsid. Figure adopted from Sabin et al. (2016) [12].*

The protrusions at the 5-fold axes are surrounded by narrow, so-called canyon, which is very shallow in the case of AiV-A1 compared to other enteroviruses. The outer wall of the canyon is *inter alia* formed by the EF loop of VP0 - in other enteroviruses, part of VP2 – which is called "puff". This protusion is very small in AiV-A1, even shorter than in human parechovirus 1, which lacks the canyons completely. The loop before the β-strand B of VP3, which in other picornaviruses also contributes to the outer canyon wall, is missing in VP3 of AiV-A1. Overall, it has a particular and specific capsid structure, and it is not

yet clear how the RNA is released from the capsid because it was impossible to find a pore at the surface [12]. For other picornaviruses, the uncoating mechanism is partly known. The majority of picornaviruses, which contain a VP4 undergo rearrangements in their structure, expose their VP4 to induce pore formation in the endosomal membrane [13, 14]. This process can be triggered by acidification of endosomes [15, 16] or, as in the case of major group rhinoviruses, by lowering the pH combined with receptor interactions [17, 18]. New insights in this direction of AiV-A1, which only carries the unprocessed VP0 comes from work published by Kelly *et al.*. in 2022. These authors find a major dependency of the uncoating of AiV-A1 on low pH, by showing a higher rate of exposed viral genome, correlating with a lower pH. The maximum effect was observed at a pH of 5 [19]. Furthermore, they demonstrate differences AiV-A1 and enterovirses in uncoating experiments, with AiV-A1 being more relying on the pH. Its capsid undergoes changes in structure that cannot be compared to the uncoating mechanism of other picornaviruses that contain VP4.

1.2. Cells and tissue

Cells

AiV-A1 is a picornavirus that is believed to cause gastroenteritis, which, however is presently exclusivey based on epidemiological data and the observation of a strong association between gasteroenteritis in animals infected with related AiV species [20]. One step further in supporting its role as a human enteric pathogen would be the demonstration, that it is able to infect cells of the human gastrointestinal system. This will not only allow to find a way to prevent infections by AiV-A1, but also to learn more about viral entry and intracellular pathways. To this end a variety of continuously growing human cell lines of gastrointestinal origin were examined for their suitability as viral hosts. Their precise origin and properties are described in the following paragraphs.

Human colonic epithelial cells (HCEC) 1CT cells are of non-malignant origin and therefore closer to primary intestinal cells compared to the tumor-derived cell lines introcuced further below. 1CT cells were isolated from biopsy material during the course of a screening colonoscopy by Roig *et al.* in 2010 [21]. The dissociated primary cells were immortalised by expressing the catalytic part of the human telomerase and the cyclin-dependent kinase 4 proteins [21]. HCEC-1CT cells express stem cell markers, such as LGR5, BMI1, CD29, and CD44, and are capable of differentiating into various epithelial lineages of the colon, which was not executed in this thesis.

T84 cells are colonic epithelial cells derived from a human colonic carcinoma. They are able to differentiate into colonocytes when grown on filter inserts. After their differentiation, these cells exhibit a high transepithelial electrical resistance, which makes them one of the best cell models in the field of

membrane trafficking and for investigations on cell entry mechanisms of numerous enteric micro-organisms [22].

Caco-2 cells were derived from a human colon adenocarcinoma. They are even capable to spontaneously differentiate into enterocyte-like cells when grown to high density in 2-D culture [23]. Therefore they have been already frequently used as an enterocyte model for studying interaction with various enteric pathogens [24]. This cell line was already use as an model organism for different viruses, for example SARS-CoV-2, human adenovirus and herpes simplex virus 1 [25].

RKO cells were derived from human colon carcinoma; they are poorly differentiated and immortalized due to an inactivated *CDX2* gene. They are nonetheless often used in experiments with viruses [26, 27].

As already mentioned before, Chen *et al...* (2013) have shown that at least one AiV-A1 representative (the Taiwanese strain) can also productively infect A549 cells [28]. This cell line was originally derived from a human caucasian lung carcinoma. When grown for a longer time, about 25 days, A549 cells rather closely resembles Type II alveolar cells lining the alveoli of the distal lung, and produce lamellar bodies as a typical hallmark [29]. They are frequently used in infection studies with viruses targeting the lower human respiratory tract, either by their simple 2D or less frequently, more elaborate 3D cultivation [30]. This is evidenced by the many studies that have been published using this cell line, focusing on entry mechanisms and cellular routing of these pathogens, such as RSV (human respiratory syncytial virus, SARS-CoV-2 (severe acute respiratory syndrome coronavirus type 2) [31, 32], and also various *Picornaviridae* [33-35].

As outlined in detail in the results section, all of the immortalized human intestinal tract-derived cell lines mentioned above (RKO, HCEC 1CT, T84 and Caco-2 cells) were tested for their permissitivity to support AiV-A1infection as a prelude for studies on its entry mechanism. T84, A549 and Vero cells served as a control as they were already found to allow replication of the Taiwanese AiV strain (20).

The human airway system and EpiAirway 3D tissue model

The human respiratory tract, in part due to its large accessible surface, is a prominent target of many so-called respiratory pathogens including numerous viruses. In several instances it also allows access to other parts of the body by their subsequent dissemination through the blood circulation [36]. The cells in the lung epithelium are divided into three structurally and functionally distinct groups, the basal, secretory, and ciliated cell types. The predominant cell type is ciliated epithelial cells, which comprise more than 50 per cent of the cells of the airway epithelium [37]. They are mainly responsible for transporting mucus from the lung to the throat by means of their cilia, thereby removing as many

microbes and debris as possible from the respiratory tract. A second type is the goblet cells, also called mucous cells, which are responsible for mucus production [38]. Serous cells resemble mucous cells morphologically but have a more electron-dense granule content compared to them [25]. The last two types are basal cells, which play an essential role in membrane attachment and are thought to serve as stem cells for ciliated and mucous cells [39, 40] and Clara cells, which have a secretory and a stem cell role [41, 42].

The EpiAirway tissue by MatTek (Ashland, USA) is a 3D model of the human tracheal/bronchial epithelium. It is obtained by cultivation of normal human cells of this region on filter inserts at the air-liquid interface for about 30 day, using a special growth medium to achieve full differentiation. It has already been used by others in experiments with rhinovirus-14, influenza, respiratory syncytial virus and adenovirus-2 [43] and has the distinct advantage of more closely reflecting the host-pathogen interactions taking place in natural infctions of the human airways [44]. One still has to keep in mind, that the innate immune response and expression of the related proteins is limited to the one donor as well.

In this thesis, the highly differentiated EpiAirway system was employed for the first time to explore the possible tropism of human aichiviruses for the human respiratory tract as hinted by the previous study using A549 cells (20). Though they are clearly a poorer mimick of the complex human respiratory tract, due to their easier handling and considerably lower costs of cultivation, all experiments on AiV internalization and uncoating were then carried out with A549 cells grown in standard 2D tissue culture.

1.3. Virus uptake and intracellular routing

Many viruses initially attach to component(s) of the glycocalyx, which consists of proteoglycans, glycoproteins and glycolipids and represents the outer layer of the cell surface. In a number of instances, the carbohydrates covalently linked to the proteins or lipids are already by themselves involved in binding, concentration and even internalization of pathogens [45]. These so-called virus receptors are frequently expressed in a cell-type specific manner and are therefore at least in part responsible for the tissue tropism of these pathogens. However, neither the receptor molecule(s) nor the components (carbohydrate, lipid and/or protein) involved in AiV binding are known up to this date [20].

This initial, receptor-mediated, contact with the host cell is essential for nearly all viruses to enter the cell. This is accompanied by their uncoating either directly from the cell surface or during/after their endocytosis, followed by replication of the released genetic material. The final steps involve packaging of the viral genome and eventually the exit of the newly assembled progeny virions by lytic and/or nonlytic mechanisms. Each of these steps in the viral life cycle may in principle serve as a target for

compounds, aiming at pharmacological inhibition of virus infection. Despite the large number of experimental anti-picornaviral drugs already described in the literature [46, 47], no one has yet been approved by authorities of different countries for patient use except as a last resource in cases of emergency. Endocytosis as one of the earliest events is a particularly attractive target for efficient inhibition of virus infection. While the mechanisms of host cell invasion have already been elucidated for a considerable number of picornaviruses, it still remains elusive for the human aichivirus. As endocytosis is by far the most common entry and transport pathway used by picornaviruses [48], it is save to assume that this is also central for the entry/uncoating of AiV. The most relevant endocytic pathways ursurped these and numerous other viruses are therefore reviewed in the following.

Ways of Endocytosis

This thesis places its focus on dynamin-dependent and dynamin independent endocytosis. Well known examples are the clathrin-mediated endocytosis (CME), fast endophilin-mediated endocytosis (FEME), macropinocytosis and the CLIC/GEEC pathway, which stands for a clathrin-independent carrier/glycosylphosphatidylinositol-anchored protein-enriched early endocytic compartment [49]. Endocytosis mediated via caveolae, which are flask-like, narrow invaginations at the plasma membrane, is also an option for pathogens to enter cells, but this is a highly discussed subject [49], with some links to picornavirus uptakes, including Poiliovirus and CVB3, which enter cells over caveolin [50, 51]. The only consensus seems to regard its eminent role in keeping a constant caveolar density on the cell surface and thereby serving in lipid, cholesterol and albumin trafficking [52]. Figure 3**C** shows the proposed molecular organization of caveolae, which, besides caveolin-1 are characterized by the presence of cavin isotypes [49]. In line with this topic, there is also conflicting data on the importance of caveolae in the endocytosis of A549 cells [42, 53]. The other pathways will be elaborated on in the following paragraphs, including the compounds used to inhibit these uptake mechanisms. Caveolin-mediated endocytosis is dynamin-dependent and hence inhibited by compounds targeting this small GTPase, such as dinasore (Reference). It is also inhibited by cholesterol-targeting compounds such as methyl-ß-cyclodextrin (MßCD), nystatin, filipin (described in more detail in a separate chapter). Caveolin-1 directly interacts with cholesterol of the plasma membrane and depletion of cholesterol results in flattening/disassembly of the caveolae, rendering them dysfunctional [54, 55]. Genistein is a broad-spectrum tyrosine kinase inhibitor that inhibits cavelae-dependent endocytosis by preventing actin depolymerization in the local cortical cytoskeleton as prerequisite for internalization of caveolar vesicles and recruitment of dynamin-2 required for their pinching-off from the plasma membrane [56]. Conversely, full disruption of the caveolae-stabilizing cortical actin filaments by latrunculin in CHO cells eliminated caveolin-1 arrays from the plasma membrane by promoting caveolar vesicle formation.

The microtubule-depolymerizing compound nocodazole was found to inhibit long-range movement of these vesicles in these cells [57].

Caveolae are usually embedded in lipid rafts. Another lipid raft-dependent endocytosis type involves certain GPI-anchored proteins and the choleratoxin B (CT-B) and depends on flotillins, forming microdomains at the plasma membrane [58]. The internalization of cargo such as CD59 or CT-B is triggered by the kinase Fyn and starts with the formation of flotillin-bearing vesicles, which appear to fuse with and/or mature into rab7 positive endosomes. This pathway is also dynamin-dependent, and, like the caveolar and many other clathrin-independent pathways, is sensitive to cholesterol-sequestretion and depletion. Of note, with respect to viral cargo, this pathway has sofar only been found important for infection of HeLa cells by respiratory syncytial virus [59]and for a plant virus in the gut of insect vector [60].

CME is a well-known and best-studied entry pathway of those mentioned above. It is the main entry route for viruses like influenza A, rhinovirus A2 (RV-A2) or foot-and-mouth disease virus (FMDV), the latter two belonging to the picornaviruses [46, 61, 62]. CME is induced by ligands like low-density-lipoprotein (LDL) on binding to the cognate almost ubiquitous LDL-receptor, starting with the recruitment of clathrins to form clathrin-coated pits (CCP). This process normally happens very fast, in only 30 to 120 seconds [63]. Another possibility is binding of ligands including viruses to recpetors already captured in preformed CCP, which comprise about 0.5 to 2% of the cell´s clathrin together with dynamin and AP2 also participating in the assembly of these structures. Ehrlich *et al...* (2004) further distinguished between shorter-lived CCP (~6 seconds residence time) involved in transferrin binding via the transferrin receptor (TfR) and more stabler CCP (~20 seconds) employed for capturing LDL [63]. Tf is a serum iron-transport glycoprotein, which, after binding to its cognate transferrin receptor (TfR), is imported via the CME. The clathrin-coated vesicles fuse with Rab5+ early endosomes, where iron releasen is triggered by the acidic pH. The TfR-bound apoTf is transferred back to the cell surface via the EGA insensitive perinuclear recycling compartment, where it dissociates from the TfR at the neutral pH [64]. Minor receptor group rhinoviruses such as RV-A2 and several other viruses including vesicular stromatitis virus (VSV)[65] have been found to exploit the LDLR for clathrin-mediated endocytosis into host cells [66]. The GTPase dynamin and actin are both required for pinching off cargo-loaded CCP resulting in the formation of clatrhin-coated vesicles. Dynamin is not directly linked to clathrin or its adaptor proteins but can interact with auxilin, Hsc70 and, through its proline-rich C-terminal segment, proteins that contain SH3 domains like amphiphysin. The latter three polypeptides in turn associate with clathrin [67, 68]. Auxilin is a protein that binds to clathrin lattices with high affinity, leading to the recruitment of Hsc70, which triggers the uncoating of the vesicle [69]. In line with above requirements, Cytochalasin D latrunculin A and jasplakinolide, which either disrupt or stabilize actin filaments, are able to inhibit CME [70-72]. Microtubules seem to be only necessary for later stages of CME [73]. The same was found for Dynasor which inhibits the rather neuron-specific dynamin 1 and

the ubiquitous dynamin II, later referred to as dynamin. Chlorpromazine (CPZ) is believed to inhibit clathrin-coated pit formation by leading to a redistribution of the clathrin along with AP2 from the PM to the early endodomes [74]. It must be noted, that one publication finds dynamin as the critical target for CPZ [75], which however, has not yet been indepentenly confirmed by others. CPZ is amphipathic and can increase the lipid fluidity of the plasma membrane, which may inhibit the formation of invaginations [76]. In addition to that, it can block phospholipase C, which regulates the dynamics of actin and macropinocytosis [77-79]. CPZ must hence be carefully titrated and used alongside appropriate controls, in order to account for its possible pleiotropic effects. Pitstop-2 was recently introduced as a new CME-specific inhibitor [80]. This compound did not become available during the course of this thesis work and later on was also found to affect other endocytic pathways (Reference). Depletion of K^+ and hypertonic sucrose shock have also been used to more or less specifically inhibit CME, which were not employed for reasons of too little experimental time.

FEME, while also requiring dynamin and actin, is completely clathrin-independent. Instead, it uses endophilin A2 and represents a faster alternative for endocytic uptake (see Figure 3**B**). FEME is involved in the endocytosis of many receptors, including the β_1-adregenic receptor (β_1-AR) and the epidermal and hepatocyte growth factor receptors (EGFR and HGFR), found by Boucrot *et al...* in 2015 [81]. These authors also described a possible interaction between endophilin A2 and dopaminergic receptors 3 and 4, muscarinic acetylcholine receptor 4 and proline-rich motifs in tumour-infiltrating lymphocytes, which is part of the α_{2a}-adregenic receptor. There are even more receptors, like the receptor tyrosine kinases PDGFR or the interleukin-2 receptor A. Mechanistically, the SH3 domain of endophilin B2 binds to the cytosolic tail of cargo receptors, and its BAR domain induces curvature and bolsters, supported by dynamin, the membrane scission to close the pit to a vesicle [82, 83]. Distinguishing it from CME, depletion of clathrin or AP2 caused no decrease in internalisation of the β_1-adregenic receptor. Except for CPZ, this pathway is inhibited by the same compounds which affect CME as mentioned above, due to their shared dependencies on actin and dynamin. It wasalready shown, that enterovirus 71 for example is using FEME in Caco-2 cells [84]. An siRNA-mediated knock-down of endophilin-A2 is therefore recommended for unambiguous verification of its role in endocytosis of a presumed cargo (e.g. [84]. Among picornaviruses, FEME-mediated endocytosis has been reported for enterovirus 71 (EV71) [84].

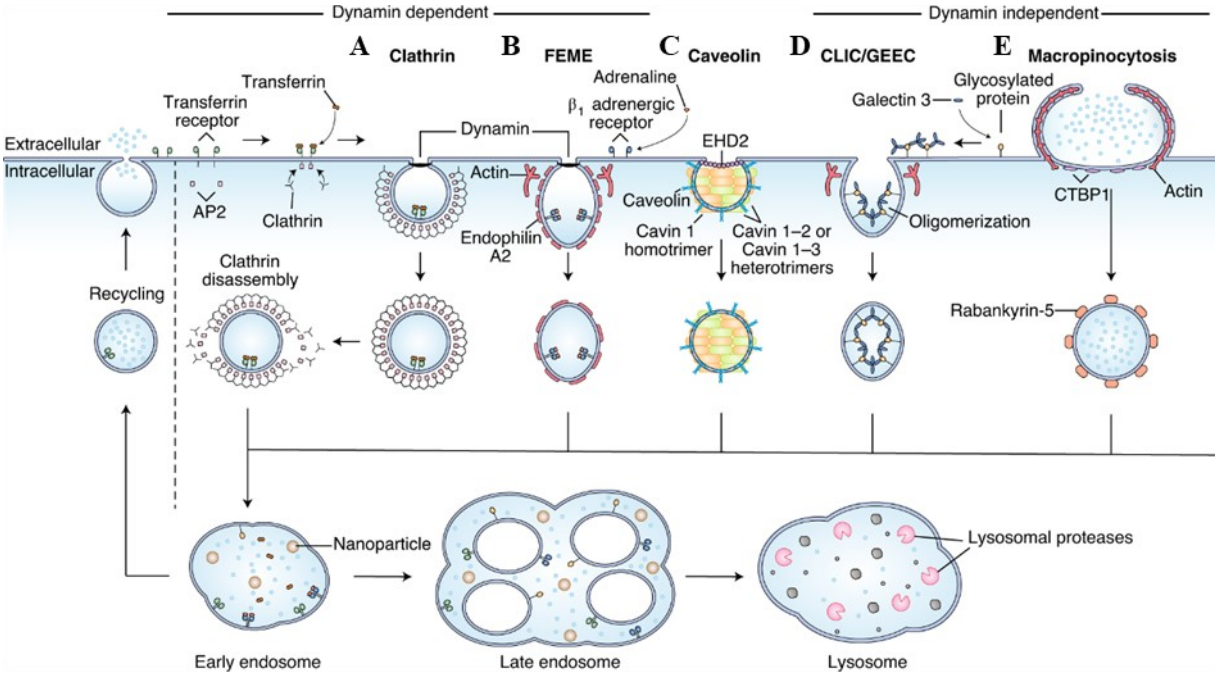

Figure 3 ***Overview of the main uptake mechanisms for viral particles.*** *The pathways can be divided into dynamin-dependent and dynamin independent uptake. CME (**A**) and FEME (**B**) are both parts of the first group, requiring dynamin to close the formed vesicle completely. In contrast, CME is carried out by clathrin recruiting, induced by bindings to transferrin or LDL receptors or using existing CCPs. FEME instead is triggered by binding to dopaminergic 3 and 4, α_{2a}-and β_1-adrenergic receptors or receptor tyrosine kinases.* ***C*** *Caveolae are formed by caveolin and cavin 1, 2 and 3 and hold or pinched off by EHD2, regulating endocytosis.* ***D*** *The CLIC/GEEC pathways include actin and the oligomerisation of galektin, but does not involve dynamin nor clathrin.* ***E*** *Macropinocytosis is dynamin independent but also needs actin for its vesicle formation. The figure was taken from Rennick et al. (2021)[49].*

The dynamin independent CLIC/GEEC uptake (Figure 3**D**) is regulated by ADP-ribosylation factor 1 and cell division protein 42, which are both small GTPases [85, 86]. CLICs are mostly found at the leading edge of migrating cells. They are uncoated tubulovesicular primary carriers which arise directly from the plasma membrane. They mature into tubular GEECs, which subsequently fuse with sorting endosomes by a mechanism dependent on Rab5, phosphatidylinositol-3-kinase and SNAREs [87]. Together this system has a high carrier capacity, able to turn the whole membrane over in fibroblasts in only 12 minutes, proving the importance of this pathway for the homoeostasis of the cell membrane [88, 89]. The CLIC/GEEC pathway is responsible for the endocytosis of a substantial part of the fluid phase, many glycosylphosphotidylinositol-anchored proteins [90], adeno-associated virus 2 [91] and toxins like cholera toxin [92] and Helicobacter pylori vacuolating toxin A [90].

The CLIC transmembrane protein CD44 is bound by the cargo protein galectin-3, which also regulates its endocytosis and is the trigger of CLIC formation. This step is dependent on glycosphingolipids (GSL), and the occurrence of CLIC formations is proportional to the expression of GSL. CLIC/GEEC

is neither dynamin nor clathrin-dependent, but as most uptake mechanisms are dependent on actin, its depletion shows a reduction of galectin-3 uptake and the formation of galectin-3/CLIC clusters. The findings of Lakshminarayan *et al.*. in 2014 also showed diversity in cargoes and endocytic structures of CLICs, which leads them to the conclusion that there are different populations of CLICs [93]. It should be noted, however, that recent data indicated an extensive cross-talk between the caveolae-dependent with the CLIC/GEEC dependent pathway (Chaudhary *et al.* (2014) PLoS Biol 12: e10011832), and the pathway also share components with macropinocytosis such as cdc42 (see below). The pathway is abolished by mild depletion of cholesterol and the perturbation of actin polymerization (Chadda *et al.* (2007) Traffic 8: 702–717). Up do date no picornavirus has been described to invade host cells via this pathway.

Macropinocytosis (Figure 3**E**) exemplifies another dynamin independent pathway. In this process, the actin skeleton actively extendes the plasma membrane (PM), allowing it to enclose a large amount of extracellular medium. The order of events of this mechanism, appropriately termed cell drinking, was described for a long time already, but recently in great detail by Condon *et al.*. in 2018 in macrophages. They used lattice light-sheet microscopy to show that two tentpole-like actin structures peak up and collapse in a circular manner, wrapping up the fluid and trapping it inside [94]. In A549 cells and several other tumor cells, macropinocytotic events are upregulated due to a K-Ras mutation [95, 96] and exhibit the second kind of macropinocytosis, so-called peripheral ruffles, where a part of the plasma membrane, driven by actin, wraps over an amount of fluid and engulfs it [97]. Cancer cells use this mechanism as a constitutive macropinocytic process to get supplied with amino acids by uptaking extracellular proteins [95]. The mechanism can be induced or upregulated by several factors like receptor tyrosine kinase family receptors, EGFR, for example, neutrophils as a viral response, and proteoglycans and G-protein-coupled receptors on binding their respective ligands, [98]. Other regulating agents are p21-activated kinases (PAKs), which highly influence macropinocytic uptake. Gain-of-function PAK1 mutations were shown to stimulate dextran internalisation and macropinocytic events [99]. CtBP1 and Rabankyrin-5 are also proteins required for the fission and formation of macropinosomes [100, 101]. One speciality of macropinocytosis is the size of the resulting vesicles, which, with more than 200 nm, is the biggest among the pathways mentioned above, permitting cells to internalise larger amounts of fluid, solutes, and membrane [98].

Macropinocytosis has many dependencies, in addition to the already mentioned on actin, CtBP1 and Rabankyrin-5. Macropinocytosis is also dependent on different motor proteins, myosin I, II and V enabling the engulfing of the vesicle and the movement of the filopodia [102, 103]. Macropinocytosis can be inhibited by Blebbistatin, which targets myosin II. It does not inhibit myosin directly but rather acts as antagonist to actin instead. Both bind to the globular head domain of myosin II. Blebbistatin, however, drastically decreases the ATPase activity of the actin bound state of the globular head domain of myosin II, blocking it and preventing the cross-linking of actomyosin [104, 105]. The productive

entry via micropinocytosis has been described in the past for several picornaviruses such as foot-and-mouth-disease viruse (FMDV) [106] and echovirus 1 (EV1) [107].

1.4. The role of cholesterol in endocytosis

Chadda *et al.*. showed in 2007 that cholesterol is essential for the recruitment of actin to the assembling site of vesicles pinching of and Cdc42 molecules, which are GTPases of the Rho family to the plasma membrane [86]. For those reasons, cholesterol targeting compounds were used as well, such as genistein, a tyrosine kinase inhibitor, proven to decrease cholesterol production [108], nystatin, which sequesters cholesterol [109] and U18666A, an inhibitor of cholesterol transport [110].Additionally, simvastatin which inhibits the HMG-CoA Reductase as a first key enzyme in the synthesis of isprepoids and then Cholesterol was used as well [111]. U18666A noncompetitively blocks the cholesterol transporter NPC1 and also inhibits at least three membrane-bound enzymes involved in cholesterol biosynthesis [110].

Filipin III has also been used to bind cholesterol and flatten the membrane at lipid rafts sites preventing membrane engulfing [112].

Despite binding cholesterol, filipin III also reduces the phosphorylation of EGFR and the protein kinase Akt [113]. Akt is an important factor facilitating the formation of the clathrin coat complex and is required for recycling events [114] while EGFR is known for being internalised by CME [115]. The last compound used to examine the role of the CLIC/GEEC pathway in the case of AiV-A1 was methyl-β-cyclodextrin (MβCD), a compound depleting the cholesterol on a cell surface and also from the internal membrane [116]. The cholesterol targeting compounds were also associated with macropinocytosis, which depends on cholesterol and MβCD additionally with CME as well [117] .

Cholesterol also plays an essential role in macropinocytosis. It was previously shown that cholesterol depletion reduces HIV-1 internalisation and the import of the Ebola virus via macropinocytosis drastically [118, 119]. All the compounds mentioned above were monitored to determine the importance of macropinocytosis for AiV-A1 infection.

Intracellular pathways

After a successful engulfing or scission of a newly formed vesicle and its fusion with an early endosome there are multiple trafficking directions an early endosome (EE) can follow. Figure 4 shows an overview of the possible pathways and the points of interference by the previously mentioned compounds.

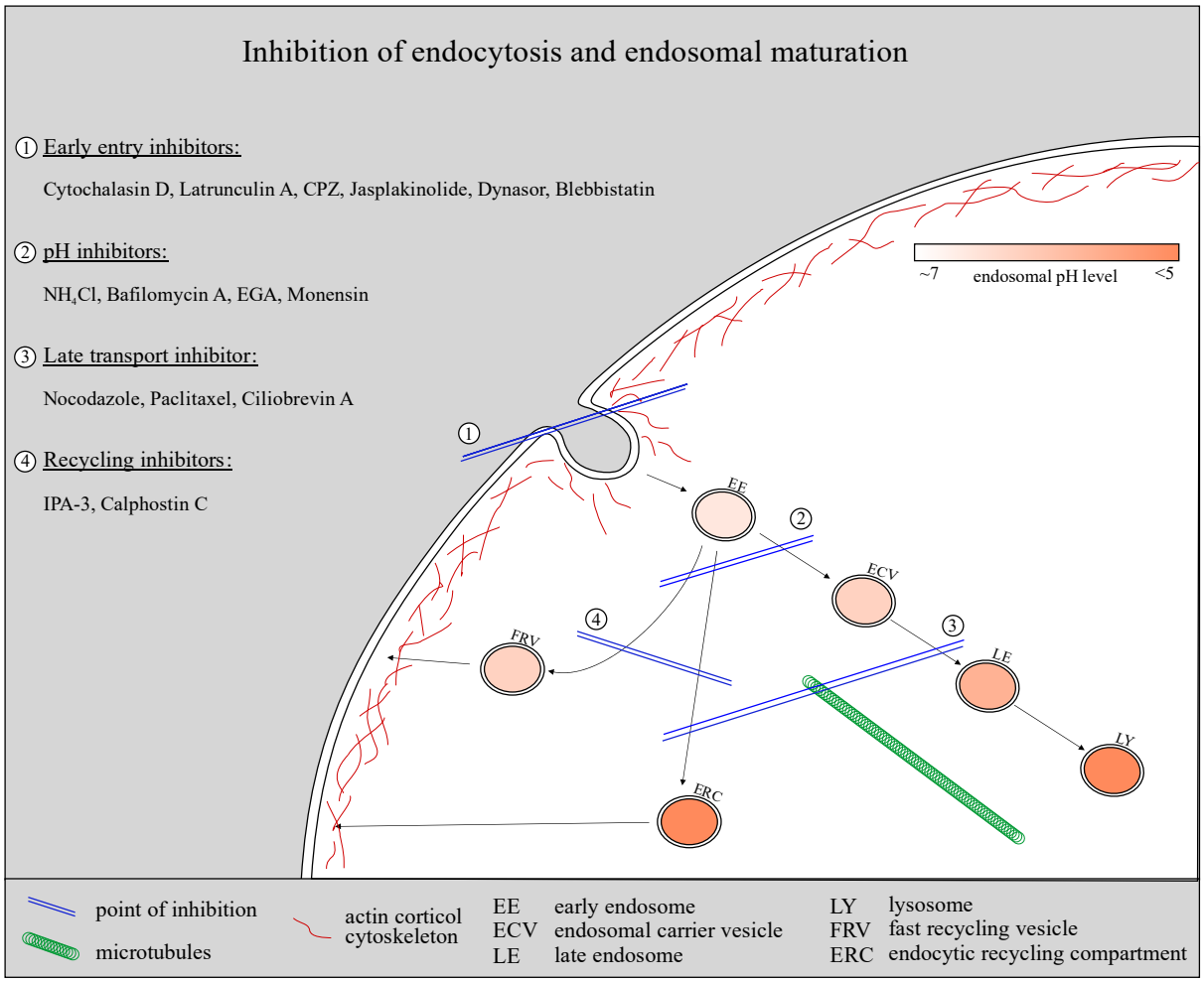

Figure 4 ***Compound inhibition on different timepoints from entry to more mature vesicles****. The entry is inhibited by compounds targeting, among other proteins, actin and dynamin ①. Agents like NH_4Cl render the vesicular pH neutral and thereby disallow the maturation of early endosomes, while EGA only act as it is behaving the same, but not influencing the pH ②. Nocodazole, paclitaxel and ciliobrevin A block the migration of early endosomes to vesicles of a lower pH for subsequent fusion by targeting microtubules or the motor protein dynein ③. IPA-3 and calphostin C pevent recycling events ④.*

The EE usually has a pH between 6.5 and 6.0 and is the first distinguishable station before the contents fate is further determined. Cargo, which is internalised through caveolar and macropinocitotic events and GLEEC is also transferred to early endosomes in many instances. EEs have the small GTPase Rab5 as a critical component, which is also used to identify these vesicle. Its tasks include maturating clathrin-coated pits and regulating the fate of EEs. Rab7 is involved in redirecting EE back to the cell membrane, which become a recycling endosome (RE) with a pH of around 7.4. This process recycles receptors responsible for endocytosis and brings them back to the plasma membrane. The transferrin receptor is

one example of receptors recycled with a half-time of 2 minutes. Diferric transferrin splits off its iron atoms when exposed to the slight acidic pH in the EE. This reaction leads to a recycling of the receptor and apotransferrin, both being reintegrated in the plasma membrane [120].

Alternatively, EE may be directed to the endocytic recycling compartment (ERC) and for receptor recycling. The ERC has a pH milieu of 5.6 or less in some cells, whereas in other cells it could be nearly neutral, depending on the cell type and this route has a half-time of about 12 minutes. The ERC is positioned around the microtubule organising centre, where the (-)-strand of the microtubule network becomes attached [120, 121]. One example of a receptor directed to the ERC is the low-density lipoprotein receptor (LDLR) [122]. LDL dissociates from LDLR in the EE at a slightly acidic pH, and the receptor is recycled to the PM via the ERC.

After sorting designated cargo into the recycling pathway, according to the maturation model, the EE with its remaining cargo matures into a late endosome (LE). Referring to the vesicle-shuttle model, the different endosomal compartments are stable entities, which communicate by exchange (shuttling) of vesicles. In BHK cells, MDCK cells and hypocampal neurons, endosomal carrier vesicle (ECV) have been shown to mediate transport from early to late endosomes [123]. In contrast to Les, this type of vesicle is relatively uniform among mammalian cells and has a diameter of about 0.5 μm [124]. An exchange of Rab5 by Rab7 is taking place at the ECV, facilitated by the C VPS/HOPS complex, which is a guanine nucleotide exchange factor [125]. The last step on this route is fusion of the late endosome with a lysosome, accompanied by a further drop in vesicular pH [126]. The late endosome can maintain a pH lower than 5.6 and lysosome lower than 5.0, which leads to the degradation of most molecules by a plethora of acid hydrolases [127]. Playing a similar role as Rab5 for the EE, Rab7 is essential for the late endosome being the main factor in guiding late endosome trafficking [128]. Therefore, these two small GTPases are often used as marker proteins for EEs and late endosomes [129]. The migration to the late endosomes and the lysosomes is dependent on microtubule dynamics, and a similar microtubule-dependence was observed for ERC [130, 131]. Nocodazole, a microtubule disrupting agent [120], does not interfere with endosome formation but prevents their their directional long-range translocation. At least in HeLa it curtails every step after the endocytic carrier vesicle [132]. By contrast, paclitaxel, which hyperstabilises microtubules by binding to the β subunit of tubulin, does not inhibit fluid-phase macropinocytosis, but reduces significantly ^{125}I-transferrin uptake via receptor mediated endocytosis by about 50% [133].

Nevertheless, compounds mainly affect the events after the early endosome formation [134]. The motor protein dynein is an important player in the translocation of endosomes. It transports the vesicles along the microtubules through the cell towards the minus-end. Ciliobrevin used in this thesis inhibits the ATPase activity required for dynein activity [135] and thereby impedes this endosomal transfer. Two additional compounds known to interfere with endocytosis were tested in preventing viral infection and

replication. The first, calphostin is a specific inhibitor of protein kinase C (PKC) [136]. PKC has many functions in cells and some are linked to intracellular trafficking being responsible for the balance of receptor recycling [137]. It also plays an important role in the uptake of distinct viruses [138-140]. The second was f-3, a chemical inhibitor of p21-activated kinase 1 (Pak1), a serine-threonine kinase. Pak1 is required for cytoskeleton reorganisation and necessary for macropinocytosis and potentially also CME [99, 141, 142].

The last group of compounds employed in this thesis inhibit maturation of early endsomal vesicles. Three of them act by dissipating the acidic vesicular pH via different mechanism. The most commonly used compound is Ammonium chloride (NH_4Cl). It is membrane permeable due to the NH_3 formed in equilibrium and its mild pH buffering capacity leads to an arrest of early endosome maturation [143, 144]. NH_4Cl has been used to retain already internalized virus particles in the EE, which prevents the pH-dependent uncoating of certain viruses such as minor group RVs [46, 122, 145]. Bafilomycin prevents endosomal acidification by acting on the electrogenic vacuolar-type ATPase [146], resulting in blockage of endosomal maturation as shown by its inhibition of receptor recycling and endosomal-lysosomal fusion [147, 148]. It is also often used as an autophagy inhibitor and is functional in many organisms, including mammals and yeast [149]. Monensin, a ionophore antibiotic, dissipates organellar transmembrane pH-gradients [150] by electroneutrally replacing protons with monovalent cations [151], and is frequently used to inhibit virus processing and replication [152, 153]. EGA, by contrast, does not perturb the organellar pH nor transferrin recycling, the retrograde endosomal to Golgi transport and phagolysosomal trafficking. However, it strongly affects the processing of low pH-dependent toxins and viruses, most likely through inhibition of trafficking between early endosomal and the more acidic late endosomes, as also demonstrated by the substantially delayed lysosomal targeting and degradation of the EGFR [154]. Despite that, its concrete target remains unknown.

1.5. Viral endosomal escape mechanisms

Once taken up by the cell, viruses need to transfer their genetic material to an appropriate intracellular destination for replication. This requires either escape of the naked genome or of subviral particles from the membranous confinement, most frequently from endosomal vesicles. Interestingly, while members of the parvovirus, the adenovirus, and the picornavirus families all exploit the endosomal escape route, they differ in the mechanistic details. Parvovirus family members possess in their VP1 a domain with homology to the cellular enzyme phospholipase A_2 (PLA2) at the so-called N-terminusVP1-unique region (VP1u). After internalisation, it is proposed that VP1u becomes exposed [155] and enzymatically damages the liposome membrane, leading to a possible endosome rupture [156]. Differently, adenoviruses undergo rearrangements of their structure after binding to integrins [157] or the Coxsackie

and adenovirus receptor (CAR) [158]. The event triggered by the virus binding allows the lytic protein-VI to interact with the endosomal membrane, again resulting in endosome membrane rupture [159].

Naked viruses developed different strategies to breach the endosomal barrier for transfer of their genetic material or (partially disassembled) nucleocapsid into the cytosol [160]. For picornaviruses, which exhibit a maturation cleavage of their VP0, two models are currently proposed, primarily based on results with rhinoviruses. One posits the formation of a discrete, about 5-10 nm wide channel within the liposomal membrane. This is built from several copies of myr-VP4 following its release from the capsid upon a receptor- and/or low pH-triggered conversion into the subviral A particle. The RNA genome is thought to exit through an opening in the A particle in continuity with this VP4-based channel, allowing unhindered passage into the cytosol [161-163]. By contrast, for rhinovirus B14, a (partial) disruption of the endosomal membrane has been suggested following its conversion into the A particle. This larger-scale damage of the lipid bilayer is presumably mediated by the membrane-inserted VP4 in combination with the exposed amphipathic N-termini of VP1, and possibly the stress excerted on the lipid bilayer on engagement of multiple receptors by the internalized virus. Uncoating of the RNA genome then occurs either concurrently or after transfer of the subviral particle into the cytosol [164]. A similar scenario has been described for adenoviruses, where viral protein-induced lysis of the endosomal vesicle enables the release of the nucleoprotein core containing the dsDNA genome [165].

Poliovirus, a member of the picornavirus family, after receptor binding triggers endocytosis and then damages the endosome's inner face. Recruiting of the cellular phospholipase PLA2G16 facilitates endosomal escape of the viral genome, though the precise mechanism if still unclear [166]. Additionally, poliovirus, in common with most other picornaviruses, feature a myristic acid attached to VP4, which is putatively involved in the endosomal escape of reovirus, which don’t have a VP4 but the same myristic motif [165, 167]. Even though AiV-A1 has no VP4, its VP0 carries VP4 and VP2 information and contains the myristyolation motif [168]. It was already proposed, that the capsid proteins could be re-incorporated in the structure of the capsid, after the genome exposure [12]. Kelly *et al.* additionally shows, that the N-terminus of VP0 fills in an analogous role as the N-terminus of VP4 found in other picornaviruses. One of the tasks is forming a pore in the endosome and it is hypothesised, that also the same sequence, conserved across the picornavirus family as well as in the VP0 of AiV, could be carried out as well [19].

1.6. Translation, processing and replication of aichiviral RNA

Once the 8.2 kb AiV-A1 RNA genome has arrived in the cytosol, translation of its single open reading frame (ORF) is initiated by ribosome subunits interacting with the internal ribosomal binding site

(IRES), located in the 5' UTR. This results in a large polyprotein that is processed by viral proteases into structural and non-structural proteins with overall similarity to other picornaviruses [168]. The AiV-A1 proteases are 3C and 3CD; 3CD seems to work together with the 2A protein, forming a complex at the VP1-2A cleavage site [6]. AiV-A1 also has a conserved motif in 2A, which it shares with eleven other picornaviruses. This domain is related to an enterovirus host factor, the phospholipase PLA2G16, mentioned before [166, 169].

In common with other picornaviruses, multiplication of the aichiviral genome takes place in replication complexes, composed of partially double-stranded viral RNA, viral and host cell proteins essential for viral replication. They are usually attached to cytosolic vesicles arising by virus-induced rearrangement of intracellular host cell membranes. These numerous, de-novo produced membraneous structures are termed replication organelles. Assembly of new virus particles furthermore takes place in close proximity of these organelles, resulting in the intimate coupling of (+) ssRNA production and packaging [170]. Notably, many picornaviruses depend on phosphatidylinositol-4-phosphate (PI4P) located to the replication sites. Kobuvirus 3A proteins recruit Acyl-coenzyme A binding domain containing 3 (ACBD3) and phosphatidylinositol-4 kinase B (PI4KB) to form a complex that can produce PI4P. This negatively charged lipid assists in electrostatic attraction of RNA-dependent RNA polymerase [171], which is encoded by the viral protein 3D, is responsible for the plus and minus-strand replication [172]. However, it must be mentioned that work by Cemaron and colleagues [173] rather identified the picornaviral 3CD protease as masterregulator of this process. The generation of the replication organelles is also critically dependent on a flow from/exchange of lipids with other organelles such as cholesterol (reviewed in [174]).

2. Material and methods

2.1. Cell culture and viruses

The cell lines HCEC 1CT, T84, Vero and Caco-2 were acquired from ATCC. A549 cells were a kind gift by Dr. Walter Berger (Institute of Cancer Research, Medical University of Vienna, Austria; originally from Sigma, 86012804), and Dr. Gijs Versteeg generously provided the RKO cells (Max Perutz Labs, Vienna, Austria; originally from ATCC, CRL-2577). All cells were cultivated at 37 °C in an atmosphere with 5% CO_2 and grown in a growth medium as recommended by the providers. For the infection assays, an infection medium was used (Table 1). All experiments were performed with Aichi virus-A1 kvgh99012632/2010 Taiwan (referred to as AiV-A1 throughout most of the text). In experiments with the EpiAirway system, the AiV-A1 strain 846/88 isolated from a patient of a gasteroenterits outbreak in Japan was also used. In one experiment (2.12), the coxsackievirus B3 strain

Nancy (CVB3) was employed, which was crudely purified as described in Corbic-Ramljak *et al.*. in 2018 [175]. The amount of virus used in the experiments is stated as multiplicity of infection (MOI), which is the ratio of virus infectious particles to the number of cells present on the assay [176]. Baculovirus tagged with GFP, which was used to detect Rab5a and Rab7 was purchased from Thermo Fisher.

Virus infectivity was evaluated by the median tissue culture infectious dose ($TCID_{50}$) method (explained in detail below) and converted to plaque-forming units (PFU) using the formulas from Reed and Muench (1938) [177] and Seeberg *et al.*. (1981) [178] based on the Poisson distribution.

2.2. Tissue preparation and culture

The human lung epithelium (EpiAirway AIR-100) model tissues were provided for free from MatTek (Ashland, USA). According to the information provided by the vendor, each batch of these model tissues were grown from preserved stem cells isolated from the tracheal/bronchial tissue obtained from a single donor. They were cultured under the conditions recommended by the manufacturer.The tissues were delivered in separate transwell inserts kept in Matrigel as the basal membrane, and where then Table 1 to MatTek medium (Table 1) upon arrival and kept at 37 °C in an atmosphere with 5% CO_2 for 24 h prior to the assays. After washing the inserts with PBS, the the basolateral medium was replaced with fresh medium.

For the infection procedure, each insert received 10^7 PFU of AiV-A1 (or CVB3 Nancy) prepared in the growth medium, replacing the growth medium at the basolateral side and adding medium containing the same amount of virus to the apical side, following an incubation of one hour at 37 °C. Subsequently, inserts were washed with PBS and fresh growth medium was added to the basal and the apical compartment. The apical medium was collected, stored at -80 °C and the cells replenished with a fresh medium every day. Aliquots from the daily collected infection medium were evaluated for the presence of infectious virus by $TCID_{50}$ measurements [177].

For fluorescence microscopy analysis, the inserts were cut out of their scaffolds, transferred to small tubes, combined with 1% paraformaldehyde solution in PBS and incubated at 25 °C for 30 minutes. After removal of the fixative, the inserts were washed three times with cold PBS and stored at 4 °C until further processing on the next day.

Table 1 Cell culture medium composition

Celltype	Growth medium	Infection medium
Vero	DMEM (Gibco, 21063029) 10 % FBS (Sigma, F7524) 1% Pen-Strep (Sigma, 15140122)	DMEM (Gibco, 21063029) 2% FBS (Sigma, F7524) 1% Pen-Strep (Sigma, 15140122)
HCEC 1CT	DMEM and Medium 199 Earle's, 4+1 (Biochrom, F0435 and FG0615) 4 mM GlutaMAXTM-1 (100X), (Gibco, 35050038) 2% Cosmic Calf Serum (Hyclone, SH30087) 20 ng/ml EGF (Sigma-Aldrich, E9644) 10 µg/ml Insulin (Sigma-Aldrich, I9278) 2 µg/ml Apo-Transferrin (Sigma-Aldrich, T2036) 5 nM Sodium-Selenite (Sigma-Aldrich, S5261) 1 µg/ml Hydrocortisone (Sigma-Aldrich, H0396)	
A549	Ham's F-12K Medium (Gibco, 21127022) 10% FBS (Sigma, F7524) 1% Pen-Strep (Sigma, 15140122)	Ham's F-12K Medium (Gibco, 21127022) 2% FBS (Sigma, F7524) 1% Pen-Strep (Sigma, 15140122)
T84	DMEM / F12 1:1 (Gibco, 11320033) 10% FBS (Sigma, F7524) 1% Pen-Strep (Sigma, 15140122)	DMEM / F12 1:1 2% FBS (Sigma, F7524) 1% Pen-Strep (Sigma, 15140122)
Caco-2	RPMI (Gibco, 21875034) 20% FBS (Sigma, F7524) 0.1 mM NEAA (Lonza, 13-114E) 1% Pen-Strep (Sigma, 15140122) 1 mM Pyruvate (Sigma, S8636)	RPMI (Gibco, 21875034) 2% FBS (Sigma, F7524) 0.1 mM NEAA (Lonza, 13-114E) 1% Pen-Strep (Sigma, 15140122) 1 mM Pyruvate (Sigma, S8636)
RKO	RPMI (Gibco, 21875034) 10% FBS (Sigma, F7524) 0.1 mM NEAA (Lonza, 13-114E) 1% Pen-Strep (Sigma, 15140122) 1 mM Pyruvate (Sigma, S8636)	RPMI (Gibco, 21875034) 2% FBS (Sigma, F7524) 0.1 mM NEAA (Lonza, 13-114E) 1% Pen-Strep (Sigma, 15140122) 1 mM Pyruvate (Sigma, S8636)
EpiAirway Medium	DMEM (company disclosed) Epidermal growth factors and other proprietary factors (concentration disclosed) Gentamicin 5 µg/ml Amphotericin B 0.25 µg/ml Other additives were disclosed	

2.3. Determining the cytotoxicity of compounds in A549 cells

This method was previously described by Chung *et al.*. (2013) [179] with modifications by Denani *et al.* (2020) [180]. In brief, five thousand cells (A549) resuspended in the corresponding growth medium were added to each well of a 384 well-plate, and the plate was transferred to an incubator and kept overnight at 37 °C in a 5% CO_2 atmosphere. On the next day, the medium was changed to the serum-reduced infection medium containing a specific test compound and 5 % DMSO or only infection medium plus 5 % DMSO as a negative control, and the plate was placed back in the incubator for an additional 24 h at 37 °C, 5% CO_2. 2 h before the next step, two wells received Triton-X100 at a final concentration of 1%, serving as a positive control for cytotoxicity. After 24 h, an equal volume of CellTiter-Glo Reagent (Promega Corporation, USA; 100 µl/well) was added to all wells, and the luminescence was measured with a VICTOR Nivo plate reader (PerkinElmer, USA) after 5 to 10 minutes.

2.4. Tissue Culture Infectious Dose 50 ($TCID_{50}$) Assay

The amount of infectious virus was determined by end-point titration. To this end, the virus-containing sample was used as starting material for preparation of 10-fold serial dilutions in infection medium. One hundred µl of each dilution was added to one well of a 96-well plate with Vero cells, about 80 % confluent and the plate was incubated for four to 5 days post-infection (p.i.) at 37 °C and 5% CO_2. The CPE was visualized by crystal violet staining (0.2% crystal violet, 150 mM NaCl, 1% Formaldehyde) [180]. The virus titre was calculated as $TCID_{50}$ according to Reed and Muench (1938) [177].

2.5. Seed virus production

Vero cells were grown to 80% confluency in 75 mm^2 and 150 mm^2 flasks and infected with AiV-A1 (MOI=0.1). After 72 h p.i., cells were harvested and collected in a Falcon tube. The cells were frozen and thawed three times by putting in liquid nitrogen for 2 to 3 minutes, depending on the volume of the sample, followed by placing in a water bath (25 °C) until the medium was thawed completely. The repeated cycles of freezing and thawing assist in releasing new virions from cellular membranes. The sample was centrifuged for 10 min at 4000 rpm to remove the cellular debris, the supernatant was collected, and the pellet was discarded. The suspension was vortexed and centrifuged in an ultracentrifuge (Beckmann-Coulter, USA) at 40000 x g at 4 °C for 2 h under a vacuum to concentrate

the virus. The supernatant was discarded and the pellet resuspended in 100 µl virus buffer (50 mM Tris/HCl pH 7.5, 25 mM NaCl). The virus titre was determined by $TCID_{50}$.

2.6. RNA Extraction

RNA was extracted from cells and viruses using TRIzol reagent (Invitrogen, USA) according to the manufacturer's protocol. In brief, 200 µl chloroform was added to the amount of cells remaining after scratching and collecting them in 1 ml TRIzol. The sample was then centrifuged for 15 min at 12000 x g at 4 °C. The upper aqueous phase was transferred to a new tube. 0.5 ml isopropanol was added, and the tube was inverted several times and the mixture incubated for 10 min at room temperature. The sample was then centrifuged for 10 min at 12000 x g at 4 °C, and the supernatant was discarded. The pellet was resuspended in 1 ml 75 % EtOH per 1 ml TRIzol, vortexed briefly and centrifuged for 5 min at 12000 x g at 4 °C. The supernatant was discarded, and the pellet was dried for 10 to 15 min until all of the EtOH was evaporated. Finally, the pellet was resuspended in 50 µl MilliQ water and incubated for another 10 to 15 min at 55 to 60 °C. The samples were then used for further experiments or stored at -80 °C.

2.7. Reverse Transcription – Quantitative Polymerase Chain Reaction (RT-qPCR)

Viral RNA and selected cellular mRNA species were quantified by RT-qPCR. A two-step RT-qPCR was performed after extracting the total (viral and/or cellular) RNA (see chapter 1.7). The required amount of input RNA for cDNA synthesis was determined by UV-Vis spectrophotometry using a NanoDrop (Thermo Fisher, USA) device. The cDNA was produced using the M-MLV reverse transcriptase of Promega (USA) according to the manufacturer's protocol. In brief, one µg of RNA was incubated with 0.5 µg of random hexamer primers and transcribed by adding buffer, nucleic acids and the reverse transcriptase (5 u/µl). An aliquot of the obtained, unpurified first-strand cDNA was used as template in a subsequent qPCR with the GoTaq DNA polymerase (Promega, USA). The pipetting scheme is shown in Table 2 Components and parameter of the RT-qPCR protocol The $2^{-(\Delta\Delta Ct)}$ method was used to calculate the gene expression. To this end the Ct value of the viral RNA was measured and normalized by the Ct value of the human Cyclophilin A (CypA; PP1A) housekeeping gene (Table contains all primers).

Table 2 Components and parameter of the RT-qPCR protocol.

Concentration	Component	qPCR step	Temperature (°C)	Time (min)
1x	5x GoTaq Colourless Reaction Buffer	Initial Denaturation	95	3 min
200 µM, each	dNTPs Mix, 10 mM each	Denaturation	95	15 sec
0.625 u	GoTaq DNA Polymerase (5 u/µl)	Annealing and Extension	60	1 min
5 µM	Syto 82 (5 mM)	Hold	4	-
0.5 µM, each	Primers (100 µM)			
1 µg	cDNA			
X	ddH2O			
25 µl	Total			

Table 3 Primers used for RT-qPCR.

Primers	Forward 5'-3'	Reverse 5'-3'
AiV-A1 Fw-SQP2	Fw: GCT CAC CCA ACT CCT CAA CT	SQP2: AGA GGA TAA GGG CTC CGG CA
AiV-A1 Rw-SQP1	SQP1: TGT ACA ACA CCC ACT CCA TGT G	Rw: TCC ACA GAG AGG GAG TTC CTG
PPIA	AGA CAA GGT CCC AAA GAC AGC AGA	TGT GAA GTC ACC ACC CTG ACA CAT

2.8. Immunofluorescence microscopy of infected cells

The cells were seeded on sterile coverslips placed in the wells of a 24-well plate and cultured to 80% confluency. Subsequently, cells were infected with AiV-A1 (or CVB3) using a MOI=5. The working volume used for coverslip treatment was 500 µl. The cells were fixed in 4% Paraformaldehyde in PBS (pH 7.4) for 5 minutes at RT and (virus-infected) tissue cultures (see above) were similarly fixed for 20 minutes. Thereafter, coverslips were washed three times with ice-cold PBS. The cells were permeabilised by adding 0.25% Triton X-100 in PBS (pH 7.4) to the coverslips for 5 min at RT and washed three times with ice-cold PBS. The cells were then incubated in blocking buffer (5% Bovine serum albumin (BSA)); 0.05% Tween 20 in PBS) for 30 min at RT to reduce unspecific binding. After removing the blocking solution, the first antibody or antibodies were added at a dilution listed in Table 5 List of used antibodies. Antibodies were diluted in blocking buffer and incubated with gentle agitation

for 1 h at RT in the dark. The antibody-containing solutions were discarded, and the cells were washed at least six times for 5 min with PBS to remove all unbound primary antibody. Thereafter, cells were incubated with the secondary antibody or antibodies (in instances of double staining) according to dilution (Table 5). The cells were washed at least six times with PBS for 5 min in the dark to remove the secondary antibody. Hoechst solution at a final concentration of 1 µg/ml (Invitrogen H3570) diluted in PBS was used to counterstain the cell nuclei. Cells were incubated with the solution for 10 minutes and washed three times with PBS for 5 minutes each. Finally, the coverslips were placed upside down on a slide with one drop of mounting medium (Prolong Glass Antifade Mountant; Invitrogen, P36982, USA). The slides were dried overnight and stored at 4 °C in the dark. Images were acquired using a fluorescence microscope, the Zeiss Axio Observer Z1 (Zeiss, Germany).

Table 4 PBS buffer and its composition.

PBS	- **137 mM NaCl** - **2.7 mM KCl** - **10 mM Na2HPO4** - **1.8 mM KH2PO4** - **pH 7.4**

Table 5 List of used antibodies.

Antibody	**Company/Reference**	**Concentration/dilution used**
AiV VP1	Chen et al. 2013	1:1000 (2mg/ml)
dsRNA (J2)		1:500 (2mg/ml)
Goat anti-Rabbit IgG (H+L) Alexa Fluor Plus 555	Invitrogen A32732	1:2000 (2mg/ml)
Goat anti-Mouse IgG (H+L) Alexa Fluor 680	Invitrogen A-21057	1:2000 (2mg/ml)
Donkey anti-Rabbit IgG (H+L) IRDye 680RD	LI-COR P/N: 926-68073	1:10000 (1mg/ml)

2.9. Fluid-phase endocytosis of fluorescent dextrane

Cells were incubated with AIV-A1 (MOI = 50) together with fluorescent dextran (10000 MW) for 15 min at 37 °C. Dextran beads of that size are preferentially internalised by macropinocytosis. Already after 5 min imported dextran can be detected in macropinosomes or early endosomes [181]. Cells were then washed, fixed and examined by IF microscopy (see chapter 2.8). TRITC-dextran from Thermo Fisher was used (10000 MW). Dextran without virus was used as a control.

2.10. Virus infection with cold synchronization in different cell lines

Cells grown to 80% confluence in a 12-well (the timepoints were taken in triplicates) plate were pre-incubated for 30 min at 4 °C and 5% CO_2. A specific amount of AiV-A1, the MOI depending on the assay, was prepared for the specific cell type and pre-chilled in the infection medium. After the pre-incubation, the growth media was replaced by the pre-chilled medium containing the virus and the cells incubated for 1 h at 4 °C. After the medium with the virus was removed, the cells were washed three times with ice-cold PBS. 1.5 ml PBS was added to three wells, harvested and collected in a 2 ml Eppendorf tube. The three wells were refilled with a 1.5 ml infection medium and incubated at 37 °C. After 72 h, the cells in the wells were detached with a cell scraper, collected in Eppendorff tubes and kept at -80 °C until they were submitted to freeze and thaw procedure as described above (chapter 2.5). The virus titre was determined by $TCID_{50}$ measurements (see chapter 2.4).

Keeping the cells during virus challenge at 4 °C allows AiV-A1 binding to the cells while preventing its internalisation. The titre measured at T0 therefore corresponds exlusively to cell-attached virus. Further, the infection in the cells kept for 72 h was synchronised on heating to 37 °C.

2.11. Measuring the inhibitory effect of endocytosis inhibitors on virus replication

In this thesis, 23 compounds, which according to literature, affected the cellular uptake and trafficking of diverse viruses by inhibiting different cellular targets involved in endocytosis were used. They are listed with the final concentration used in Suppl. 1.

A549 cells were used to test these compounds. Cells were grown to 80% confluency in 6-well plates and treated with the compounds diluted in infection medium for 30 minutes at 4 °C prior to the AiV-A1 infection. The virus was added using a MOI=1 and incubated at four °C for 30 minutes. Thereafter, cells

were incubated for additional 8 h at 37 °C. The medium was discarded, the cells were washed with PBS, and TRIzol was added directly to the wells and the lysate used for RNA extraction. Thereafter, first-strand cDNA was produced and quantified by qPCR. The viral RNA yield of the treated samples was compared with the virus control without any compounds, using the ΔΔCt-method. Cells incubated without any drugs were used as a negative control.

Each condition was performed in triplicate, including the Mock infected condition (the control without AiV-A1) and non-treated (the control without compound).

Chlorpromazine, EIPA, MβCD and Jasplakinolide turned out to be too toxic for the A549 cells when present for a total of 9 h as used for all other compounds. To overcome this problem, cells were pre-incubated with each one of these drugs for just 15 minutes at 4 °C, followed by one-hour incubation in the presence of AiV-A1 at 37 °C. After removing the virus and compound containing medium, cells were washed with PBS, and fresh infection medium containing 50 mM NH_4Cl was added. This weak based efficiently blocks infection by AiV (see results) and was used here to prevent uncoating of AiV, which has not yet entered the cells during the 1 h incubation periode. The infection was allowed to continue for additional 8 h, then the cells were washed with PBS, lysed with TRIzol and processed as in above.

2.12. Comparing AiV-A1 and Coxsackievirus B3 based on the cytopathic effect

A549 cells were infected with AiV-A1 and in parallel, with CVB3 to reveal a possibly distinct infection pattern. MOIs of 1 and 0.1 were used for both viruses. Viruses were diluted in infection medium, then added to the cells grown in a 24-wells plate to 90 % confluency and incubated for 24 h at 37 °C, 5% CO_2. After that, cells were imaged in brightfield, using the fluorescence microscope Zeiss Axio Observer Z1 (Zeiss, Germany).

2.13. *In vivo* determination of virus-induced endosomal damage

Instead of a more common method using fluorophore-virus conjugates [182], we used Quinacrine (QC), as a reporter for detection of endosome perforation or disruption possibly accompanying AiV-A1 uncoating. QC is a fluorescent aminoacridine dye that can freely diffuse through biological membranes in its neutral pH form. It accumulates in acidic vesicles after acquiring a positive charge in the low pH environment, preventing its back-crossing through the membrane [183]. Due to its high quantum yield and resistance to photobleaching, it can be sensitively detected by fluorescent microscopy over long

periods of time [184]. QC was co-internalized with the aichivirus for labelling of acidic vesicles including those carrying viral cargo. A possible virus-mediated damage of the endosomal bilayer should result in leakage of the dye, detectable by a loss of fluorescence, with a kinetics dependent on the extent of membrane perturbation. A549 cells were grown to 70% confluency in a glass-bottom dish from MatTek (Ashland, USA). Cells received AiV-A1 (MOI=10) diluted in infection medium supplemented with one µM QC and 50 mM NH_4Cl or, as a non-endosomolytic control, RV-A2 (MOI=10), diluted in the same QC containing infection medium. Cells receiving only infection medium with QC served as negative control. The cells were then incubated at 37°C in the dark for 30 minutes in the and washed three times with PBS containing 50 mM NH_4Cl. After the last washing step, cells were kept in PBS containing 50 mM NH_4Cl and quickly transferred to a fluorescence microscope. After selecting the cells to be imaged (field with 6-10 non-overlapping cells), the PBS containing 50 mM NH_4Cl was replaced by PBS and the fluorescence signals from these selected cells were recorded for 10 minutes in 15 seconds intervals. Each condition was repeated two times, and in every instance, three cells were arbitrarily chosen and three vesicles per selected cell were then evaluation for dye leakage, all with a diameter of about 500 nm. This size is close to the average size of early endosomes in A549 cells (Shearer and Petersen (2019) Helyon 5: e02375)). The fluorescenc signal was quantified using the software ImageJ and the fluorescence intensity was plotted against the time. The signal was normalized by the minimal intensity to erase the bias caused by different sizes of vesicles.

3. Results

3.1. Models for studying AiV-A1 infection

Examination of human colonic and lung-derived cell lines for susceptibility to AiV-A1

Kobuviruses of the species AiV-A1 (previously named human aichiviruses) are routinely propagated in Vero cells. This is a immortalized cell line, which has been established from the kidney of an African green monkey and is commonly employed in virological studies due to its ability to support growth of a large variety of viruses [185]. Attempts by others at growing the prototypic Japanese AiV-A1 strain A846/88 (GenBank accession no. JQ281544; Yamashita *et al.* (1998)) in various human cell lines have failed [168]. By contrast, more recently Taiwanese researchers have reported the productive replication of the AiV-A1 strain kvgh99012632/2010 (gb JX564249) isolated from an infected female neonate (Chang *et al.* (2013)) (herewith named AiV-A1) in human DBTRG-05MG gliablastoma cells, HEK293T cells, A549 lung carcinoma cells, and T84 intestinal carcinoma cells, but not in HeLa cells [186]. The latter aichivirus strain was obtained by us from the Taiwanese group to independently assess T84 and A549 cells for permessivity to this virus. As AiV-A1 is believed to infect the human

gasterointestinal tract, three more human cell lines originating from this organ were included in our study: Two were derived from cancerous tissue (Caco-2 cells, RKO cells) and one was an immortalized colonic epithelial cell line created from a healthy adult patient colonic biopsy (HCEC-1CT cells). The cells were grown to around 70% confluency and infected with AiV-A1 at an MOI of 0.1. The virus titre at timepoint 0 (= T0, due to cell-attached but not yet internalized virions) and after 72 h p.i. (= T72, reporting on newly produced virus) was measured as $TCID_{50}$ (**Fehler! Verweisquelle konnte nicht gefunden werden.B**). The highest titre at T0 was obtained in Caco-2 cells with a mean around $1x10^4$ $TCID_{50}$/ml, dropping to approximately $1x10^3$ $TCID_{50}$/ml at T72. Unexpectedly, a decrease in virus titer 3 days post infection (p.i.) was also found for T84 cells, though less pronounced. In all other cell types the titre significantly increased 72 h p.i.. The total increase was the smallest for 1CT ($\sim 3x10^1$ $TCID_{50}$/ml), somewhat higher for RKO cells ($5x10^2$ $TCID_{50}$/ml) and nearly $4x10^4$ $TCID_{50}$/ml for the Vero cells. The highest titre ($2x10^8$ $TCID_{50}$/ml) was clearly obtained with A549 cells. Taken together, our data with A549 cells corroborated the findings (based on immunofluorescence analysis of newly produced AiV-A1 VP1 protein) by Chen *et al.*, while in our hands, the T84 cells reproducibly did not at all support AiV-A1 replication. The other human intestinal tract-derived cell lines similarly resulted in no to only low titres after 72 h p.i.. Of note, the titre of AiV-A1 produced in RKO cells (but not in the other intestinal cell lines) infected at an MOI of 0.1 significantly increased at longer times p.i. (beyond T72). The increase in virus production was confirmed by a RT-qPCR analysis of the newly produced viral RNA (Figure 5**C**).

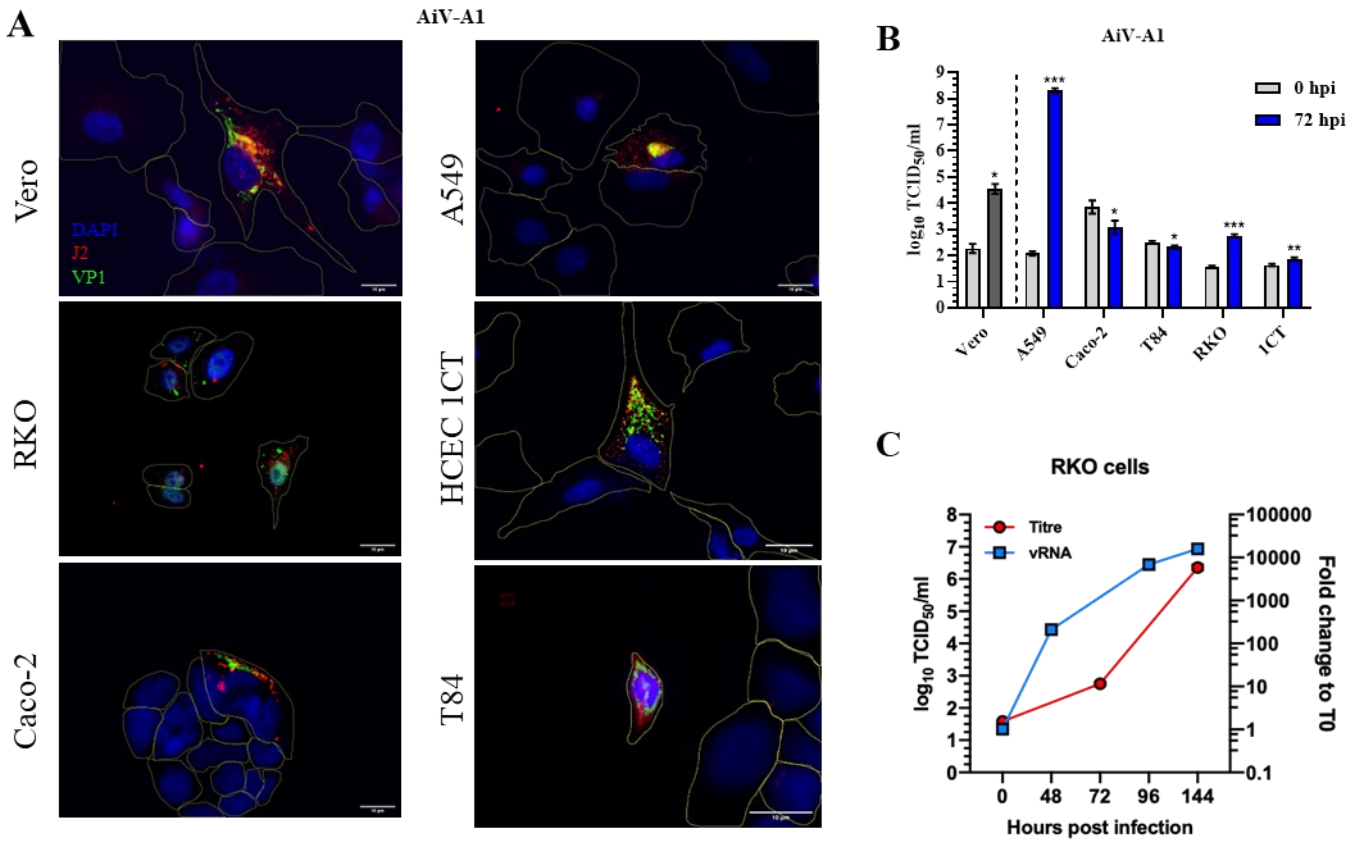

Figure 5 ***AiV-A1 shows a varying efficiency of infection in different cell types.*** *Cells of the specified type were grown to 50 % confluency on coverslips in a 24-well plate and infected with A1V-A1 (MOI=1) for 1 hour at 37 °C. After that, the cells were incubated for another 8 h in a fresh infection medium at 37 °C. They were then fixed in 4 % paraformaldehyde and washed with ice-cold PBS. Viral protein VP1 was detected with rabbit-anti-VP1 antibody and viral RNA with J2, a mouse-anti-dsRNA antibody in combination with a goat anti-rabbit Alexa Fluor Plus 555 (here shown in green) and goat anti-mouse Alexa Fluor 680 (shown in red), respectively. The nuclei were counterstained with Hoechst, represented in blue. Areas appearing yellow correspond to overlapping signals of VP1 and dsRNA. Pictures were taken under the fluorescence microscope with a 100x objective. Cell borders were manually drawn using brightfield images. Scale bar: 10 µm. B Cells grown in 12-well plates were preincubated at 4 °C for 30 min following infection with AiV-A1 (MOI=0.1) for 1 hour at 4 °C. The medium was removed amd cells washed with ice-cold PBS three times, followed by addition of fresh infection medium. Virus titer was determined immediately after the washing step (T0) and 72 h p.i. (T72). The number of independent replicates n = 3 for all conditions. Graphed is the mean ± standard deviation. The significance of the change in titre over time was determined by performing a Student's t-test. All differences were significant (*: p-value<0.05; **: p-value<0.005; ***: p-value<0.0005; p(Vero)=0.0136; p(A549)=0.0009; p(Caco-2)=0.0485; p(T84)=0.0175; p(RKO)=0.0002; p(1CT)=0.0089). C Titre and vRNA kinetics in RKO cells after AiV-A1 infection (MOI=0.1), determined by RT-qPCR.*

Virus replication was independently evaluated by the detection of newly synthesized viral RNA and protein via immunofluorescence microscopy. Confluent cells were challenged for one hour with AiV-A1 (MOI of 1) and stained 9 h p.i. with the monoclonal antibody J2, which binds to ds RNA [187] (arising as an essential intermediate during the infection cycle of (+) ssRNA viruses), and a polyclonal antiserum against AiV-A1 VP1[155, 186]. The cells were counterstained with the Hoechst dye to reveal the nuclei. The same images were also used to determine the ratio of infected cells after 8 h of infection (Suppl. 2).

*Figure 5***A** shows a positive J2 signal for double-stranded RNA (in red) as well as a clear signal for viral protein VP1 (in green) 9 h p.i. in every cell type tested, though only in a small percentage of cells (see Suppl. 2). The borders of all visible cells were outlined manually with the help of the respective brightfield image. In all cases, cells with signals in both channels could be found as expected for true replication. Colocalization of VP1 and dsRNA was, however, only infrequently observed. In most instances, the signal for J2 clustered in a punctate pattern around the nucleus (in blue), most likely representing replication organelles as shown for other picornaviruses, such as poliovirus [188]. The more speckled pattern of the VP1-specific signal (in green) was largely centrally to peripherally located, presumably resulting from intracellularly accumulating progeny virions.

Characterization of the cytopathic effect of AiV-A1-infected A549 cells in comparison to CVB3

The previous experiments demonstrated, that the human lung non-small cell cancer-derived A549 cells are fully permissive for AiV-A1, suggesting their suitability for more detailed investigations of its life cycle. An important end-point for assessing the infectivity of many viruses including picornaviruses such as rhinovirus [189] and coxsackievirus [190] is the cytopathic effect (CPE). This term describes the characteristic morphological changes of the virus-infected cell, which can vary with the virus species, the type of host cell, and the MOI. Since A549 cells are also permissive for coxsackievirus B3 (CVB3, a human pathogen belonging to the genus enteroviruses. species B within the *Picornaviridae* family), they were next infected in parallel with AiV-A1 and CVB3 and assessed for the developing cytopathic effect (CPE) at 24 h p.i.. Two phenomena could be noted: First, even though the same MOI was used, the CPE appeared in a considerably lower fraction of cells infected with AiV-A1. When infected with CVB3, even at an MOI of 0.1, already about one-third of all cells were dead after 24 h, whereas AiV-A1 infection resulted in just around five per cent of dead cells at the same MOI (based on titration of the respective virus stocks on Vero cells). At an MOI of 1, almost 100 percent of the cells were killed by CVB3 after 24 h versus roughly ten percent by AiV-A1. Whether this difference is due to a host cell heterogeneity [191] with greater importance for AiV-A1 and/or other factors remains to be investigated. The second observation concerned the distribution of the dead cells. A549 cells killed by

CVB3 eventually completely detached from the surface of the cell culture dish, resulting in their uniform distribution in the medium. In stark contrast, AiV-A1 infection resulted in discete clusters of rounded cells, which seem to hover above a layer of still normal appearing cells. These patches of dead cells (which we termed infection **ce**nters) expanded during progression of the infection. While this phenomenon was not further examined it suggested, that the cells killed by AiV may have an exceptional tendency to stick together and/or the virus for unclear reasons spreads preferentially locally (Figure **6**).

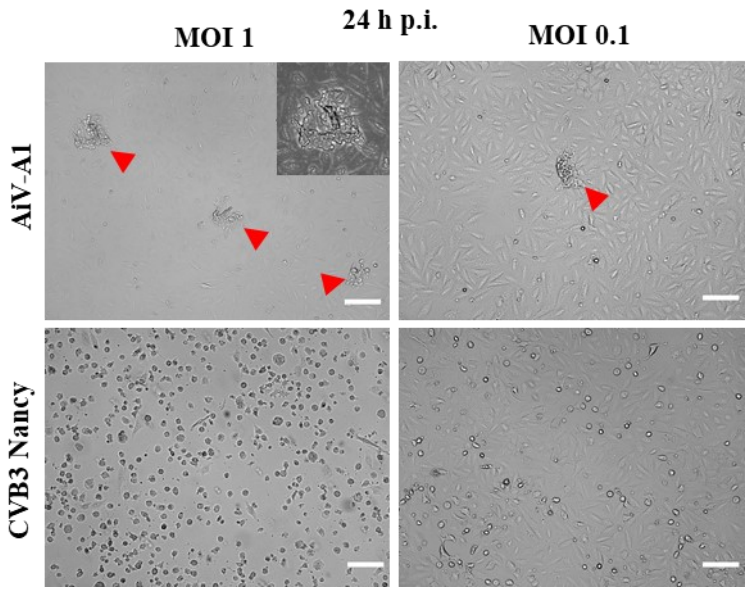

Figure 6 ***AiV-A1 infection pattern emerges from hotspots*** *A549 cells grown to confluency were infected with either AiV-A1 or CVB3 Nancy at a MOI of 0.1 and 1 for each virus. After 24 h incubation at 37 °C, pictures were taken with a light microscope using a 20x objective. Infection centers of AiV-A1 are marked with red arrows.*

The replicational potential of AiV-A1 in human EpiAirway 3D tissues

The productive replication of AiV-A1in A549 cells with similarity to pulmonary type II epithelial cells [192] raised the possibility, that at least certain strains of human aichiviruses may have a broader tropism in the human host, by also acting as respiratory tract pathogen. Tumor cells lines, however, particularly when kept in 2D culture, do not adequately represent their primary cells of origin normally residing in the context of a complex tissue or organ[193]. Therefore, to substantiate above hypothesis, the EpiAirway system available from MatTek (Ashland, USA) was tested for its infectibility by AiV-A1. This system consists of fully differentiated airway epithelial cells grown in 3D, closely mimicking the bronchiolar tract of the human lung, a prominent target of respiratory viruses. While handling this tissue-

like model is more demanding than working with cells kept in simple 2D culture, viral titre and viral RNA can be determined as well (see [194] and [195]). Both parameters were measured over 120 h following the infection of individual EpiAirway inserts with 10^7 PFU each of AiV-A1. Apical supernatants were harvested in 24 h intervals and immediately replaced with fresh medium. The viral titre measurement (Figure 7**A**) of these supernatants revealed a small increase in $TCID_{50}$/ml by one log from T0 to T48. The titre then dropped to values ranging from $1x10^4$ to $1x10^5$ $TCID_{50}$/ml for the last 3 timepoints up to 120 h. The fold change of the viral RNA (Figure 3**B**) over the same time window was determined in parallel by RT-qPCR of total RNA extracted from the infected tissue inserts. It showed a 1.25 fold increase from T0 to T24 and a drop after 48 h p.i. to about one fourth of input virus, and then stayed rather constant for the next three timepoints until T120 (the last time point examined).

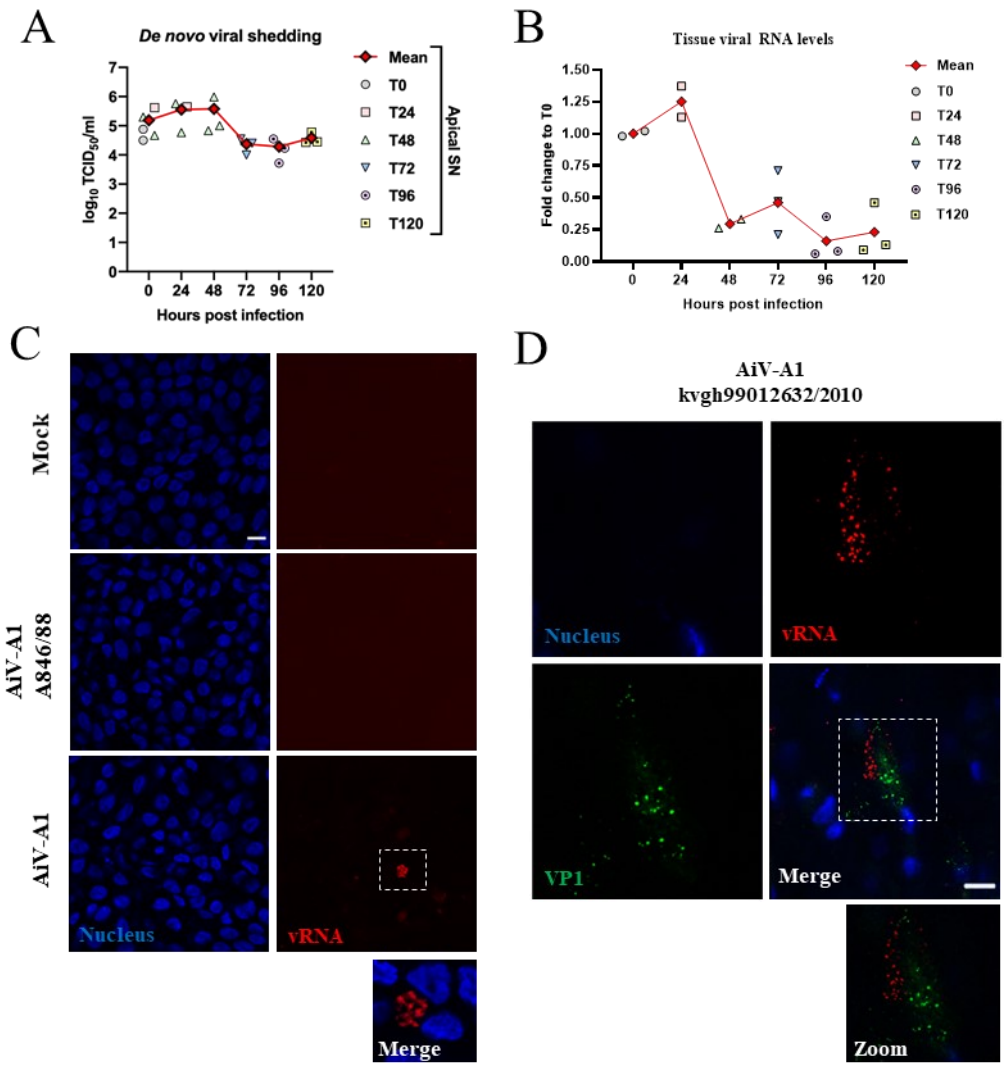

Figure 7 ***AiV-A1 replicates in human airway epithelium (EpiAirway). A-B*** *EpiAirway was exposed to AiV-A1 (PFU 10^7) simultaneously from the apical and basolateral side for 1 h at 37°C. (A) Depicted are the measured titres from the apical surface until indicated times p.i.. Each individual symbol represents the result of an*

independently produced EpiAirway tissue (B) Replication profile of vRNA in the airway epithelium over time by RT-qPCR. N=3. ***C*** *Confocal micrographs stained with mAb J2 for vRNA (red) in EpiAirway infected with AiV-A1 A846/88 or AiV-A1, 24 h p.i. respectively. Nuclei were counterstained with Hoechst. A zoomed in image of the white boxed area is shown at the bottom of the respective panel.* ***D*** *Confocal microscopy of EpiAirway infected with AiV-A1 immunostained for viral RNA (red) and capsid protein VP1 (green) at 24 h p.i..*

The titration and RT-qPCR results indicated only a rather modest growth of AiV-A1 in the highly differentiated EpiAirway tissue model which rapidly dropped to negligible values after the peak at 24 h p.i. (viral RNA) and progeny virus production (48 h p.i.). In order to further corroborate genuine virus replication in this lung-like tissue, newly produced VP1 and dsRNA were detected by immunostaining. This analysis was carried out with both, the Japanese AiV-A1 strain (AiV-A1 A846/88) and the Taiwanese AiV-A1 strain (AiV kvgh99012632/2010 = AiV-A1) for comparison, as the former was previously found by us not to replicate in A549 cells [196]. Figure 7**C** shows confocal images of EpiAirway tissue infected with AiV-A1, AiV-A1 A846/88 and a mock-infected negative control. As a positive control, the tissue was identically infected with human rhinovirus A2 (RV-A2), which is a pathogen preferentially infecting the upper, but also the lower respiratory tract [197]. Newly produced viral RNA was detected with the J2 monoclonal antibody as before (red fluorescence signal). For better discrimination of cells, nuclei were counterstained with Hoechst. As expected, practically no signal was observed in cells of the mock-infected tissues sample. EpiAirway inserts infected with AiV-A1 A846/88 were also clearly negative for dsRNA. Conversely, the same tissue infected with AIV-A1 gave rise to a specific signal with J2, though restricted to very few cells, similar to the results with J2 in the AiV-A1-infected human cell-lines (Figure 5).

It is known that dsRNA can also be produced in normal (uninfected) cells [198], though the amounts are apparently too low for their detection in cells of the mock-infected EpiIntestinal system. The J2 positive signal therefore most likely resulted from a genuine virus replication in a few permissive target cells within the lung-like tissue. Furthermore, EpiAirway challenged with the RV-A2 positive control showed a comparable outcome (Suppl. 3 EpiAirway infected with RV-A2Suppl. 3). To further strengthen this point, EpiAirway inserts infected with AiV-A1 were double-stained with J2 and the anti-VP1 polyclonal antibody. As shown in Figure 7**D**, replication of viral RNA (detected by J2) and production of viral protein VP1 occured within the same cell. This strongly indicated, that the Taiwanese AiV-A1 strain, in contrast to the Japanese strain, is capable to infect the human lung-tissue like model, though with low frequency. This likely explains the low virus titre and level of aichiviral (+)RNA quantified by bulk analysis of the infected EpiAirway system (Figures 7**A** and 7**B**).

3.2. AiV-A1 entry and intracellular pathways

Dependence of AiV-A1 on dynamin, actin and pH

As already mentioned in the introduction, many viruses initially need to bind to receptor(s) for uptake by the host cell via endocytosis, followed by transport to a suitable compartment for their (partial) uncoating. These are critical steps in the viral life cycle and hence promising anti-viral drug targets. Given the multifaceted nature of the cellular entry and endosomal transport pathways [49, 122], their role in the host cell invasion by pathogens must be explored on a case-by-case basis. This thesis part focused on unravelling the major endocytic pathway(s) responsible for productive infection of A549 cells by the Taiwanese AIV-A1. To this end, an assortment of compounds was used, which were previously shown to interfere with distinct cellular uptake mechanisms and/or specific intracellular transport routes (see Figure 4). If such a pathway is important for virus entry, infectivity will be delayed, curtailed or even abrogated as reflected by an appropriate readout for the amount of progeny virus produced in absence/presence of such mechanistic inhibitors.

All compounds used in the infectivity assay were initially tested for their potential cytotoxicity on A549 cells at the selected concentrations by measuring the ATP level after a 24 h incubation. If not already available from the literature for A549 cells, the concentrations chosen were in the range of those routinely employed in other cell lines. The method used is based on the luciferin/luciferase binary system, which leads to luminescens in dependency on the amount of ATP [180]. Since cell death results in a drastic drop in ATP levels, the measured luminescence is negatively correlated to the % cell death caused by a compound. Figure 8 shows the cytotoxicity after 24 h in percentage of the positive control (cells lysed by treatment with Triton X-100, resulting in 100% cell death). The negative control was cells treated with an infection medium only.

The cytotoxicity assay allowed the identification of appropriate (i.e. not to low cytotoxic, less than 50 % cell death) concentrations for most of the tested compounds (Suppl. Table 1). These concentrations were then selected for the infection of A549 cells with AiV-A1 (MOI = 1) in presence of each one of these substances. The impact on cell entry and uncoating pathway(s) was quantified by the reduction in the level of the viral RNA synthesis as a proxy, similarly as described in a study on hepatitis A virus uptake by Rivera-Serrano *et al.* [199]. Cells were lysed 9 h p.i., the amount of viral RNA was measured by RT-qPCR and normalized to the similarly determined RNA level of the house keeping gene (PPIA). The fold-change expression relative to a mock-infected control was calculated with the ΔΔCt method [200].

In contrast to the majoritiy of the tested chemicals, the cytotoxicity assay showed a drastic drop in the ATP level of 50% up to 100% after the 9 h treatment of A549 cells with Chlorpromazine, EIPA and MβCD and Jasplakinolide (Figure 8**A**). Those compounds were therefore tested differently from the

other substances as specified in more detail further below (due to limited ressources and time left for experiments, different lower concentrations could not be assayed).

The first group of compounds tested specifically targeted the cellular cholesterol, which plays a prominent role in raft/caveolae-mediated endocytosis as detailed in the introduction. Neither Nystatin (complexing lipid membrane resident cholesterol) nor Simvastatin (inhibiting HMG-CoA reductase, the rate limiting enzyme of the cholesterol biosynthesis pathway) nor U18666A (which blocks the cholesterol transporter NPC1 and the endogenous cholesterol production) showed any reduction in viral RNA. Surprisingly, despite sequestering plasma membrane cholesterol analogous to Nystatin, Filipin treatment caused a significant drop in AiV-A1 replication by about 50% (Figure 8**B**). As elaborated in more detail later on, a short-term treatment with the cholesterol-depleting agent MβCD led to a 35% reduction in viral RNA (Figure 8**G**). Taken together, based on these data, the role for AiV-A1 endocytosis mediated by lipid rafts/caveolae seems rather unikely but cannot not be fully ruled out.

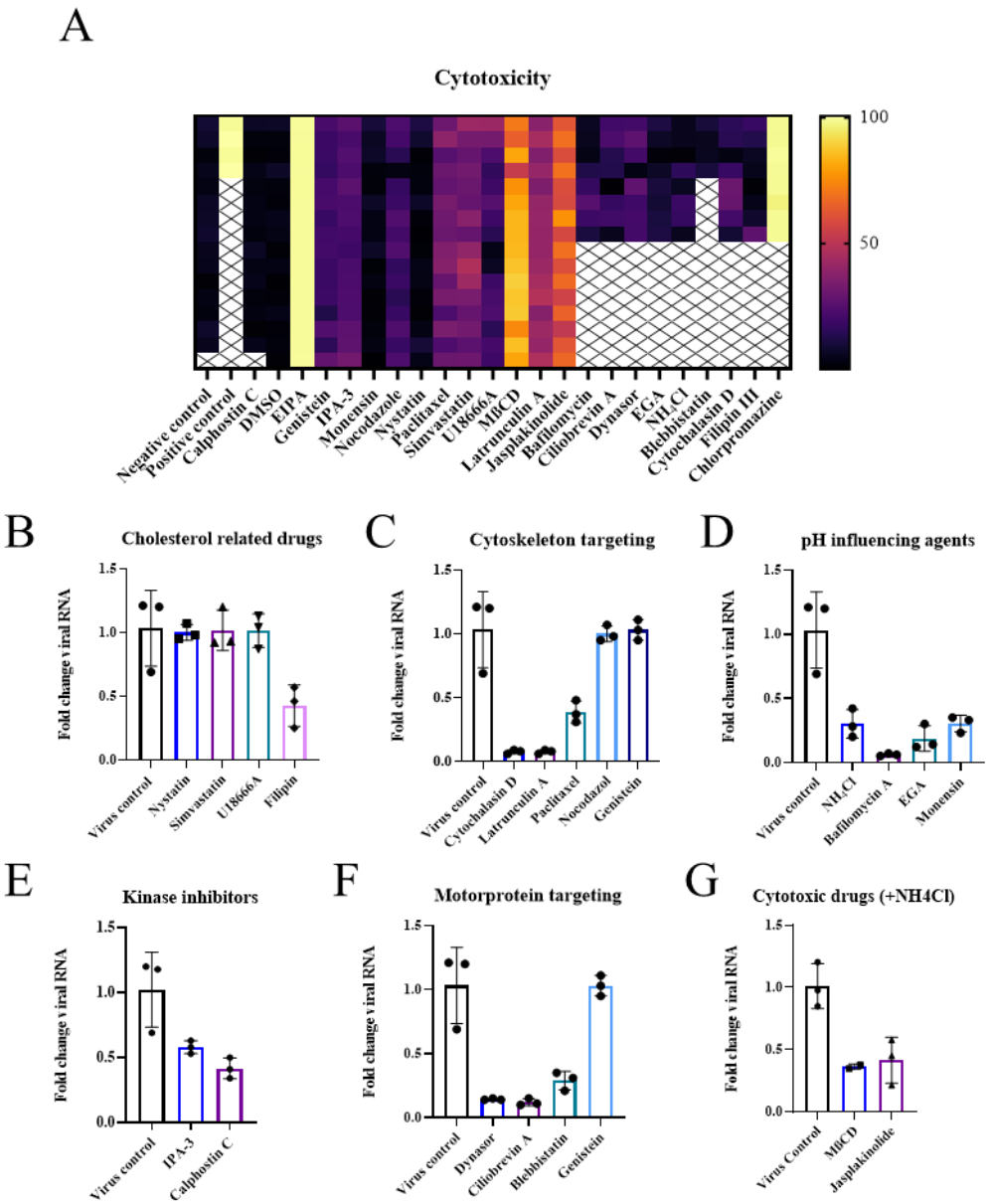

Figure 8 ***Impact on AiV-A1 infection of compounds targeting different steps in endocytosis, vesicle maturation and intracellular transport.*** ***A*** *Confluent A549 cells were incubated at 37 °C with the compounds shown (for used concentrations see Suppl. Tab.1) for 24 h. After that, the CellTitre Glo compound was added, and the ATP level measured via luminescence. The ATP-level is plotted in relation to the ATP level of cells lysed with Triton X-100.* ***B-F*** *Confluent A549 cells were preincubated with infection medium containing the appropriate chemical compound for 30 minutes and infected with AiV-A1 (MOI=1) for 9 h at 37 °C. The viral RNA was measured by RT-qPCR and the fold change was calculated using the* $2^{-\Delta\Delta Ct}$ *method, relating to the control only treated with virus. The compounds were divided by their mode of action into those sequestering membrane cholesterol, targeting the cytoskeleton, influencing the pH, or causing similar effects like EGA inhibiting kinases and in targeting motorproteins.* ***G*** *A549 were treated for 30 minutes with the cytotoxic compounds at 37 °C, following another 1 h together with virus and their subsequent removal by washing with PBS containing* NH_4Cl*. The cells*

*were then incubated for another 9 h in infection medium containing NH_4Cl. RNA was measured using the same method as in **B-F.** The used concentrations are displayed in Suppl. Table1.*

Infection of A549 cells in the presence of the compounds affecting cytoskeleton components (Figure 8**C**) showed a drastic impact of the actin polymerisation blocking agents Cytochalasin D and Latrunculin A, reducing the viral RNA level down to five percent. Paclitaxel treatment, which stabilizes microtubules, resulted in a reduction of viral replication to about 40%. Given this result, it was somewhat unexpected that Nocodazole, which depolymerizes microtubules, had practically no effect on the viral RNA level and consequently AiV-A1 cell entry. Genistein, which inhibits tyrosine kinases controlling several steps in the caveolar-mediated uptake, but has also been implicated in src-activated macropinocytosis [201], also did not decrease the viral RNA production.

As can be seen in Figure 8**D**, the acidic endocytic pH plays a key role in the productive infection of A549 cells by AIV-A1: Each of the tested lysosomotropic compounds, which neutralize the organellar pH by a different mechanism, substantially diminished the RNA synthesis of AiV-A1. NH_4Cl or Monensin treatment caused a reduction by about 70%. The V-ATPase inhibitor Bafilomycin A was most potent, reducing the RNA levels down to 1%. EGA, which inhibits the early to late endosomal maturation/transport without influencing the vesicular pH also had a major impact on the viral RNA production, decreasing it by about 85%.

The kinase inhibitors IPA-3 and Calphostin, which block the protein Ser/Thr kinases Pak1 and PKC, respectively, implicated in macropinocytosis (see also introduction), decreased the amount of viral RNA to 60 and 40 percent, respectively (Figure 8**E**).

The effect of Dynasor and Ciliobrevin A is shown in Figure 8**F**. The former inhibits Dynamin II responsible for pinching off vesicles in CME and several forms of CIE (see introduction) and the latter targets dynein, which transports vesicles along the microtubules towards the end. Both compounds led to a strong, about 80% and 90%, reduction of the viral RNA compared to the solvent control. The myosin II inhibitor Blebbistatin decreased the level by about 70%.

For the four compounds, which were highly toxic towards A549 cells during the 9 h exposure (see above), the incubation time was shortend to 90 minutes to attenuate their adverse effect. This comprised a 30 minutes preincubation of A549 cells with the drug and additional 60 minutes together with the AIV-A1 inoculum (MOI = 1), always at 37 °C. The medium containing drug and virus was removed, cells were washed with PBS and replenished with fresh infection medium containing 50 mM NH_4Cl. The latter (based on the results presented above) should prevent uncoating of AiV-A1, which has not yet entered the host cell during the 1h time window. Incubation was then continued for 8 h at 37 °C.

In the cases of EIPA (a inhibitor of micropinocytosis) and Chlorpromazine (interfering with CME), the Ct values obtained for the housekeeping gene were always considerably higher for the drug-treated

compared to untreated cells (data not shown), which disallowed their use for normalization of the measured viral RNA levels. The results with these compounds were therefore considered unreliable and are thus not presented here. This problem did not arise with the other two long-term cytotoxic drugs, which allowed the proper quantitation of their effect on the viral RNA synthesis. Both, treatment with the cholesterol-depleting agent MβCD and with the actin- polymerization-inducer and stabilizer Jasplakinolide showed a similar decrease in viral RNA production by around 35% and about 40%, respectively (Figure 8**G**).

In summary, of all the successfully tested substances, EGA, the ones inhibiting acidification and actin polymerization, as well as those blocking dynamin and dynein had the biggest impact on the level of viral replication. It suggests, that AIV-A1 uptake into A549 cells proceeds predominantly via a dynamin- and acto-myosin dependent endocytosis mechanism, while the role of the dynein motor protein in the absence of any effect of Cytochalasin D on viral internalization/uncoating remains unclear. In addition, results with inhibitors of PAK1 and PKC point to a non-ignorable role of macropinocytosis. Due to the viral RNA normalization problem when using Chlorpromazine and EIPA mentioned above as well as the somewhat inconclusive results with the cholesterol-targeting compounds, the specific entry pathway (clathrin or non-clathrin mediated and/or macropinocytosis) could not be mapped out in further detail at that stage. The pivotal importance of the acidic pH, combined with the role of dynactin and the profound inhibitory activity of EGA furthermore indicated a requirement for transfer of the virus to the late endosomal/lysosomal compartment for uncoating of its RNA genome.

Endosomal localization of internalized AiV-A1

We next carried out a double-labeling immunofluorescence microscopy analysis to concurrently visualize intracellular AiV-A1 and possible endocytic transport pathways(s) ursurped by the virus. One prominent route taken by many viruses leads from the early endosome (EE) to the late endosome (LE). These vesicles can be distinguished by their association with the small GTPase rab5 (EE) or rab7 (LE). After an overnight incubation with a recombinant baculovirus expressing the small GTPase Rab5a tagged with GFP (30 particles per cell; [202]), A549 cells were combined with AiV-A1 (MOI = 50) and incubated in the cold for 30 min, which allows cell-binding but not internalization of the viral particles. Unbound virus was washed away and synchronized infectious cell entry of attached virions initiated by warming cells to 37 °C. Thirty min p.i. (the time where all cargo usually reaches the early endosomes [125]), cells were fixed and probed for VP1 expression with the anti-VP1-antiserum as described before. Immunofluorescence images of sections showed an extensive colocalization of the VP1 signal (red colour) with Rab5a-GFP (green colour), which manifested in yellow coloured spots close to the cell´s periphery (Figure 9**A,** upper row). Note, that the corresponding endosomes were infrequent in number

and also appeared rather large, most likely due to fusion of smaller EE as a known consequence of wt Rab5a overexpression [203].

The finding strongly suggested that after cell entry, AiV is initially transferred to the Rab5a+ early endosomes. The role of CME in this process was assessed by using chlorpromazine (CPZ). To further reduce its adverse effect on cell viability, the drug was added to the cultivated A549 cells for 30 min before and just a 30 min period of challenge with AIV-A1 in the cold. Drug and unbound virus were washed away and cell entry of attached virions initiated by heating to 37 ° C. Thirty min p.i. cells were fixed and stained for VP1. No VP1 signal (red colour) could be reproducibly observed inside the cells in the presence of CPZ. Instead, isolated clusters of virus particles remained attached to the cell surface. This was accompanied by a massive intracellular clustering of Rab5a+ structures (Figure 9**A,** lower row), similarly as reported by Uytterhoeven *et al.*. [204]. This is not unexpected, as CPZ acts by sequestering clathrin, causing it to assemble around endosomal membranes thereby preventing its recycling to the plasma membrane. Altogether these results showed that CME most likely functions a the key entry pathway for AIV-A1 into A549 cells.

To determine, whether AiV-A1 needs to access the late endosomal compartment as strongly suggested by the lysosomotropic inhibitors and EGA, A549 cells were preincubated for 24 h with a recombinant baculovirus expressing a GFP-tagged Rab7. This was followed by infection with AIV-A1 for 45 minutes before immunofluorescence analysis of the fixed cells. The time was adopted from Rink *et al.*. (2005) showed complete conversion from Rab5 to Rab7 after around 45 minutes in A431 cells [125]. The image showed clear signals for Rab7 marking the late endosomes and for VP1, but practically without any colocalization (Figure 9**B**, upper panels). Addition of Nocodazole during the infection with AiV to block microtubule formation required for maturation of early into late endosomes had no effect on the colocation of the VP1 signal and Rab7 compared to untreated cells (Figure 9**B**, lower panels). Altogether, these immunofluorescence-based results unexpectedly seem to indicate, that AIV-A1 does not enter late endosomes nor lysosomes for uncoating, in apparent disagreement with the outcome of the abovementioned inhibitor study.

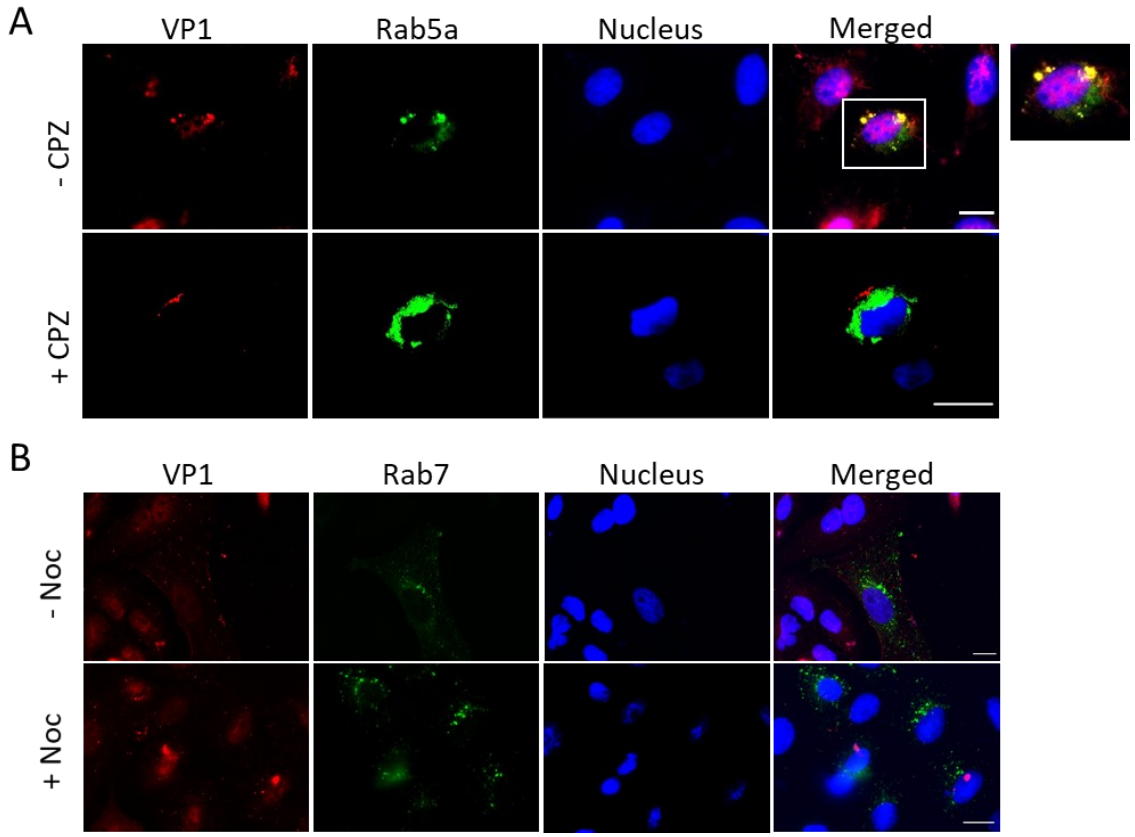

Figure 9 ***AiV-A1 leaves the early endosome.*** ***A*** *A549 cells were cultured to 50 % confluency and infected for 20 hours with a recombinant baculovirus expressing a GFP-tagged Rab5a (green colour). Prior to the infection with AIV-A1, the cells were preincubated with infection medium (control) or infection medium containing Chlorpromazine (CPZ) at 50 µM for 30 minutes at 4 °C. AiV-A1 at a MOI of 50 was added without media change and allowed to attach to the A549 cells for another 30 minutes at 4 °C. Drugs and unattached virus were removed and cells washed 3 times with cold PBS. New warm infection medium without chlorpromazine was added, the cells were kept at 37 °C for 30 minutes, washed as before and fixed in 4 % Paraformaldehyde. VP1 was detected with a primary mouse anti-VP1 antibody and an AlexaFluor-555-labled secondary antibody (Red colour). Nuclei were stained with DAPI (Blue colour).* ***B*** *Cells were treated as in* ***A****, except labelling Rab7 instead of Rab5a, + and - Nocodazole and incubating 45 minutes after washing. Staining was performed as in* ***A****. Scalebar = 10 µm.*

AiV-A1 exploits CME but not macropinocytosis for cell entry

The previous results pointed toward CME as the dominant entry mechanism for AIV-A1. To further strengthen our reasoning, we co-internalized virus particles with transferrin (Tf). Colocalization of other cell ligands or receptors with Tf is often used to proof their CME and their possible transport to recycling endosomes at later times [35]. The confocal IF image of the 5 min endocytosis sample exhibited an extensive overlap of the signal from the green channel (Transferrin) and the red channel (VP1). This was manifested by numerous yellow dots next to the inner side of the plasma membrane, indicating a colocalization of the AiV and Tf in the early endosome (Figure 10**B**, upper panels). After an incubation of 30 minutes, the colocalization was almost lost and the virus particles and Tf were distributed differently throughout the cells (Figure 10**B**, lower panels). The data further furnish CME of AiV-A1 as the most prominent if not exclusive entry route. The absence of virus/Tf colocalization at 30 min of cointernalization indicated, that AiV is furthermore most likely not transferred to the recycling endosomes.

The Tf colocalization experiments clearly demonstrated that alternative cell entry pathways are if at all, only infrequently utilized by AIV-A1 at the conditions used in these experiments. One of these minor pathways might be micropinocytosis, which, according to the mechanistic inhibitor studies, should play a significant role. In order to sort this out, we investigated its putative function in aichivirus uptake more directly by cointernalization of AIV-A1 with TRITC-labled 10 kD dextran as a commonly used fluid phase marker. Internalized virions were detected with the mouse anti-VP1 antiserum and a secondary IRDye 680RD-labled goat anti-mouse antibody. Importantly, in contrast to many other cell lines, A549 cells constitutively upregulate macropinocytosis as a consequence of an oncogenic K-ras mutation (Quian *et al.* (2014) Cancer Lett 351: 242–51) though this contradicts older work by Garcia-Perez and coworker, who found only negligible macropinocytic uptake of fluorescent dextrane [97]. Our results were more in line with the report by Quin *et al.*, as the A549 cells clearly showed a moderate uptake of TRITC-dextrane (Figure 10**A**, right panel). However, virtually no colocalization of the signals from VP1 (red colour) and the fluorescent dextran (green colour) could be detected (Figure 10**A**, left panel).

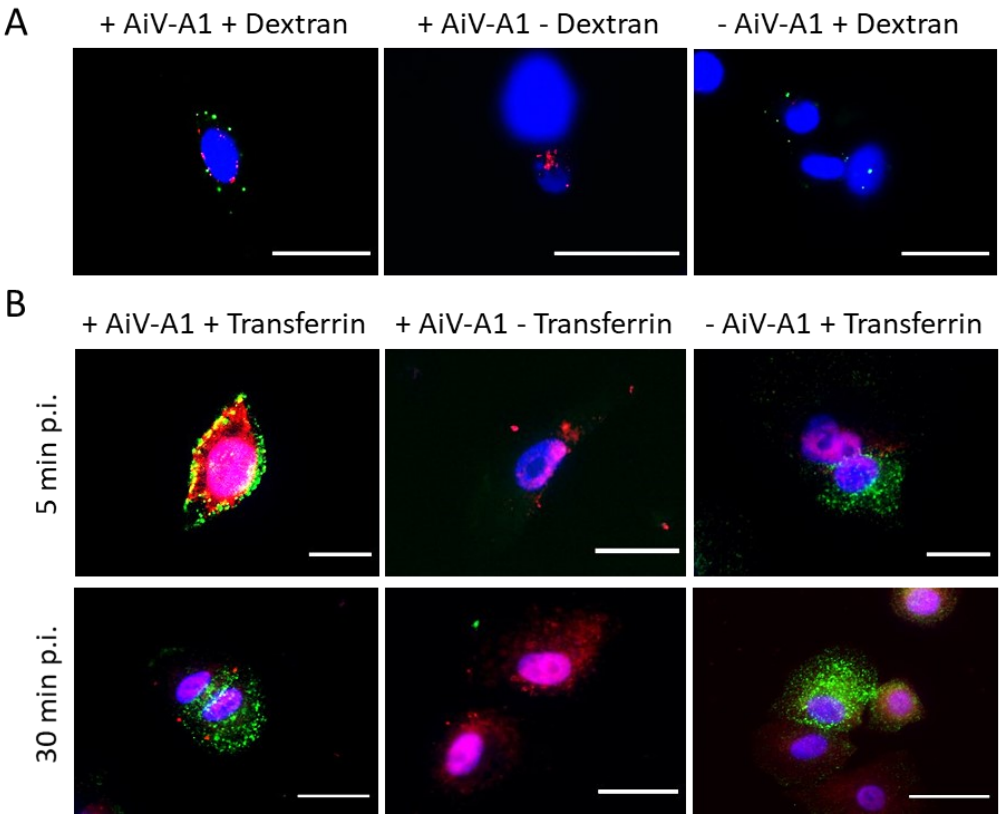

Figure 10 ***AiV-A1 shows colocalisation with Transferrin after 5 minutes. A*** *A549 cells were infected with AIV-A1 (MOI = 50) with or without Dextran TRITC (10 µM) for 15 minutes at 37 °C. Cells incubated with Dextran TRITC alone served as a control (green signal). The cells were fixed and VP1 was labelled with IRDye 680RD against mouse (red signal).* ***B*** *After preincubation at 4 °C, confluent A549 cells were infected with AIV-A1 (MOI of 50) in precooled infection medium with or without Transferrin From Human Serum, Alexa Fluor™ 568 Conjugate (final concentration of 25 µg/ml) for 30 minutes at 4 °C. Cells incubated with transferrin alone were used as a control. After that, the cells were washed two times with cold PBS before warm infection medium was added and incubated for another 30 or 5 minutes. Finally the cells were fixed in 4 % PFA and stained. VP1 was labelled with IRDye 680RD*

These data evidently ruled out micropinocytosis as additional (minor) uptake mechanism for AIV-A1 at least in A549 cells in the absence of the blockage of other entry pathways.

AiV-A1 induces rupture of early endosomes membrane

A critical step in picornavirus life cycle is the facile transfer of the uncoating RNA genome across the endosomal membrane into the cytosol. As detailed in the introduction, where examined, this is achieved through a channel assembled from several copies of the myristoylated viral protein VP4 inserted in the lipid bilayer or by (partial) disruption of the endocytic vesicle. The latter results in the release of subviral particles into the cytosol during or after uncoating. These mechanisms of endosomal breaching were discovered using picornaviruses, which undergoe a maturation cleavage of their VP0 capsid protein. However, aichiviruses maintain VP0 in their infectious particle, therefore, RNA uncoating and endosomal transfer likely differ from the majority of picornaviruses. Very recently, the Tuthill group reported an *in vitro* analysis demonstrating the ability of AiV-A1 to introduce small pores into liposomes particularly at low pH. They suggest a conformational change into an A-like particle, presumably resulting in the insertion of exposed VP0 N-termini (equivalent to VP4) into the liposomal bilayer. We investigated a possible *in vivo* endosomal damage during the early stage of AiV-A1 infection by co-internalization of the small, noncytotoxic fluorescent dye QC [205]. NH_4Cl was included in the medium to prevent acidification of the endocytic vesicles as prerequisite for AiV-A1 uncoating shown before. 30 min p.i. the medium was replaced with PBS lacking NH_4Cl, which allows quick recovery of the low endocytic pH and hence synchronized uncoating of AiV-A1. The fluorescence signal of QC was immediately recorded from three arbitrarily chosen ~ 500 nm wide vesicles (which according to the rab5-GFP expressing A549 cells should be mostly early endosomes) per cell every 15 seconds. As positive control, A549 cells were separately infected in parallel with RV-A2. The myr-VP4 released during the low pH-triggered conformational alteration of this rhinovirus species was previously shown to perforate the endosomal membrane, resulting in openings large enough for diffusive leakage of 10 kD dextrans. considerably smaller QC molecules into the cytosol [206]. Mock infected cells served as a negative control.

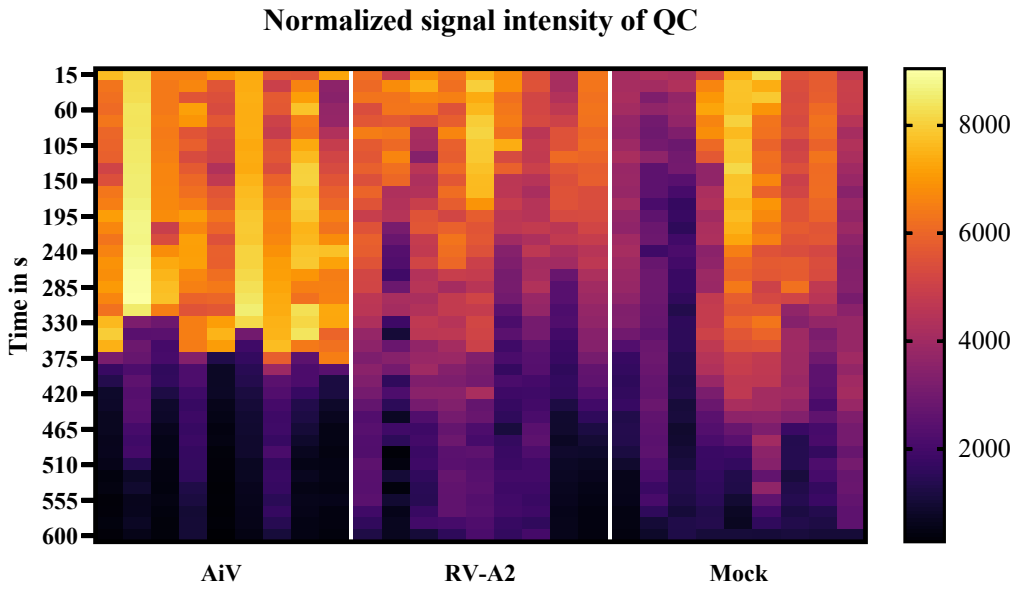

Figure 11 ***AiV-A1 ruptures early endosomes.*** *A549 cells were infected with AiV-A1, RV-A2 (both MOI=10) or mock infected in the presence of NH_4Cl (50 mM) and Quinacrine (1 µM) in infection medium for 30 minutes in the dark. After three times washing with PBS containing NH_4Cl, PBS without the base was added and the fluorescent signal was immediately recorded in fourty intervals of 15 sec each, with a 15 sec pause between each measurement to avoid excessive photobleaching. The fluorescence intensity of three vesicles each in three arbitrarily selected cells was quantified with ImageJ and the normalized (see 2.13) and individually plotted as heat map versus the observation time.*

Figure 11 shows a heat map of the background corrected fluorescence intensity of the endocytosed QC, from individual measurements of nine vesicles for each sample (3 vesicles/cell of 3 arbitrarily chosen cells), done in 40 intervals of 15 seconds up to 10 min after removing NH_4Cl. The gradual decrease of the fluorescent signal in the vast majority of mock infected cells likely results from the rare spontaneous endosomal damage in combination with progressive photobleaching of the QC dye over time of exposure. Unexpectedly, the RV-A2 infected positive control showed a similar change of the fluorescence intensity for QC as the negative control. In stark contrast, AiV-A1 infected cells uniformly exhibited a sudden steep drop of the initially bright fluorescent intensity after about 6 min, clearly distinguishable from the time course of the RV-A2 and mock infected control sample. This indicated that AiV likely triggers endosomal damage different as described for RV-A2, which in this experimental approach was not appearent in comparison to the negative control. There occur differences in the initial timesteps, according to the signal intensity.Those differences are attributed to the usage of unedited data, which has not undergone any corrections, to prevent losing information. Therefore the raw data is shown, including small differences, which were not resolved by normalising.

4. Discussion

After some years that AiV-A1 has been studied, it has only been described yet, how the virus behaves on a clinical level and in cell culture. It neither could have been shown, which cell types AiV-A1 infects in humans, nor how the infection dynamics look like in human tissue. This thesis aimed at solving those questions in one part and managed to answer the majority in the first half. Additionally, the possible tissue tropism was further illuminated.

4.1. AiV-A1 in human cells and tissue

Aichiviruses are known for being present throughout the population on all continents. They were first discovered in Asia and then in more countries located in southern and northern America, as well as Europe. The detection of aichiviruses is most of the time linked to patients suffering from gastroenteritis, leading so far to the conclusion, that they have to infect intestinal cells in human [20]. Surprisingly Chen *et al.*. found out in 2013, that AiV-A1 is also able to infect A549 but they did not dig more into this phenomenon [28]. This was not the first example of this type of tropism, it was already described for some Influenza virus strains [207]. That is the reason for these experiments, taking a closer look at the differences between an AiV-A1 infection in various human intestinal cells, human lung cells and human lung tissue.

By comparing the appearing cytopathic effect of AiV-A1 with CVB3 Nancy, we could recognise a pattern of accumulated cytopathic cells in the case of AiV-A1, while the effect was equally distributed in cells infected with CVB3 Nancy. Unpublished observations resulted in the same appearance of this phenomenon on Vero cells, infected with the japanese AiV-A1 strain 846/88. This leads to the conclusion, that it seems to be virus specific, not dependent on the cells.

It was shown that AiV-A1 overall had a surprisingly low infection rate in all tested intestinal cell lines. Suppl. 2 shows that only around 1.5 to 2 percent of all RKO, HCEC 1CT and T84 cells were infected. Caco-2 cells had the highest rate with about 6 percent after 9 h p.i.. The majority of Vero and A549 cells were infected with a rate between 2.5 and 5 percent. But in the end, all cell types showed at least a small production of viral RNA, which was detected with the J2 antibody (Figure 5**A**). The titre measurements also confirmed the small number of binding and infection events showing only a small titre after binding and washing. But after 72 hours, the differences between the cell types are getting bigger. A549 cells show an increase in the collected titre by the factor 1 million, whereas the intestinal cell lines show either no increase or just a small one like RKO cells do (Figure 5**B**). RKO cells additionally seem to be

the intestinal cell line which produces AiV-A1 in the most effective manner, producing a constant increasing amount of RNA and infectious particles (Figure 5**C**).

One reason for the huge differences in the infection behaviour and low overall infection rates could be the need of a certain probably unknown receptor which is needed for the virus to bind the cells, or could be only poorly expressed in the cell population. In addition, the used MOIs were not as high as in other studies and could therefore influence the infection rate as well.

Since the outbreak of the Coronavirus disease 2019 (COVID-19), focus was again set on cell tropism of viruses. Patients infected with SARS-CoV-2 show a high rate of gastro-intestinal symptoms, additional to respiratory symptoms [208]. Short after that in 2021, Han *et al.* proved the permissiveness of hPSC-derived colonic organoids for SARS-CoV-2, giving another important example of tissue tropism in humans [209]. Taking the previously discussed results into consideration, one could assume that AiV-A1 might be able to infect human lung tissue as well.

The experiments regarding the infection of human airway tissue were able to proof the permissiveness of the human airway epithelium for AiV-A1, additionally to the lung cell line. Even though the infected inserts showed a drop in viral RNA and new shed virus particles after two days, both parameters slightly started increasing again after four days. There are two untypical phenomena in this result, which suggest not just showing a loss in infectivity. First, the drop in titre is very small, compared to other viruses. Then it drops just a little more than one log to the base of ten. The RNA also drops down to about one fourth relative to T0. In the most cases of cells not susceptible to a virus, the titre and the RNA usually drop down several levels on a log scale to the base of ten [210].

In future experiments it would be important to keep the measurements going for a longer time period to see, whether the small increase in both cases keeps growing after five days or not. In the context of this master thesis, it was not possible to gather those results due to the limited time period the inserts can be used.

Nevertheless, labelling AiV-A1 infected cells with immunofluorescent markers and using confocal microscopy as a read out method brought more findings to proof a positive infection of the tissue. Using a confocal microscope to evaluate the infected inserts was the preferred method over light microscopy. It has a higher range of its depth of field and can provide a better focus in one of many cell layers, while the signal under the light microscope produces a lot of background noise and gets therefore less reliable. The images displayed only very few cells, whose inner showed the distinct signal of the J2 antibody, which indicates dsRNA referring to virus. It only exists in cells, if a successful infection has happened and the RNA could be replicated. The pattern is similar to other viruses like different human rhinoviruses and CVB3 or CVB4 [24, 187]. Distinct and ellipse-shaped signals, perinuclearly distributed in the cell indicate the presence of replicated viral dsRNA. Another strain of AiV-A1, AiV-A1 A846/88, which

shows no infection of A549 cells, was also used and showed no signals of dsRNA at all and looked like the uninfected negative control (Figure 5**C**).

Additionally, another insert was labelled with a combination of primary antibodies, also including an antibody for VP1, targeting the viral capsid. The results showed revealed cells in the tissue, positive for both markers, VP1 and dsRNA. Those images proved the presence of viral capsids and viral RNA in some cells of the human lung tissue. An uninfected control for the VP1 antibody could not be prepared because no insert was left for the experiment, but the signal could only be detected in cells, which were also positive for J2. To gather more evidence, more control inserts with other different viruses and uninfected controls would be necessary to prepare in the future.

In the end, the handling and working with tissue is still expensive and time consuming and therefore remains more suitable for qualitative analyses. That's the reason why the experiments regarding to the entry and intracellular routing mechanisms of AiV-A1 were still performed in the human lung cell line A549.

4.2. Cell entry, trafficking and influencing counterparts

Again said, there is a vast field of possibilities, viruses as well as bacteria can enter a cell and migrate to induce replication in the end. The second half of this thesis narrowed down the entry and intracellular pathways of AiV-A1 in A549 cells and shows the virus uncoating. To make sure, that none of the compounds would harm the cells and create a bias, the method using the CellTiter-Glo reagent was adapted and exerted. All compounds which held the cell viability above 50 percent after 24 hours were kept in the selection for the assays. For the others the duration of the treatment was reduced drastically. One still has to be reminded, that all compounds could cause pleiotropic effects, which were not discovered or described for that cell type.

Actin emerged as the most important targeted protein. All reagents manipulating or inhibiting actin lead to a decrease in viral RNA of at least 50 percent. This can be explained by the mere importance of actin to lots of cellular processes [211]. Already the FEME, the CLIC/GEEC and macropinocytotic entry are dependent on actin, requiring it to close and stabilise the vesicle. The compounds cytochalasin D, latrunculin A and jasplakinolide all reduced the viral RNA production remarkable (Figure 8**C,G**).

The compounds dynasor and ciliobrevin A both caused a huge drop in produced viral RNA, decreasing it to 14 and 12 percent of the control. Dynasor proved the dependency of AiV-A1 internalisation on dynamin, making the macropinocytic entry pathway much less likely and setting the focus on CME and FEME. The results for ciliobrevin A display the importance of the motor protein dynein, which is apparently necessary for the intracellular transport of AiV-A1. The about 70 percent drop blebbistatin is causing would contrarily point towards macropinocytosis because it is often used as its specific

inhibitor. But as mentioned in the introduction, blebbistatin is also indirectly affecting the actin skeleton by accumulating and stabilising the intermediate power-stroke actomyosin state, which could be enough to perturb the balance of the actin network [212], whose importance for AiV-A1 was stated in the previous paragraph.

At least in HeLa cells, neutralization of the vesicular pH by bafilomycin A additionally prevented early to late endosome transport and a similar effect was found for NH_4Cl [213]. The latter reportedly had no such effect in A549 cells [214].

Interestingly, nocodazole had no effect on the RNA yield. This finding provides strong evidence, that AiV-A1 is not utilising the longer pathways, heading to the lysosome or the ERC. The microtubules are responsible for the endosome translocation and in the end the fusion with a lysosome. Consequently, AiV-A1 must already leave the endosome before a certain drop in pH and the involvement of the microtubule network. Paclitaxel treatment reduced the measured RNA below 50 percent, contraindicating microtubule independency on the first sight. But unlike nocodazole, paclitaxel hyperstabilises microtubules, which further disrupts membrane trafficking [134].

Another regulator of cellular processes, especially including the membrane is cholesterol. None of the tested compounds, showed a decrease of viral RNA production after the indicated time, except filipin III and MβCD. One reason, why this single compound could have caused an effect, where the others didn't, can be its additional influence on the membrane by flatten it and changing the conformation [215]. Another reason can be its inhibition of EGFR, taking into consideration that EGFR is being exploited by various viruses for entry and replication, what could be the same case for AiV-A1 [216]. MβCD also had an initial inhibiting effect on the viral infection. Even though the cells and the virus were incubated with the compound just for 60 minutes, the RNA yield was decreased to roughly 37 percent. It was previously shown, that MβCD is efficiently and selectively extracting cholesterol from the membrane even blocking clathrin coated vesicle formation [217]. This result points towards CME as the major endocytic pathway as well.

The small inhibitory effect of IPA-3 (Figure 8**E**), which is suspected to influence actin polymerisation could affirm, that in some cases AiV-A1 also is capable of using the CLIC/GEEC entry. Calphostin C instead contributes another hint on CME usage by causing decrease of RNA of about 60 percent. This can be explained by the indirectly CME promoting function of PKC, which mediates the ubiquitinylation of EGFR, which is required for CME. PKC is inhibited by calphostin C [218].

A second indispensable factor is the pH-value. The pH-value is a known important factor for viruses, especially the uncoating. Examples for viruses, whose uncoating depends on the pH are RV-A2, influenza A (H3N2) and enterovirus 71 [219-221]. Besides the previous mentioned viruses, which are in need of a low pH to get uncoated, many more viruses are sensitive to pH-changes. Some enveloped

viruses need a drop in pH to fuse the envelope with membrane of the cell or the endosome, for example hepatitis C virus [222]. All three compounds influencing the pH-value and EGA lead to a drop in viral RNA with a minimum of 70 percent, with the front runner bafilomycin A with remaining RNA yield of six percent of the untreated control. Kelly *et al.* (2022) showed a dependency on a low pH for uncoating, but they tested only NH_4Cl [19].

These results speak for a dependency on the pH-value. The subsequent microscopic experiments showed contrary results, detecting no virus particles in late endosomes or the ERC, which was partly contrary to the results of Kelly *et al.* (2022) who showed that the uncoating of AiV-A1 is indeed pH dependent [19]. The immunofluorescence signals showed no colocalization of virus and the late endosome marker Rab7 (Figure 9**B**). However, the signals of AiV-A1 and Rab5 were colocalised. Under CPZ treatment, virus particles can only be detected what looks like the outside of the cell, distinct from Rab5a, which looks distributed as in the untreated sample (Figure 9**B**). Already Shearer *et al.* (2019) [129] showed, the Rab5 is distinguishable in A549 cells, which is not the case in the presence of CPZ. This condensing was also observed by Saitoh *et al.* in 2017, who had similar IF signals of Rab5 in the presence of CPZ. It could be, that the co-import of transferrin and AiV-A1 showed no colocalisation after 30 minutes, where transferrin is usually located in the ERC and again an overlay of the signals after 5 minutes, presumably in the early endosome (Figure 10**B**). Dextran likewise is not colocalised with AiV-A1 after the entry, which rules out macropinocytosis as the entry mechanism for AiV-A1.

Summing up the last findings, AiV-A1 is neither located in the late endosome nor the endocytic recycling compartment, even though its uncoating is highly dependent on an acidic pH. the virus has either to be uncoated in the EE or the endocytic carrier vesicle, which is kind of a pre-state of the late endosome or it has to leave the EE in some way, but is not proven to be found in A549 cells yet [124, 165].

4.3. Viral escape

By taking a look on all the results so far, AiV-A1 is not present in late endosomes or the ERC, due to the microscope analysis and its independence on nocodazole, but is still dependent on the pH, validated by the results of treatments with four different compounds. This leads to the assumption that AiV-A1 is exiting the endosomal pathway either from the early endosome or the endocytic carrier vesicle.

The VP0 of AiV-A1 resembles the uncleaved combination of VP1 and VP4. Those two play essential roles in the endosomal escape of poliovirus. Both viruses induce the membrane transmission or disruption by exposing VP1. It is known, that this VP0 still has its myristic acid, which is used in the VP4 of poliovirus and rhinoviruses [7]. AiV-A1 could also form a pore, induced by the VP4 equivalent part of VP0, to release the RNA in the cytosol. PLA2G16, recruited by poliovirus, enhances the RNA release, when the pore was formed. This protein is a homolog AiV-A1s protein 2A, which has no proved function yet and could be needed for some kind of similar interaction [223].

This first possibility would be the most probable one, especially based on the relation to other picornaviruses. But it is unclear whether QC could still leak from the endosome, because the endosomes wouldn't be disrupted, only perforated at the locations, the pores would form and the virus bind. The second possibility suits more the results of the co-import in the cell. In this case, the whole capsid escapes through the disrupted membrane. The way adenoviruses manage to do so is less plausible for AiV-A1, because the genetic requirements for this kind of rupture, including coding for the essential protein VI and for fibres are not fulfilled in AiV-A1 [224]. Parvoviruses also disrupt the endosomal membrane. After internalisation, the capsid undergoes a conformational change, when the pH reaches a lower value. This leads to an exposition of VP1, whose PLA2 domain in its activated state triggers membrane remodelling. This new emerged permeability enables the virus particles to escape the endosome, leaving it disrupted. A mechanism of this kind could also enable the leakage of quinacrine, generating a loss in fluorescence. The discrepancy would be the low pH, which triggers the change in the capsid of parvoviruses. This chain of events is only described in late endosomes yet. AiV-A1 could not be detected in late endosomes, which indicates an escape before the low pH is reached. It would be possible, that the mechanism is similar to the one of parvovirus, but is already being triggered in the early endosome, or the endocytic carrier vesicle, at least for A549 cells.

Clearly, the combination of both, mechanistic inhibitors, loss of function and gain of function genetic experiments will substantially strengthen conclusions initially drawn on a type of entry pathway exploited by a cargo, based on the use of dedicated drugs. However, there was not enough time available during this thesis work to integrate these approaches in the analysis of the AiV-1 entry pathway and needs to be implemented in future follow-up investigations.

This thesis collected a lot of evidence, illuminating the entry process and the intracellular routing as well as its preferences regarding human cells and tissue types. It is to say, AiV-A1 seems also to be a human pathogen for lung cells, showing positive infection in RKO cells, as well a human intestinal cell line and

human airway tissue. Both results were proven by titre and RNA measurements, in addition to fluorescence microscopic indication. Further several compounds were proven to inhibit the production of viral RNA, narrowing the entry possibilities down to CME and the CLIC/GEEC pathway. We could also proof the dependency on the pH of AiV-A1 infection. Finally, using fluorescence microscopy, we could also show that the virus leaves the endosomal system from early endosomes or the endocytic carrier vesicle.

5. Appendix

Suppl. 1 List of compounds, including the final concentration and a reference.

Substance	Final concentration	Reference
Bafilomycin	200 nM	Ganjian *et al.*. 2017
Blebbistatin	50 µM	Delorme-Axford *et al.*. 2013
Calphostin C	100 nM	Huber *et al.*. 1997
Chlorpromazine	100 µM	Ganjian *et al.*. 2017
Ciliobrevin A	20 µM	Conzemius *et al.*. 2016
Cytochalasin D	20 µM	Ganjian *et al.*. 2017
DMSO (Dimethyl sulfoxide)	0.1 %	Conzemius *et al.*. 2016
Dynasore	80 µM	Ganjian *et al.*. 2017
EGA	20 µM	Conzemius *et al.*. 2016
EIPA	100 µM	Delorme-Axford *et al.*. 2013
Filipin	5 µg/ml	Ganjian *et al.*. 2017
Genistein	74 µM	Delorme-Axford *et al.*. 2013
IPA-3	15 µM	Han, SC *et al.*. 2016
Jasplakinolide	2 µM	Heikkilä *et al.*. 2010
Latrunculin A	1 µM	Heikkilä *et al.*. 2010
MβCD	5 mM	Delorme-Axford *et al.*. 2013
Monensin	200 nM	D C Johnson and P G Spear
NH4CL	50 mM	Conzemius *et al.*. 2016
Nocodazole	20 µM	Conzemius *et al.*. 2016
Nystatin	25 µg/ml	Delorme-Axford *et al.*. 2013
Paclitaxel	20 µg/ml	Ryang *et al.*. 2019
Simvastatin	20 µM	Delorme-Axford *et al.*. 2013
U18666A	2 µg/ml	Elgner *et al.*. 2016

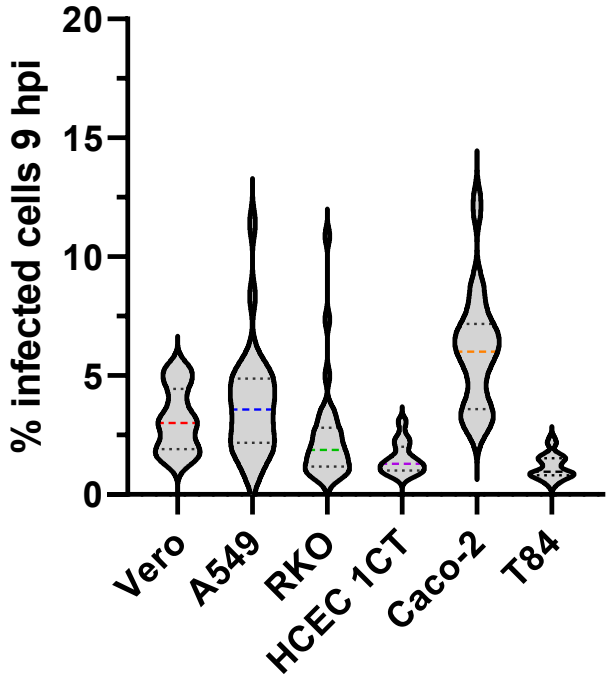

*Suppl. 2 Infection rate of AiV-A1 in different cells. The different cells were treated as described in chapter 2.8 and Figure 5**A**. The signal of the J2 antibody was used to determine the percentage of infected cells after 9 h incubation. Evaluated were the J2 positive cells in ten different fields of view relative to the whole number of cells in the field of view. The figure includes 10 fields of view per 3 replicates per cell type.*

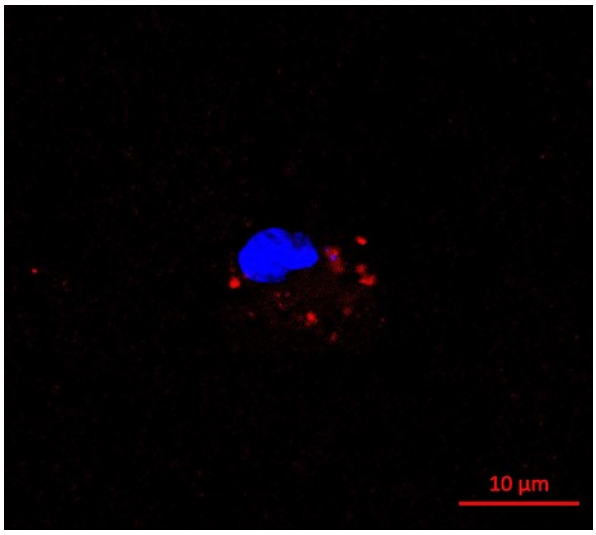

Suppl. 3 EpiAirway infected with RV-A2.

6. Bibliography

[1] A.M.Q. King, (2000) Picornaviridae, Virus taxonomy : seventh report of the International Committee on Taxonomy of Viruses (1999) 657-673.

[2] G. Lu, X. Zhang, J. Luo, Y. Sun, H. Xu, J. Huang, J. Ou, S. Li, First report and genetic characterization of feline kobuvirus in diarrhoeic cats in China, Transbound Emerg Dis 65(5) (2018) 1357-1363.

[3] R. Zell, E. Delwart, A.E. Gorbalenya, T. Hovi, A.M.Q. King, N.J. Knowles, A.M. Lindberg, M.A. Pallansch, A.C. Palmenberg, G. Reuter, P. Simmonds, T. Skern, G. Stanway, T. Yamashita, C. Ictv Report, ICTV Virus Taxonomy Profile: Picornaviridae, The Journal of general virology 98(10) (2017) 2421-2422.

[4] J.-T. Chang, Y.-S. Chen, B.-C. Chen, D. Chao, T.-H. Chang, Complete genome sequence of the first aichi virus isolated in taiwan, Genome announcements 1(1) (2013) e00107-12.

[5] A. Sadiq, C.k. Yinda, W. Deboutte, J. Matthijnssens, N. Bostan, Whole genome analysis of Aichivirus A, isolated from a child, suffering from gastroenteritis, in Pakistan, Virus Research 299 (2021) 198437.

[6] J. Sasaki, K. Ishikawa, K. Taniguchi, 3CD, but not 3C, cleaves the VP1/2A site efficiently during Aichi virus polyprotein processing through interaction with 2A, Virus Res 163(2) (2012) 592-8.

[7] L. Zhu, X. Wang, J. Ren, A. Kotecha, T.S. Walter, S. Yuan, T. Yamashita, T.J. Tuthill, E.E. Fry, Z. Rao, D.I. Stuart, Structure of human Aichi virus and implications for receptor binding, Nat Microbiol 1(11) (2016) 16150.

[8] H.H. Rabouw, L.J. Visser, T.C. Passchier, M.A. Langereis, F. Liu, P. Giansanti, A.L.W. van Vliet, J.G. Dekker, S.G. van der Grein, J.G. Saucedo, A.A. Anand, M.E. Trellet, A.M.J.J. Bonvin, P. Walter, A.J.R. Heck, R.J. de Groot, F.J.M. van Kuppeveld, Inhibition of the integrated stress response by viral proteins that block p-eIF2–eIF2B association, Nature Microbiology (2020).

[9] J. Sasaki, K. Taniguchi, Aichi virus 2A protein is involved in viral RNA replication, Journal of virology 82(19) (2008) 9765-9.

[10] E. Jan, I. Mohr, D. Walsh, A Cap-to-Tail Guide to mRNA Translation Strategies in Virus-Infected Cells, Annu Rev Virol 3(1) (2016) 283-307.

[11] J. Sasaki, K. Taniguchi, The 5'-end sequence of the genome of Aichi virus, a picornavirus, contains an element critical for viral RNA encapsidation, Journal of virology 77(6) (2003) 3542-3548.

[12] C. Sabin, T. Fuzik, K. Skubnik, L. Palkova, A.M. Lindberg, P. Plevka, Structure of Aichi virus 1 and its empty particle: clues towards kobuvirus genome release mechanism, Journal of virology (2016).

[13] M.P. Davis, G. Bottley, L.P. Beales, R.A. Killington, D.J. Rowlands, T.J. Tuthill, Recombinant VP4 of human rhinovirus induces permeability in model membranes, Journal of virology 82(8) (2008) 4169-74.

[14] T.J. Tuthill, D. Bubeck, D.J. Rowlands, J.M. Hogle, Characterization of early steps in the poliovirus infection process: receptor-decorated liposomes induce conversion of the virus to membrane-anchored entry-intermediate particles, Journal of virology 80(1) (2006) 172-80.

[15] T.J. Tuthill, K. Harlos, T.S. Walter, N.J. Knowles, E. Groppelli, D.J. Rowlands, D.I. Stuart, E.E. Fry, Equine rhinitis A virus and its low pH empty particle: clues towards an aphthovirus entry mechanism?, PLoS Pathog 5(10) (2009) e1000620.

[16] N. Malik, A. Kotecha, S. Gold, A. Asfor, J. Ren, J.T. Huiskonen, T.J. Tuthill, E.E. Fry, D.I. Stuart, Structures of foot and mouth disease virus pentamers: Insight into capsid dissociation and unexpected pentamer reassociation, PLoS Pathog 13(9) (2017) e1006607.

[17] E. Groppelli, T.J. Tuthill, D.J. Rowlands, Cell Entry of the Aphthovirus Equine Rhinitis A Virus Is Dependent on Endosome Acidification, Journal of virology 84(12) (2010) 6235-6240.

[18] G. Nurani, B. Lindqvist, J.M. Casasnovas, Receptor priming of major group human rhinoviruses for uncoating and entry at mild low-pH environments, Journal of virology 77(22) (2003) 11985-91.

[19] J.T. Kelly, J. Swanson, J. Newman, E. Groppelli, N.J. Stonehouse, T.J. Tuthill, Membrane interactions and uncoating of Aichi virus, a picornavirus that lacks a VP4, bioRxiv (2022) 2022.01.10.475380.

[20] E. Rivadulla, J.L. Romalde, A Comprehensive Review on Human Aichi Virus, Virologica Sinica (2020).

[21] A.I. Roig, U. Eskiocak, S.K. Hight, S.B. Kim, O. Delgado, R.F. Souza, S.J. Spechler, W.E. Wright, J.W. Shay, Immortalized epithelial cells derived from human colon biopsies express stem cell markers and differentiate in vitro, Gastroenterology 138(3) (2010) 1012-21.e1-5.

[22] K. Dharmsathaphorn, J.A. McRoberts, K.G. Mandel, L.D. Tisdale, H. Masui, A human colonic tumor cell line that maintains vectorial electrolyte transport, Am J Physiol 246(2 Pt 1) (1984) G204-8.

[23] F. Zucco, A.F. Batto, G. Bises, J. Chambaz, A. Chiusolo, R. Consalvo, H. Cross, G. Dal Negro, I. de Angelis, G. Fabre, F. Guillou, S. Hoffman, L. Laplanche, E. Morel, M. Pincon-Raymond, P. Prieto, L. Turco, G. Ranaldi, M. Rousset, Y. Sambuy, M.L. Scarino, F. Torreilles, A. Stammati, An inter-laboratory study to evaluate the effects of medium composition on the differentiation and barrier function of Caco-2 cell lines, Altern Lab Anim 33(6) (2005) 603-18.

[24] M.L. Stanifer, C. Kee, M. Cortese, C.M. Zumaran, S. Triana, M. Mukenhirn, H.-G. Kraeusslich, T. Alexandrov, R. Bartenschlager, S. Boulant, Critical Role of Type III Interferon in Controlling SARS-CoV-2 Infection in Human Intestinal Epithelial Cells, Cell Reports 32(1) (2020) 107863.

[25] R. Ramani, J.M. Laplante, T.M. Church, G.M. Farrell, D.M. Lamson, K. St George, CACO-2 cells: A continuous cell line with sensitive and broad-spectrum utility for respiratory virus culture, J Virol Methods 293 (2021) 114120.

[26] M.G. Brattain, A.E. Levine, S. Chakrabarty, L.C. Yeoman, J.K. Willson, B. Long, Heterogeneity of human colon carcinoma, Cancer Metastasis Rev 3(3) (1984) 177-91.

[27] L.T. da Costa, T.-C. He, J. Yu, A.B. Sparks, P.J. Morin, K. Polyak, S. Laken, B. Vogelstein, K.W. Kinzler, CDX2 is mutated in a colorectal cancer with normal APC/β-catenin signaling, Oncogene 18(35) (1999) 5010-5014.

[28] Y.-S. Chen, B.-C. Chen, Y.-S. Lin, J.-T. Chang, T.-S. Huang, J.-J. Chen, T.-H. Chang, Detection of Aichi virus with antibody targeting of conserved viral protein 1 epitope, Applied Microbiology and Biotechnology 97(19) (2013) 8529-8536.

[29] J.R. Cooper, M.B. Abdullatif, E.C. Burnett, K.E. Kempsell, F. Conforti, H. Tolley, J.E. Collins, D.E. Davies, Long Term Culture of the A549 Cancer Cell Line Promotes Multilamellar Body Formation and Differentiation towards an Alveolar Type II Pneumocyte Phenotype, PloS one 11(10) (2016) e0164438-e0164438.

[30] M. Lieber, G. Todaro, B. Smith, A. Szakal, W. Nelson-Rees, A continuous tumor-cell line from a human lung carcinoma with properties of type II alveolar epithelial cells, International Journal of Cancer 17(1) (1976) 62-70.

[31] W.E. Müller, M. Neufurth, S. Wang, R. Tan, H.C. Schröder, X. Wang, Morphogenetic (mucin expression) as well as potential anti-corona viral activity of the marine secondary metabolite polyphosphate on A549 cells, Marine Drugs 18(12) (2020) 639.

[32] D.C. Munday, E. Emmott, R. Surtees, C.-H. Lardeau, W. Wu, W.P. Duprex, B.K. Dove, J.N. Barr, J.A. Hiscox, Quantitative proteomic analysis of A549 cells infected with human respiratory syncytial virus, Molecular & Cellular Proteomics 9(11) (2010) 2438-2459.

[33] J. Mazzolini, R.J. Weber, H.S. Chen, A. Khan, E. Guggenheim, R.K. Shaw, J.K. Chipman, M.R. Viant, J.Z. Rappoport, Protein Corona Modulates Uptake and Toxicity of Nanoceria via Clathrin-Mediated Endocytosis, Biol Bull 231(1) (2016) 40-60.

[34] E.K. Benedikz, D. Bailey, C.N.L. Cook, D. Gonçalves-Carneiro, M.M.C. Buckner, J.M.A. Blair, T.J. Wells, N.F. Fletcher, M. Goodall, A. Flores-Langarica, R.A. Kingsley, J. Madsen, J. Teeling, S.L. Johnston, C.A. MacLennan, P. Balfe, I.R. Henderson, L.J.V. Piddock, A.F. Cunningham, J.A. McKeating, Bacterial flagellin promotes viral entry via an NF-kB and Toll Like Receptor 5 dependent pathway, Scientific Reports 9(1) (2019) 7903.

[35] O. Heikkilä, P. Susi, T. Tevaluoto, H. Härmä, V. Marjomäki, T. Hyypiä, S. Kiljunen, Internalization of coxsackievirus A9 is mediated by {beta}2-microglobulin, dynamin, and Arf6 but not by caveolin-1 or clathrin, Journal of virology 84(7) (2010) 3666-3681.

[36] T. Flerlage, D.F. Boyd, V. Meliopoulos, P.G. Thomas, S. Schultz-Cherry, Influenza virus and SARS-CoV-2: pathogenesis and host responses in the respiratory tract, Nature Reviews Microbiology 19(7) (2021) 425-441.

[37] D.A. Knight, S.T. Holgate, The airway epithelium: structural and functional properties in health and disease, Respirology 8(4) (2003) 432-46.

[38] A. Tam, S. Wadsworth, D. Dorscheid, S.F.P. Man, D.D. Sin, The airway epithelium: more than just a structural barrier, Therapeutic Advances in Respiratory Disease 5(4) (2011) 255-273.

[39] M.J. Evans, R.A. Cox, S.G. Shami, B. Wilson, C.G. Plopper, The role of basal cells in attachment of columnar cells to the basal lamina of the trachea, Am J Respir Cell Mol Biol 1(6) (1989) 463-9.

[40] J.E. Boers, A.W. Ambergen, F.B. Thunnissen, Number and proliferation of basal and parabasal cells in normal human airway epithelium, Am J Respir Crit Care Med 157(6 Pt 1) (1998) 2000-6.

[41] R. De Water, L.N. Willems, G.N. Van Muijen, C. Franken, J.A. Fransen, J.H. Dijkman, J.A. Kramps, Ultrastructural localization of bronchial antileukoprotease in central and peripheral human airways by a gold-labeling technique using monoclonal antibodies, Am Rev Respir Dis 133(5) (1986) 882-90.

[42] K.U. Hong, S.D. Reynolds, A. Giangreco, C.M. Hurley, B.R. Stripp, Clara cell secretory protein-expressing cells of the airway neuroepithelial body microenvironment include a label-retaining subset and are critical for epithelial renewal after progenitor cell depletion, Am J Respir Cell Mol Biol 24(6) (2001) 671-81.

[43] L. Shi, H. Xiong, J. He, H. Deng, Q. Li, Q. Zhong, W. Hou, L. Cheng, H. Xiao, Z. Yang, Antiviral activity of arbidol against influenza A virus, respiratory syncytial virus, rhinovirus, coxsackie virus and adenovirus in vitro and in vivo, Arch Virol 152(8) (2007) 1447-55.

[44] X. Cao, J.P. Coyle, R. Xiong, Y. Wang, R.H. Heflich, B. Ren, W.M. Gwinn, P. Hayden, L. Rojanasakul, Invited review: human air-liquid-interface organotypic airway tissue models derived from primary tracheobronchial epithelial cells—overview and perspectives, In Vitro Cellular & Developmental Biology - Animal 57(2) (2021) 104-132.

[45] M. Koehler, M. Delguste, C. Sieben, L. Gillet, D. Alsteens, Initial Step of Virus Entry: Virion Binding to Cell-Surface Glycans, Annual Review of Virology 7(1) (2020) 143-165.

[46] H. Ganjian, C. Zietz, D. Mechtcheriakova, D. Blaas, R. Fuchs, ICAM-1 Binding Rhinoviruses Enter HeLa Cells via Multiple Pathways and Travel to Distinct Intracellular Compartments for Uncoating, Viruses 9(4) (2017).

[47] H. Vandesande, M. Laajala, T. Kantoluoto, V. Ruokolainen, A.M. Lindberg, V. Marjomäki, Early entry events in Echovirus 30 infection, Journal of virology (2020) JVI.00592-20.

[48] A.V. Nicola, H.C. Aguilar, J. Mercer, B. Ryckman, C.M. Wiethoff, Virus Entry by Endocytosis, Advances in Virology 2013 (2013) 469538.

[49] J.J. Rennick, A.P.R. Johnston, R.G. Parton, Key principles and methods for studying the endocytosis of biological and nanoparticle therapeutics, Nature Nanotechnology 16(3) (2021) 266-276.

[50] C.B. Coyne, L. Shen, J.R. Turner, J.M. Bergelson, Coxsackievirus entry across epithelial tight junctions requires occludin and the small GTPases Rab34 and Rab5, Cell host & microbe 2(3) (2007) 181-92.

[51] C.B. Coyne, K.S. Kim, J.M. Bergelson, Poliovirus entry into human brain microvascular cells requires receptor-induced activation of SHP-2, Embo j 26(17) (2007) 4016-28.

[52] O. Muriel, M. Sánchez-Álvarez, R. Strippoli, M.A. del Pozo, Role of the Endocytosis of Caveolae in Intracellular Signaling and Metabolism, in: C. Lamaze, I. Prior (Eds.), Endocytosis and Signaling, Springer International Publishing, Cham, 2018, pp. 203-234.

[53] D. Volonte, A.R. Vyas, C. Chen, S. Dacic, L.P. Stabile, B.F. Kurland, S.R. Abberbock, T.F. Burns, J.G. Herman, Y.P. Di, F. Galbiati, Caveolin-1 promotes the tumor suppressor properties of oncogene-induced cellular senescence, J Biol Chem 293(5) (2018) 1794-1809.

[54] T. Zhao, L. Cui, X. Yu, Z. Zhang, X. Shen, X. Hua, Entry of sapelovirus into IPEC-J2 cells is dependent on caveolae-mediated endocytosis, Virology Journal 16(1) (2019) 37.

[55] X.D. Zhu, Y. Zhuang, J.J. Ben, L.L. Qian, H.P. Huang, H. Bai, J.H. Sha, Z.G. He, Q. Chen, Caveolae-dependent endocytosis is required for class A macrophage scavenger receptor-mediated apoptosis in macrophages, J Biol Chem 286(10) (2011) 8231-8239.

[56] L. Pelkmans, D. Puntener, A. Helenius, Local actin polymerization and dynamin recruitment in SV40-induced internalization of caveolae, science 296(5567) (2002) 535-539.

[57] D.I. Mundy, T. Machleidt, Y.-s. Ying, R.G. Anderson, G.S. Bloom, Dual control of caveolar membrane traffic by microtubules and the actin cytoskeleton, Journal of cell science 115(22) (2002) 4327-4339.

[58] M. Meister, R. Tikkanen, Endocytic trafficking of membrane-bound cargo: a flotillin point of view, Membranes (Basel) 4(3) (2014) 356-371.

[59] X. Xiong, Y. Zhao, S. Zhuge, H. Zhou, Y. Cui, Small interfering RNA-mediated inhibition of respiratory syncytial virus infections in Hela cells, Int. J. Clin. Exp. Med 12 (2019) 12264-12270.

[60] W. Wang, L. Qiao, H. Lu, X. Chen, X. Wang, J. Yu, J. Zhu, Y. Xiao, Y. Ma, Y. Wu, Flotillin 2 Facilitates the Infection of a Plant Virus in the Gut of Insect Vector, Journal of virology 96(7) (2022) e02140-21.

[61] M.-N. Bao, L.-J. Zhang, B. Tang, D.-D. Fu, J. Li, L. Du, Y.-N. Hou, Z.-L. Zhang, H.-W. Tang, D.-W. Pang, Influenza A Viruses Enter Host Cells via Extracellular Ca2+ Influx-Involved Clathrin-Mediated Endocytosis, ACS Applied Bio Materials 4(3) (2021) 2044-2051.

[62] M.A. Martín-Acebes, M. González-Magaldi, K. Sandvig, F. Sobrino, R. Armas-Portela, Productive entry of type C foot-and-mouth disease virus into susceptible cultured cells requires clathrin and is dependent on the presence of plasma membrane cholesterol, Virology 369(1) (2007) 105-118.

[63] M. Ehrlich, W. Boll, A. Van Oijen, R. Hariharan, K. Chandran, M.L. Nibert, T. Kirchhausen, Endocytosis by random initiation and stabilization of clathrin-coated pits, Cell 118(5) (2004) 591-605.

[64] K.M. Mayle, A.M. Le, D.T. Kamei, The intracellular trafficking pathway of transferrin, Biochimica et biophysica acta 1820(3) (2012) 264-281.

[65] D. Finkelshtein, A. Werman, D. Novick, S. Barak, M. Rubinstein, LDL receptor and its family members serve as the cellular receptors for vesicular stomatitis virus, Proc Natl Acad Sci U S A 110(18) (2013) 7306-11.

[66] L. Snyers, H. Zwickl, D. Blaas, Human Rhinovirus Type 2 Is Internalized by Clathrin-Mediated Endocytosis, Journal of virology 77(9) (2003) 5360-5369.

[67] S.L. Newmyer, A. Christensen, S. Sever, Auxilin-dynamin interactions link the uncoating ATPase chaperone machinery with vesicle formation, Dev Cell 4(6) (2003) 929-40.

[68] C. David, P.S. McPherson, O. Mundigl, P. de Camilli, A role of amphiphysin in synaptic vesicle endocytosis suggested by its binding to dynamin in nerve terminals, Proc Natl Acad Sci U S A 93(1) (1996) 331-5.

[69] E. Ungewickell, H. Ungewickell, S.E. Holstein, R. Lindner, K. Prasad, W. Barouch, B. Martin, L.E. Greene, E. Eisenberg, Role of auxilin in uncoating clathrin-coated vesicles, Nature 378(6557) (1995) 632-5.

[70] M. Schliwa, Action of cytochalasin D on cytoskeletal networks, The Journal of cell biology 92(1) (1982) 79-91.

[71] I. Fujiwara, M.E. Zweifel, N. Courtemanche, T.D. Pollard, Latrunculin A Accelerates Actin Filament Depolymerization in Addition to Sequestering Actin Monomers, Curr Biol 28(19) (2018) 3183-3192.e2.

[72] M.R. Bubb, I. Spector, B.B. Beyer, K.M. Fosen, Effects of jasplakinolide on the kinetics of actin polymerization. An explanation for certain in vivo observations, J Biol Chem 275(7) (2000) 5163-70.

[73] A.B. Fielding, S.J. Royle, Mitotic inhibition of clathrin-mediated endocytosis, Cell Mol Life Sci 70(18) (2013) 3423-33.

[74] L.H. Wang, K.G. Rothberg, R.G. Anderson, Mis-assembly of clathrin lattices on endosomes reveals a regulatory switch for coated pit formation, The Journal of cell biology 123(5) (1993) 1107-17.

[75] J.A. Daniel, N. Chau, M.K. Abdel-Hamid, L. Hu, L. von Kleist, A. Whiting, S. Krishnan, P. Maamary, S.R. Joseph, F. Simpson, V. Haucke, A. McCluskey, P.J. Robinson, Phenothiazine-Derived Antipsychotic Drugs Inhibit Dynamin and Clathrin-Mediated Endocytosis, Traffic 16(6) (2015) 635-654.

[76] M.C. Giocondi, Z. Mamdouh, C. Le Grimellec, Benzyl alcohol differently affects fluid phase endocytosis and exocytosis in renal epithelial cells, Biochim Biophys Acta 1234(2) (1995) 197-202.

[77] R.W. Walenga, E.E. Opas, M.B. Feinstein, Differential effects of calmodulin antagonists on phospholipases A2 and C in thrombin-stimulated platelets, J Biol Chem 256(23) (1981) 12523-8.

[78] A. Wells, M.F. Ware, F.D. Allen, D.A. Lauffenburger, Shaping up for shipping out: PLCγ signaling of morphology changes in EGF-stimulated fibroblast migration, Cell Motility 44(4) (1999) 227-233.

[79] M. Amyere, B. Payrastre, U. Krause, P. Van Der Smissen, A. Veithen, P.J. Courtoy, Constitutive macropinocytosis in oncogene-transformed fibroblasts depends on sequential permanent activation of phosphoinositide 3-kinase and phospholipase C, Molecular biology of the cell 11(10) (2000) 3453-3467.

[80] A.K. Willox, Y.M. Sahraoui, S.J. Royle, Non-specificity of Pitstop 2 in clathrin-mediated endocytosis, Biol Open 3(5) (2014) 326-31.

[81] E. Boucrot, A.P.A. Ferreira, L. Almeida-Souza, S. Debard, Y. Vallis, G. Howard, L. Bertot, N. Sauvonnet, H.T. McMahon, Endophilin marks and controls a clathrin-independent endocytic pathway, Nature 517(7535) (2015) 460-465.

[82] M. Meinecke, E. Boucrot, G. Camdere, W.C. Hon, R. Mittal, H.T. McMahon, Cooperative recruitment of dynamin and BIN/amphiphysin/Rvs (BAR) domain-containing proteins leads to GTP-dependent membrane scission, J Biol Chem 288(9) (2013) 6651-61.

[83] E. Boucrot, A. Pick, G. Çamdere, N. Liska, E. Evergren, H.T. McMahon, M.M. Kozlov, Membrane fission is promoted by insertion of amphipathic helices and is restricted by crescent BAR domains, Cell 149(1) (2012) 124-36.

[84] S.-L. Chen, Y.-G. Liu, Y.-T. Zhou, P. Zhao, H. Ren, M. Xiao, Y.-Z. Zhu, Z.-T. Qi, Endophilin-A2-mediated endocytic pathway is critical for enterovirus 71 entry into caco-2 cells, Emerg Microbes Infect 8(1) (2019) 773-786.

[85] S. Kumari, S. Mayor, ARF1 is directly involved in dynamin-independent endocytosis, Nat Cell Biol 10(1) (2008) 30-41.

[86] R. Chadda, M.T. Howes, S.J. Plowman, J.F. Hancock, R.G. Parton, S. Mayor, Cholesterol-sensitive Cdc42 activation regulates actin polymerization for endocytosis via the GEEC pathway, Traffic 8(6) (2007) 702-17.

[87] R.A. Fratti, J.M. Backer, J. Gruenberg, S. Corvera, V. Deretic, Role of phosphatidylinositol 3-kinase and Rab5 effectors in phagosomal biogenesis and mycobacterial phagosome maturation arrest, The Journal of cell biology 154(3) (2001) 631-644.

[88] M.T. Howes, M. Kirkham, J. Riches, K. Cortese, P.J. Walser, F. Simpson, M.M. Hill, A. Jones, R. Lundmark, M.R. Lindsay, D.J. Hernandez-Deviez, G. Hadzic, A. McCluskey, R. Bashir, L. Liu, P. Pilch, H. McMahon, P.J. Robinson, J.F. Hancock, S. Mayor, R.G. Parton, Clathrin-independent carriers form a high capacity endocytic sorting system at the leading edge of migrating cells, The Journal of cell biology 190(4) (2010) 675-91.

[89] M. Kalia, S. Kumari, R. Chadda, M.M. Hill, R.G. Parton, S. Mayor, Arf6-independent GPI-anchored protein-enriched early endosomal compartments fuse with sorting endosomes via a Rab5/phosphatidylinositol-3'-kinase-dependent machinery, Molecular biology of the cell 17(8) (2006) 3689-3704.

[90] N.C. Gauthier, P. Monzo, V. Kaddai, A. Doye, V. Ricci, P. Boquet, Helicobacter pylori VacA cytotoxin: a probe for a clathrin-independent and Cdc42-dependent pinocytic pathway routed to late endosomes, Molecular biology of the cell 16(10) (2005) 4852-4866.

[91] M. Nonnenmacher, T. Weber, Adeno-associated virus 2 infection requires endocytosis through the CLIC/GEEC pathway, Cell host & microbe 10(6) (2011) 563-76.

[92] M. Kirkham, A. Fujita, R. Chadda, S.J. Nixon, T.V. Kurzchalia, D.K. Sharma, R.E. Pagano, J.F. Hancock, S. Mayor, R.G. Parton, Ultrastructural identification of uncoated caveolin-independent early endocytic vehicles, The Journal of cell biology 168(3) (2005) 465-76.

[93] R. Lakshminarayan, C. Wunder, U. Becken, M.T. Howes, C. Benzing, S. Arumugam, S. Sales, N. Ariotti, V. Chambon, C. Lamaze, D. Loew, A. Shevchenko, K. Gaus, R.G. Parton, L. Johannes, Galectin-3 drives glycosphingolipid-dependent biogenesis of clathrin-independent carriers, Nature Cell Biology 16(6) (2014) 592-603.

[94] N.D. Condon, J.M. Heddleston, T.-L. Chew, L. Luo, P.S. McPherson, M.S. Ioannou, L. Hodgson, J.L. Stow, A.A. Wall, Macropinosome formation by tent pole ruffling in macrophages, The Journal of cell biology 217(11) (2018) 3873-3885.

[95] C. Commisso, S.M. Davidson, R.G. Soydaner-Azeloglu, S.J. Parker, J.J. Kamphorst, S. Hackett, E. Grabocka, M. Nofal, J.A. Drebin, C.B. Thompson, J.D. Rabinowitz, C.M. Metallo, M.G. Vander Heiden, D. Bar-Sagi, Macropinocytosis of protein is an amino acid supply route in Ras-transformed cells, Nature 497(7451) (2013) 633-637.

[96] Y.-K. Yoon, H.-P. Kim, S.-W. Han, D.Y. Oh, S.-A. Im, Y.-J. Bang, T.-Y. Kim, KRAS mutant lung cancer cells are differentially responsive to MEK inhibitor due to AKT or STAT3 activation: Implication for combinatorial approach, Molecular Carcinogenesis 49(4) (2010) 353-362.

[97] X.P. Lin, J.D. Mintern, P.A. Gleeson, Macropinocytosis in Different Cell Types: Similarities and Differences, Membranes (Basel) 10(8) (2020) 177.

[98] J.P. Lim, P.A. Gleeson, Macropinocytosis: an endocytic pathway for internalising large gulps, Immunol Cell Biol 89(8) (2011) 836-43.

[99] S. Dharmawardhane, A. Schürmann, M.A. Sells, J. Chernoff, S.L. Schmid, G.M. Bokoch, Regulation of macropinocytosis by p21-activated kinase-1, Molecular biology of the cell 11(10) (2000) 3341-3352.

[100] P. Liberali, E. Kakkonen, G. Turacchio, C. Valente, A. Spaar, G. Perinetti, R.A. Böckmann, D. Corda, A. Colanzi, V. Marjomaki, A. Luini, The closure of Pak1-dependent macropinosomes requires the phosphorylation of CtBP1/BARS, Embo j 27(7) (2008) 970-81.

[101] J. Gilleron, W. Querbes, A. Zeigerer, A. Borodovsky, G. Marsico, U. Schubert, K. Manygoats, S. Seifert, C. Andree, M. Stöter, H. Epstein-Barash, L. Zhang, V. Koteliansky, K. Fitzgerald, E. Fava, M. Bickle, Y. Kalaidzidis, A. Akinc, M. Maier, M. Zerial, Image-based analysis of lipid nanoparticle-mediated siRNA delivery, intracellular trafficking and endosomal escape, Nat Biotechnol 31(7) (2013) 638-46.

[102] A.J. Edgar, J.P. Bennett, Circular ruffle formation in rat basophilic leukemia cells in response to antigen stimulation, Eur J Cell Biol 73(2) (1997) 132-40.

[103] A. Zidovska, E. Sackmann, On the mechanical stabilization of filopodia, Biophys J 100(6) (2011) 1428-37.

[104] M. Kovács, J. Tóth, C. Hetényi, A. Málnási-Csizmadia, J.R. Sellers, Mechanism of blebbistatin inhibition of myosin II, J Biol Chem 279(34) (2004) 35557-63.

[105] J. Jiang, A.L. Kolpak, Z.-Z. Bao, Myosin IIB isoform plays an essential role in the formation of two distinct types of macropinosomes, Cytoskeleton (Hoboken) 67(1) (2010) 32-42.

[106] S.-C. Han, H.-C. Guo, S.-Q. Sun, Y. Jin, Y.-Q. Wei, X. Feng, X.-P. Yao, S.-Z. Cao, D. Xiang Liu, X.-T. Liu, Productive Entry of Foot-and-Mouth Disease Virus via Macropinocytosis Independent of Phosphatidylinositol 3-Kinase, Scientific Reports 6(1) (2016) 19294.

[107] S.E. Krieger, C. Kim, L. Zhang, V. Marjomaki, J.M. Bergelson, Echovirus 1 entry into polarized Caco-2 cells depends on dynamin, cholesterol, and cellular factors associated with macropinocytosis, Journal of virology 87(16) (2013) 8884-95.

[108] M. Notarnicola, C. Messa, A. Orlando, B. D'Attoma, V. Tutino, R. Rivizzigno, M.G. Caruso, Effect of genistein on cholesterol metabolism-related genes in a colon cancer cell line, Genes Nutr 3(1) (2008) 35-40.

[109] S. Baek, S.M. Kim, S.A. Lee, B.Y. Rhim, S.K. Eo, K. Kim, The cholesterol-binding antibiotic nystatin induces expression of macrophage inflammatory protein-1 in macrophages, Biomol Ther (Seoul) 21(1) (2013) 42-8.

[110] R.J. Cenedella, Cholesterol Synthesis Inhibitor U18666A and the Role of Sterol Metabolism and Trafficking in Numerous Pathophysiological Processes, Lipids 44(6) (2009) 477-487.

[111] W.C. Duane, D.B. Hunninghake, M.L. Freeman, P.A. Pooler, L.A. Schlasner, R.L. Gebhard, Simvastatin, a competitive inhibitor of HMG-CoA reductase, lowers cholesterol saturation index of gallbladder bile, Hepatology 8(5) (1988) 1147-1150.

[112] P.A. Orlandi, P.H. Fishman, Filipin-dependent inhibition of cholera toxin: evidence for toxin internalization and activation through caveolae-like domains, The Journal of cell biology 141(4) (1998) 905-915.

[113] Y. Ohnishi, H. Yasui, K. Kakudo, M. Nozaki, Cetuximab-resistant oral squamous cell carcinoma cells become sensitive in anchorage-independent culture conditions through the activation of the EGFR/AKT pathway, Int J Oncol 47(6) (2015) 2165-2172.

[114] J.-W. Hsu, M. Bai, K. Li, J.-S. Yang, N. Chu, P.A. Cole, M.J. Eck, J. Li, V.W. Hsu, The protein kinase Akt acts as a coat adaptor in endocytic recycling, Nature Cell Biology 22(8) (2020) 927-933.

[115] S. Sigismund, E. Argenzio, D. Tosoni, E. Cavallaro, S. Polo, P.P. Di Fiore, Clathrin-mediated internalization is essential for sustained EGFR signaling but dispensable for degradation, Dev Cell 15(2) (2008) 209-19.

[116] S. Mahammad, I. Parmryd, Cholesterol homeostasis in T cells. Methyl-β-cyclodextrin treatment results in equal loss of cholesterol from Triton X-100 soluble and insoluble fractions, Biochimica et Biophysica Acta (BBA) - Biomembranes 1778(5) (2008) 1251-1258.

[117] J. Huang, C. Li, F. Fan, N. Liu, F. Boadi, X. Shen, B. Hao, Methyl-Beta-Cyclodextrin-Induced Macropinocytosis Results in Increased Infection of Sf21 Cells by Bombyx Mori Nucleopolyhedrovirus, Viruses 11(10) (2019).

[118] C. Jin, B. Che, Z. Guo, C. Li, Y. Liu, W. Wu, S. Wang, D. Li, Z. Cui, M. Liang, Single virus tracking of Ebola virus entry through lipid rafts in living host cells, Biosafety and Health 2(1) (2020) 25-31.

[119] N.Q. Liu, A.S. Lossinsky, W. Popik, X. Li, C. Gujuluva, B. Kriederman, J. Roberts, T. Pushkarsky, M. Bukrinsky, M. Witte, M. Weinand, M. Fiala, Human immunodeficiency virus type 1 enters brain microvascular endothelia by macropinocytosis dependent on lipid rafts and the mitogen-activated protein kinase signaling pathway, Journal of virology 76(13) (2002) 6689-6700.

[120] G. Baravalle, D. Schober, M. Huber, N. Bayer, R.F. Murphy, R. Fuchs, Transferrin recycling and dextran transport to lysosomes is differentially affected by bafilomycin, nocodazole, and low temperature, Cell and Tissue Research 320(1) (2005) 99-113.

[121] F.R. Maxfield, T.E. McGraw, Endocytic recycling, Nature Reviews Molecular Cell Biology 5(2) (2004) 121-132.

[122] R. Conzemius, H. Ganjian, D. Blaas, R. Fuchs, ICAM-1 Binding Rhinoviruses A89 and B14 Uncoat in Different Endosomal Compartments, Journal of virology 90(17) (2016) 7934-42.

[123] J. Gruenberg, H. Stenmark, The biogenesis of multivesicular endosomes, Nature Reviews Molecular Cell Biology 5(4) (2004) 317-323.

[124] C.C. Scott, F. Vacca, J. Gruenberg, Endosome maturation, transport and functions, Seminars in Cell & Developmental Biology 31 (2014) 2-10.

[125] J. Rink, E. Ghigo, Y. Kalaidzidis, M. Zerial, Rab conversion as a mechanism of progression from early to late endosomes, Cell 122(5) (2005) 735-49.

[126] J. Huotari, A. Helenius, Endosome maturation, EMBO J 30(17) (2011) 3481-500.

[127] J.A. Mindell, Lysosomal Acidification Mechanisms, Annual Review of Physiology 74(1) (2012) 69-86.

[128] C. Bucci, P. Thomsen, P. Nicoziani, J. McCarthy, B. van Deurs, Rab7: a key to lysosome biogenesis, Molecular biology of the cell 11(2) (2000) 467-480.

[129] L.J. Shearer, N.O. Petersen, Distribution and Co-localization of endosome markers in cells, Heliyon 5(9) (2019) e02375.

[130] F. Aniento, N. Emans, G. Griffiths, J. Gruenberg, Cytoplasmic dynein-dependent vesicular transport from early to late endosomes, The Journal of cell biology 123(6 Pt 1) (1993) 1373-87.

[131] E. Daro, P. van der Sluijs, T. Galli, I. Mellman, Rab4 and cellubrevin define different early endosome populations on the pathway of transferrin receptor recycling, Proceedings of the National Academy of Sciences 93(18) (1996) 9559.

[132] M.V. Kharchenko, M.V. Zlobina, R.S. Kamentseva, E.S. Kornilova, Microtubules and Actin Filaments Facilitate Fusions and Separations of Vesicules on the Endocytic Pathway of EGF-Receptor Complexes, Cell and Tissue Biology 14(6) (2020) 464-473.

[133] S.B. Horwitz, Taxol (paclitaxel): mechanisms of action, Ann Oncol 5 Suppl 6 (1994) S3-6.

[134] S.F. Hamm-Alvarez, M. Sonee, K. Loran-Goss, W.-C. Shen, Paclitaxel and Nocodazole Differentially Alter Endocytosis in Cultured Cells, Pharmaceutical Research 13(11) (1996) 1647-1656.

[135] A.J. Firestone, J.S. Weinger, M. Maldonado, K. Barlan, L.D. Langston, M. O'Donnell, V.I. Gelfand, T.M. Kapoor, J.K. Chen, Small-molecule inhibitors of the AAA+ ATPase motor cytoplasmic dynein, Nature 484(7392) (2012) 125-9.

[136] E. Kobayashi, H. Nakano, M. Morimoto, T. Tamaoki, Calphostin C (UCN-1028C), a novel microbial compound, is a highly potent and specific inhibitor of protein kinase C, Biochem Biophys Res Commun 159(2) (1989) 548-53.

[137] F. Alvi, J. Idkowiak-Baldys, A. Baldys, J.R. Raymond, Y.A. Hannun, Regulation of membrane trafficking and endocytosis by protein kinase C: emerging role of the pericentrion, a novel protein kinase C-dependent subset of recycling endosomes, Cellular and Molecular Life Sciences 64(3) (2007) 263-270.

[138] M.Y. Nakano, K. Boucke, M. Suomalainen, R.P. Stidwill, U.F. Greber, The first step of adenovirus type 2 disassembly occurs at the cell surface, independently of endocytosis and escape to the cytosol, Journal of virology 74(15) (2000) 7085-95.

[139] C.N. Root, E.G. Wills, L.L. McNair, G.R. Whittaker, Entry of influenza viruses into cells is inhibited by a highly specific protein kinase C inhibitor, J Gen Virol 81(Pt 11) (2000) 2697-2705.

[140] S.N. Constantinescu, C.D. Cernescu, L.M. Popescu, Effects of protein kinase C inhibitors on viral entry and infectivity, FEBS Lett 292(1-2) (1991) 31-3.

[141] Z.M. Jaffer, J. Chernoff, p21-activated kinases: three more join the Pak, Int J Biochem Cell Biol 34(7) (2002) 713-7.

[142] A. Grassart, V. Meas-Yedid, A. Dufour, J.-C. Olivo-Marin, A. Dautry-Varsat, N. Sauvonnet, Pak1 Phosphorylation Enhances Cortactin–N-WASP Interaction in Clathrin-Caveolin-Independent Endocytosis, Traffic 11(8) (2010) 1079-1091.

[143] P.D. Hart, M.R. Young, Ammonium chloride, an inhibitor of phagosome-lysosome fusion in macrophages, concurrently induces phagosome-endosome fusion, and opens a novel pathway: studies of a pathogenic mycobacterium and a nonpathogenic yeast, The Journal of experimental medicine 174(4) (1991) 881-889.

[144] E.H. Morgan, Inhibition of reticulocyte iron uptake by NH4Cl and CH3NH2, Biochimica et Biophysica Acta (BBA) - Biomembranes 642(1) (1981) 119-134.

[145] A. Real-Hohn, R. Zhu, H. Ganjian, N. Ibrahim, P. Hinterdorfer, H. Kowalski, D. Blaas, Catching Common Cold Virus with a Net: Pyridostatin Forms Filaments in Tris Buffer That Trap Viruses-A Novel Antiviral Strategy?, Viruses 12(7) (2020).

[146] R. Wang, J. Wang, A. Hassan, C.-H. Lee, X.-S. Xie, X. Li, Molecular basis of V-ATPase inhibition by bafilomycin A1, Nature communications 12(1) (2021) 1782.

[147] C. Mauvezin, T.P. Neufeld, Bafilomycin A1 disrupts autophagic flux by inhibiting both V-ATPase-dependent acidification and Ca-P60A/SERCA-dependent autophagosome-lysosome fusion, Autophagy 11(8) (2015) 1437-1438.

[148] L.S. Johnson, K.W. Dunn, B. Pytowski, T.E. McGraw, Endosome acidification and receptor trafficking: bafilomycin A1 slows receptor externalization by a mechanism involving the receptor's internalization motif, Molecular Biology of the Cell 4(12) (1993) 1251-1266.

[149] E.J. Bowman, A. Siebers, K. Altendorf, Bafilomycins: a class of inhibitors of membrane ATPases from microorganisms, animal cells, and plant cells, Proc Natl Acad Sci U S A 85(21) (1988) 7972-6.

[150] H.H. Mollenhauer, D.J. Morré, L.D. Rowe, Alteration of intracellular traffic by monensin; mechanism, specificity and relationship to toxicity, Biochimica et biophysica acta 1031(2) (1990) 225-246.

[151] B.C. Pressman, Biological Applications of Ionophores, Annual Review of Biochemistry 45(1) (1976) 501-530.

[152] M. Marsh, J. Wellsteed, H. Kern, E. Harms, A. Helenius, Monensin inhibits Semliki Forest virus penetration into culture cells, Proc Natl Acad Sci U S A 79(17) (1982) 5297-301.

[153] Y. Maeda, S. Shibutani, K. Onishi, H. Iwata, Ibaraki virus enters host cells by macropinocytosis, Virus Research 302 (2021) 198492.

[154] E.J. Gillespie, C.-L.C. Ho, K. Balaji, D.L. Clemens, G. Deng, Y.E. Wang, H.J. Elsaesser, B. Tamilselvam, A. Gargi, S.D. Dixon, B. France, B.T. Chamberlain, S.R. Blanke, G. Cheng, J.C. de la Torre, D.G. Brooks, M.E. Jung, J. Colicelli, R. Damoiseaux, K.A. Bradley, Selective inhibitor of endosomal trafficking pathways exploited by multiple toxins and viruses, Proceedings of the National Academy of Sciences 110(50) (2013) E4904.

[155] G.A. Farr, L.-g. Zhang, P. Tattersall, Parvoviral virions deploy a capsid-tethered lipolytic enzyme to breach the endosomal membrane during cell entry, Proceedings of the National Academy of Sciences of the United States of America 102(47) (2005) 17148-17153.

[156] S. Canaan, Z. Zádori, F. Ghomashchi, J. Bollinger, M. Sadilek, M.E. Moreau, P. Tijssen, M.H. Gelb, Interfacial enzymology of parvovirus phospholipases A2, J Biol Chem 279(15) (2004) 14502-8.

[157] T.J. Wickham, P. Mathias, D.A. Cheresh, G.R. Nemerow, Integrins alpha v beta 3 and alpha v beta 5 promote adenovirus internalization but not virus attachment, Cell 73(2) (1993) 309-19.

[158] J.M. Bergelson, J.A. Cunningham, G. Droguett, E.A. Kurt-Jones, A. Krithivas, J.S. Hong, M.S. Horwitz, R.L. Crowell, R.W. Finberg, Isolation of a common receptor for Coxsackie B viruses and adenoviruses 2 and 5, Science 275(5304) (1997) 1320-3.

[159] S. Luisoni, M. Suomalainen, K. Boucke, Lukas B. Tanner, Markus R. Wenk, Xue L. Guan, M. Grzybek, Ü. Coskun, Urs F. Greber, Co-option of Membrane Wounding Enables Virus Penetration into Cells, Cell host & microbe 18(1) (2015) 75-85.

[160] R. Fuchs, D. Blaas, Uncoating of human rhinoviruses, Rev Med Virol 20(5) (2010) 281-97.

[161] V.U. Weiss, X. Subirats, A. Pickl-Herk, G. Bilek, W. Winkler, M. Kumar, G. Allmaier, D. Blaas, E. Kenndler, Characterization of rhinovirus subviral A particles via capillary electrophoresis, electron microscopy and gas-phase electrophoretic mobility molecular analysis: Part I, Electrophoresis 33(12) (2012) 1833-41.

[162] R. Fuchs, D. Blaas, Productive entry pathways of human rhinoviruses, Adv Virol 2012 (2012) 826301.

[163] A. Panjwani, A.S. Asfor, T.J. Tuthill, The conserved N-terminus of human rhinovirus capsid protein VP4 contains membrane pore-forming activity and is a target for neutralizing antibodies, J Gen Virol 97(12) (2016) 3238-3242.

[164] D. Blaas, R. Fuchs, Mechanism of human rhinovirus infections, Mol Cell Pediatr 3(1) (2016) 21-21.

[165] J. Staring, M. Raaben, T.R. Brummelkamp, Viral escape from endosomes and host detection at a glance, Journal of Cell Science 131(15) (2018).

[166] J. Staring, E. von Castelmur, V.A. Blomen, L.G. van den Hengel, M. Brockmann, J. Baggen, H.J. Thibaut, J. Nieuwenhuis, H. Janssen, F.J.M. van Kuppeveld, A. Perrakis, J.E. Carette, T.R. Brummelkamp, PLA2G16 represents a switch between entry and clearance of Picornaviridae, Nature 541 (2017) 412.

[167] B.A. Mainou, T.S. Dermody, Transport to late endosomes is required for efficient reovirus infection, Journal of virology 86(16) (2012) 8346-8358.

[168] T. Yamashita, K. Sakae, H. Tsuzuki, Y. Suzuki, N. Ishikawa, N. Takeda, T. Miyamura, S. Yamazaki, Complete nucleotide sequence and genetic organization of Aichi virus, a distinct member

of the Picornaviridae associated with acute gastroenteritis in humans, Journal of virology 72(10) (1998) 8408-12.

[169] J. Baggen, Y. Liu, H. Lyoo, A.L.W. van Vliet, M. Wahedi, J.W. de Bruin, R.W. Roberts, P. Overduin, A. Meijer, M.G. Rossmann, H.J. Thibaut, F.J.M. van Kuppeveld, Bypassing pan-enterovirus host factor PLA2G16, Nature communications 10(1) (2019) 3171.

[170] G.A. Belov, Dynamic lipid landscape of picornavirus replication organelles, Curr Opin Virol 19 (2016) 1-6.

[171] A. Dubankova, J. Humpolickova, M. Klima, E. Boura, Negative charge and membrane-tethered viral 3B cooperate to recruit viral RNA dependent RNA polymerase 3Dpol, Scientific Reports 7(1) (2017) 17309.

[172] Y. Lu, S. Song, L. Zhang, Emerging Role for Acyl-CoA Binding Domain Containing 3 at Membrane Contact Sites During Viral Infection, Front Microbiol 11(608) (2020).

[173] S. Banerjee, D. Aponte-Diaz, C. Yeager, S.D. Sharma, G. Ning, H.S. Oh, Q. Han, M. Umeda, Y. Hara, R.Y.L. Wang, C.E. Cameron, Hijacking of multiple phospholipid biosynthetic pathways and induction of membrane biogenesis by a picornaviral 3CD protein, PLOS Pathogens 14(5) (2018) e1007086.

[174] H.M. van der Schaar, C.M. Dorobantu, L. Albulescu, J. Strating, F.J.M. van Kuppeveld, Fat(al) attraction: Picornaviruses Usurp Lipid Transfer at Membrane Contact Sites to Create Replication Organelles, Trends in microbiology 24(7) (2016) 535-546.

[175] I. Corbic Ramljak, J. Stanger, A. Real-Hohn, D. Dreier, L. Wimmer, M. Redlberger-Fritz, W. Fischl, K. Klingel, M.D. Mihovilovic, D. Blaas, H. Kowalski, Cellular N-myristoyltransferases play a crucial picornavirus genus-specific role in viral assembly, virion maturation, and infectivity, PLoS pathogens 14(8) (2018) e1007203-e1007203.

[176] S.T. Abedon, E. Bartom, Multiplicity of Infection, in: S. Maloy, K. Hughes (Eds.), Brenner's Encyclopedia of Genetics (Second Edition), Academic Press, San Diego, 2013, pp. 509-510.

[177] L.J. Reed, H. Muench, A SIMPLE METHOD OF ESTIMATING FIFTY PER CENT ENDPOINTS12, American Journal of Epidemiology 27(3) (1938) 493-497.

[178] S. Seeberg, A. Brandberg, S. Hermodsson, P. Larsson, S. Lundgren, Hospital outbreak of hepatitis A secondary to blood exchange in a baby, Hospital outbreak of hepatitis A secondary to blood exchange in a baby. 1 (1981) 1155-1156.

[179] D.-H. Chung, B.P. Moore, D.S. Matharu, J.E. Golden, C. Maddox, L. Rasmussen, M.I. Sosa, S. Ananthan, E.L. White, F. Jia, C.B. Jonsson, W.E. Severson, A cell based high-throughput screening approach for the discovery of new inhibitors of respiratory syncytial virus, Virology Journal 10(1) (2013) 19.

[180] C.B. Denani, A. Real-Hohn, C.A.M. de Carvalho, A.M.d.O. Gomes, R.B. Gonçalves, Lactoferrin affects rhinovirus B-14 entry into H1-HeLa cells, Archives of Virology 166(4) (2021) 1203-1211.

[181] J.T.H. Wang, R.D. Teasdale, D. Liebl, Macropinosome quantitation assay, MethodsX 1 (2014) 36-41.

[182] S. Bartlett Jeffrey, R. Wilcher, R.J. Samulski, Infectious Entry Pathway of Adeno-Associated Virus and Adeno-Associated Virus Vectors, Journal of virology 74(6) (2000) 2777-2785.

[183] A. Pierzyńska-Mach, P.A. Janowski, J.W. Dobrucki, Evaluation of acridine orange, LysoTracker Red, and quinacrine as fluorescent probes for long-term tracking of acidic vesicles, Cytometry Part A 85(8) (2014) 729-737.

[184] M.A. Kolber, P.A. Henkart, Quantitation of secretion by rat basophilic leukemia cells by measurements of quinacrine uptake, Biochim Biophys Acta 939(3) (1988) 459-66.

[185] Y. Yasumura, Y. Kawakita, A line of cells derived from African green monkey kidney, Nippon Rinsho 21 (1963) 1209-1210.

[186] Y.S. Chen, B.C. Chen, Y.S. Lin, J.T. Chang, T.S. Huang, J.J. Chen, T.H. Chang, Detection of Aichi virus with antibody targeting of conserved viral protein 1 epitope, Appl Microbiol Biotechnol 97(19) (2013) 8529-36.

[187] A. Jurgeit, S. Moese, P. Roulin, A. Dorsch, M. Lötzerich, W.-M. Lee, U. Greber, An RNA replication-center assay for high content image-based quantifications of human rhinovirus and coxsackievirus infections, Virology journal 7 (2010) 264.

[188] A.L. Richards, J.A. Soares-Martins, G.T. Riddell, W.T. Jackson, Generation of unique poliovirus RNA replication organelles, MBio 5(2) (2014) e00833-13.

[189] S. Hamilton, D. Wyatt, B. Wahlgren, M. O'Dowd, J. Morrissey, D. Daniels, J. Lednicky, Higher titers of some H5N1 and recent human H1N1 and H3N2 influenza viruses in Mv1 Lu vs. MDCK cells, Virology journal 8 (2011) 66.

[190] Y. Cui, R. Peng, H. Song, Z. Tong, X. Qu, S. Liu, X. Zhao, Y. Chai, P. Wang, G.F. Gao, J. Qi, Molecular basis of Coxsackievirus A10 entry using the two-in-one attachment and uncoating receptor KRM1, Proceedings of the National Academy of Sciences 117(31) (2020) 18711.

[191] J.E. Jones, V. Le Sage, S.S. Lakdawala, Viral and host heterogeneity and their effects on the viral life cycle, Nature Reviews Microbiology 19(4) (2021) 272-282.

[192] K.A. Foster, C.G. Oster, M.M. Mayer, M.L. Avery, K.L. Audus, Characterization of the A549 cell line as a type II pulmonary epithelial cell model for drug metabolism, Exp Cell Res 243(2) (1998) 359-66.

[193] K. Białkowska, P. Komorowski, M. Bryszewska, K. Miłowska, Spheroids as a type of three-dimensional cell cultures—examples of methods of preparation and the most important application, International Journal of Molecular Sciences 21(17) (2020) 6225.

[194] M.O. Pohl, I. Busnadiego, V. Kufner, I. Glas, U. Karakus, S. Schmutz, M. Zaheri, I. Abela, A. Trkola, M. Huber, S. Stertz, B.G. Hale, SARS-CoV-2 variants reveal features critical for replication in primary human cells, PLoS biology 19(3) (2021) e3001006-e3001006.

[195] N. Huang, P. Pérez, T. Kato, Y. Mikami, K. Okuda, R.C. Gilmore, C.D. Conde, B. Gasmi, S. Stein, M. Beach, E. Pelayo, J.O. Maldonado, B.A. Lafont, S.-I. Jang, N. Nasir, R.J. Padilla, V.A. Murrah, R. Maile, W. Lovell, S.M. Wallet, N.M. Bowman, S.L. Meinig, M.C. Wolfgang, S.N. Choudhury, M. Novotny, B.D. Aevermann, R.H. Scheuermann, G. Cannon, C.W. Anderson, R.E. Lee, J.T. Marchesan, M. Bush, M. Freire, A.J. Kimple, D.L. Herr, J. Rabin, A. Grazioli, S. Das, B.N. French, T. Pranzatelli, J.A. Chiorini, D.E. Kleiner, S. Pittaluga, S.M. Hewitt, P.D. Burbelo, D. Chertow, N.C.-A. Consortium, H.C.A. Oral, N. Craniofacial Biological, K. Frank, J. Lee, R.C. Boucher, S.A. Teichmann, B.M. Warner, K.M. Byrd, SARS-CoV-2 infection of the oral cavity and saliva, Nature medicine 27(5) (2021) 892-903.

[196] M. Groznica, Studying aichivirus A1 infection: from 2D to 3D cell culture systems, Wien, 2021.

[197] C. Rajput, M. Han, T. Ishikawa, J. Lei, S. Jazaeri, J.K. Bentley, M.B. Hershenson, Early-life heterologous rhinovirus infections induce an exaggerated asthma-like phenotype, Journal of Allergy and Clinical Immunology 146(3) (2020) 571-582. e3.

[198] Y.G. Chen, S. Hur, Cellular origins of dsRNA, their recognition and consequences, Nat Rev Mol Cell Biol 23(4) (2022) 286-301.

[199] E.E. Rivera-Serrano, O. Gonzalez-Lopez, A. Das, S.M. Lemon, Cellular entry and uncoating of naked and quasi-enveloped human hepatoviruses, eLife 8 (2019).

[200] K.J. Livak, T.D. Schmittgen, Analysis of relative gene expression data using real-time quantitative PCR and the 2(-Delta Delta C(T)) Method, Methods 25(4) (2001) 402-8.

[201] M. Mettlen, A. Platek, P. Van Der Smissen, S. Carpentier, M. Amyere, L. Lanzetti, P. de Diesbach, D. Tyteca, P.J. Courtoy, Src triggers circular ruffling and macropinocytosis at the apical surface of polarized MDCK cells, Traffic 7(5) (2006) 589-603.

[202] M. Mairhofer, M. Steiner, U. Salzer, R. Prohaska, Stomatin-like protein-1 interacts with stomatin and is targeted to late endosomes, J Biol Chem 284(42) (2009) 29218-29229.

[203] O. Grbovic, P. Mathews, Y. Jiang, S. Schmidt, R. Dinakar, N. Summers-Terio, B. Ceresa, R. Nixon, A. Cataldo, Rab5-stimulated Up-regulation of the Endocytic Pathway Increases Intracellular -Cleaved Amyloid Precursor Protein Carboxyl-terminal Fragment Levels and A Production, J Biol Chem 278 (2003) 31261-8.

[204] V. Uytterhoeven, S. Kuenen, J. Kasprowicz, K. Miskiewicz, P. Verstreken, Loss of skywalker reveals synaptic endosomes as sorting stations for synaptic vesicle proteins, Cell 145(1) (2011) 117-32.

[205] R. Ehsanian, C. Van Waes, S.M. Feller, Beyond DNA binding - a review of the potential mechanisms mediating quinacrine's therapeutic activities in parasitic infections, inflammation, and cancers, Cell Commun Signal 9 (2011) 13-13.

[206] E. Prchla, C. Plank, E. Wagner, D. Blaas, R. Fuchs, Virus-mediated release of endosomal content in vitro: different behavior of adenovirus and rhinovirus serotype 2, The Journal of cell biology 131(1) (1995) 111-123.

[207] W. Tombari, I. ElBehi, F. Amouna, A. Ghram, Variability of tropism and replicative capacity of two naturally occurring influenza A H9N2 viruses in cell cultures from different tissues, Avian Pathol 45(2) (2016) 212-20.

[208] L. Pan, M. Mu, P. Yang, Y. Sun, R. Wang, J. Yan, P. Li, B. Hu, J. Wang, C. Hu, Y. Jin, X. Niu, R. Ping, Y. Du, T. Li, G. Xu, Q. Hu, L. Tu, Clinical Characteristics of COVID-19 Patients With Digestive Symptoms in Hubei, China: A Descriptive, Cross-Sectional, Multicenter Study, Am J Gastroenterol 115(5) (2020) 766-773.

[209] Y. Han, X. Duan, L. Yang, B.E. Nilsson-Payant, P. Wang, F. Duan, X. Tang, T.M. Yaron, T. Zhang, S. Uhl, Y. Bram, C. Richardson, J. Zhu, Z. Zhao, D. Redmond, S. Houghton, D.-H.T. Nguyen, D. Xu, X. Wang, J. Jessurun, A. Borczuk, Y. Huang, J.L. Johnson, Y. Liu, J. Xiang, H. Wang, L.C. Cantley, B.R. tenOever, D.D. Ho, F.C. Pan, T. Evans, H.J. Chen, R.E. Schwartz, S. Chen, Identification of SARS-CoV-2 inhibitors using lung and colonic organoids, Nature 589(7841) (2021) 270-275.

[210] M.C. Freeman, A.I. Wells, J. Ciomperlik-Patton, M.M. Myerburg, L. Yang, J. Konopka-Anstadt, C.B. Coyne, Respiratory and intestinal epithelial cells exhibit differential susceptibility and innate immune responses to contemporary EV-D68 isolates, eLife 10 (2021) e66687.

[211] V.B. Dugina, G.S. Shagieva, P.B. Kopnin, Biological Role of Actin Isoforms in Mammalian Cells, Biochemistry (Moscow) 84(6) (2019) 583-592.

[212] M.A. Rahman, M. Ušaj, D.E. Rassier, A. Månsson, Blebbistatin Effects Expose Hidden Secrets in the Force-Generating Cycle of Actin and Myosin, Biophysical journal 115(2) (2018) 386-397.

[213] N. Bayer, D. Schober, E. Prchla, R.F. Murphy, D. Blaas, R. Fuchs, Effect of bafilomycin A1 and nocodazole on endocytic transport in HeLa cells: implications for viral uncoating and infection, Journal of virology 72(12) (1998) 9645-55.

[214] J. Oppliger, G. Torriani, A. Herrador, S. Kunz, Lassa Virus Cell Entry via Dystroglycan Involves an Unusual Pathway of Macropinocytosis, Journal of virology 90(14) (2016) 6412-6429.

[215] J. Milhaud, Permeabilizing action of filipin III on model membranes through a filipin-phospholipid binding, Biochim Biophys Acta 1105(2) (1992) 307-18.

[216] K. Zheng, K. Kitazato, Y. Wang, Viruses exploit the function of epidermal growth factor receptor, Reviews in Medical Virology 24(4) (2014) 274-286.

[217] S.K. Rodal, G. Skretting, O. Garred, F. Vilhardt, B. van Deurs, K. Sandvig, Extraction of cholesterol with methyl-beta-cyclodextrin perturbs formation of clathrin-coated endocytic vesicles, Mol Biol Cell 10(4) (1999) 961-74.

[218] I.M. González-González, N. García-Tardón, C. Giménez, F. Zafra, PKC-dependent endocytosis of the GLT1 glutamate transporter depends on ubiquitylation of lysines located in a C-terminal cluster, Glia 56(9) (2008) 963-74.

[219] E. Prchla, E. Kuechler, D. Blaas, R. Fuchs, Uncoating of human rhinovirus serotype 2 from late endosomes, Journal of virology 68(6) (1994) 3713-3723.

[220] S. Li, C. Sieben, K. Ludwig, C.T. Höfer, S. Chiantia, A. Herrmann, F. Eghiaian, I.A. Schaap, pH-Controlled two-step uncoating of influenza virus, Biophysical journal 106(7) (2014) 1447-1456.

[221] M. Dang, X. Wang, Q. Wang, Y. Wang, J. Lin, Y. Sun, X. Li, L. Zhang, Z. Lou, J. Wang, Molecular mechanism of SCARB2-mediated attachment and uncoating of EV71, Protein & cell 5(9) (2014) 692-703.

[222] M. Tscherne Donna, T. Jones Christopher, J. Evans Matthew, D. Lindenbach Brett, A. McKeating Jane, M. Rice Charles, Time- and Temperature-Dependent Activation of Hepatitis C Virus for Low-pH-Triggered Entry, Journal of virology 80(4) (2006) 1734-1741.

[223] P.J. Hughes, G. Stanway, The 2A proteins of three diverse picornaviruses are related to each other and to the H-rev107 family of proteins involved in the control of cell proliferation, J Gen Virol 81(Pt 1) (2000) 201-7.

[224] C.M. Wiethoff, H. Wodrich, L. Gerace, G.R. Nemerow, Adenovirus protein VI mediates membrane disruption following capsid disassembly, Journal of virology 79(4) (2005) 1992-2000.